ANGULAR DISTRIBUTION AND INTERCEPTION OF DIFFUSE SOLAR RADIATION

by

M.D. STEVEN, B.Sc., M.Sc.

Thesis submitted to the University of Nottingham
for the degree of Doctor of Philosophy

October 1977

Department of Physiology and Environmental Studies
University of Nottingham School of Agriculture
Sutton Bonington, Loughborough, Leics.

ACKNOWLEDGEMENTS

First and foremost I am grateful to my supervisor Dr. M.H. Unsworth and to Prof. J.L. Monteith for helpful criticism and guidance at all stages in my work.

I would also like to thank the workshop staff for instrumental.work; members of the Biometry Unit for assistance with computing; Mr. Paul Dunn of Loughborough University for help with a laser; and all members of the Environmental Studies Section who have contributed much help and useful criticism. I am also grateful to NERC for financial support.

Finally, special thanks go to Miss Edna Lord for typing this thesis under difficult circumstances.

ABSTRACT

The estimation of the irradiance of sloping surfaces from standard meteorological measurements requires knowledge of the geometrical distribution of scattered radiation from the sky. Measurements of the radiance distribution of cloudless skies were made with a Linke-Feussner actinometer. When measurements of sky radiance N were expressed relative to the diffuse irradiance D of a horizontal surface, the angular distributions of N/D were remarkably independent of atmospheric turbidity. Standard distributions of N/D, drawn up for different solar zenith angles, were used to estimate the diffuse irradiance of slopes under cloudless skies.

A new actinometer was designed for the measurement of the radiance of cloudy skies. A theoretical analysis of the energy budget of a thermopile in relation to the actinometer design is presented. Nine actinometers were used to measure mean distributions of radiance for partly cloudy and overcast skies. Results for overcast conditions indicated that the mean radiance near the horizon was larger than the value predicted by the 'Standard Overcast Sky' formula, but the increase in estimated irradiance of vertical surfaces was only about 2%.

A computer model was formulated for estimating the global irradiance of slopes using the new results for diffuse radiation. The model was applied to climatological mean radiation data from the Meteorological Office for Kew, Eskdalemuir, Aberporth and Lerwick.

C O N T E N T S

LIST of APPENDICES

LIST of FIGURES

LIST of TABLES

NOTATION

In all equations in the text, parentheses ( ) denote functional relationships whereas curly or square brackets are used for grouping of terms. When given on their own, the symbols for radiation values B , D , G , R refer to the irradiance of a horizontal surface; I refers to the direct solar beam at normal incidence. The irradiance of a slope is indicated by its functional dependence on angle, e.g. $B(\alpha,\psi)$, $D(\alpha)$.

The principal symbols used in the text are :

$\vec{A}$	unit vector normal to slope
A_2, A_3	cross sectional areas of wires
B	direct solar beam
b	width of shade ring
D	diffuse solar radiation
D*	diffuse irradiance of horizontal surface intercepted by shade ring
D_o^*	D* based on assumption of isotropic sky
D'	background diffuse radiation
D_b	blue sky part of diffuse radiation
D_c	circumsolar diffuse radiation
D_g	cloudy sky part of diffuse radiation
d	thickness of thermopile
f	horizontal view factor of shade ring
G	global radiation
G_e	irradiance of an extraterrestrial horizontal surface
g	geometric shade ring correction

h	anisotropy correction for shade ring
h_s	relative sunshine hours
I	direct solar beam at normal incidence
K	total shade ring correction
k_1 to k_6	thermal conductivities
L	latitude
l	characteristic dimension for convection
m	air mass number
N	radiance of sky
Nu	Nusselt number
n	cloud amount
n_j	number of function pairs
n_o/n_t	frequency with which the sun is obscured by cloud
q	relative horizontal irradiance of region of sky obscured by shade ring
R	reflected radiation
R_n	net radiation
r	shade ring radius; scale length of scattering elements
S	solar radiation
s	ratio of circumsolar radiation D_c to diffuse radiation D in a cloudless sky
T	temperature
t_o	hour angle at sunset
V	voltage
z	zenith angle of sun
α	angle of tilt
β	radiance distribution parameter
γ	absorptivity
Δ	temperature difference between the black and white painted parts of a thermopile

δ	solar declination
δT	temperature difference
ε	emissivity
ζ	angle of refraction in water
η	angle between a point source and the normal to a surface
θ	zenith angle
λ	wavelength
μ	refractive index
ν	thermoelectric potential of thermocouples
ξ	scattering angle
ρ	albedo, reflection coefficient
ρ_a	dimensionless particle size $2\pi r/\lambda$
ρ_b	coefficient of backscattering in water
ρ_d	coefficient of reflection for diffuse radiation
ρ_f	Fresnel coefficient of reflection
σ	Stefan-Boltzmann constant
τ	atmospheric turbidity
ϕ	azimuth angle
ψ	azimuth of slope
$d\vec{\Omega}$	vector element of solid angle

I. INTRODUCTION

1.1 Introduction

The sun is the primary source of energy for natural processes on the earth's surface and stored solar energy is still by far the largest source of energy for mankind. Recently there has been a revival of interest in the direct use of solar energy and in the design of solar energy devices (see e.g. Brinkworth, 1972). The potential for using solar energy however depends on a number of meteorological factors which have been only partially studied: e.g. the spectral composition of the radiation; the geometric distribution; the variability; and the dependence of energy losses on temperature and wind speed. These factors need to be related to the way in which solar energy is used. For example, Kern and Harris (1975) point out that the tilt of solar energy collectors "... can only be optimised with respect to a well defined objective function". All these considerations point to the need for a better understanding of the nature of solar radiation.

Solar radiation at the earth's surface consists of the direct beam from the sun and diffuse radiation scattered by the atmosphere and clouds. In Britain, diffuse radiation accounts for 60% of the average annual receipt on a horizontal surface (UKISES, 1976), but there have been few studies of its characteristics. Global and diffuse radiation are measured routinely on horizontal surfaces in many parts of the world but for many aspects of solar energy use the solar irradiance of sloping surfaces is required. This study was to investigate the geometrical distribution of the diffuse component of solar radiation and to investigate the importance of the distribution to the radiation balance of slopes.

1.2 Solar Radiation

Solar radiation at the top of the atmosphere has a spectrum generally characteristic of a black body at 6000°K; about 97% of the energy is in the waveband 300 to 3000 nm. The extra-terrestrial irradiance at normal incidence varies by ±3% through the year due to the changing earth - sun distance. The currently accepted mean value of the 'solar constant' is 1353 W m^{-2} but there are claims that the 'constant' varies by as much as 3% (Thekaekara, 1976).

On an annual basis in the atmosphere above Britain (Kew), 34% of this energy is scattered to space, mostly by clouds and 30% is absorbed by the atmosphere, mainly by water vapour and other gaseous constituents. The rest reaches the earth's surface, either as direct radiation (15%) or diffuse (21%), (Monteith, 1973). Most of the absorption takes place in the infra-red whereas scattering, especially scattering by the atmosphere, is more important at shorter wavelengths. The spectrum of scattered radiation is consequently different from that of direct radiation and the quality of radiation scattered by clouds differs from that scattered by clear skies.

Radiation fluxes at the surface are very variable due to the changeability of atmospheric conditions. Below clear skies when the solar elevation exceeds about 30°, diffuse irradiance may vary from 15 to 35% of global irradiance, depending on turbidity (Unsworth and Monteith, 1972). Cloud however, is a more significant cause of variation and global radiation can fluctuate rapidly, changing by a factor of 4 or 5 within a few minutes. In the longer term, monthly mean values of global radiation at stations in Britain vary greatly from year to year with a standard deviation of 11% and up to 27% in

winter (UKISES, 1976). The variability of diffuse radiation is appreciably less, showing that most of the variation is in the direct component.

1.3 Scales of Radiation Measurement

Solar radiation may be measured fundamentally in radiometric (energy) units. There has been much confusion however due to two other systems: quantum measurement and photometric measurement. These have distinct fields of applicability but they have frequently been used where radiometric units would be more appropriate.

Quantum measurements describe the number of photons or quanta measured, independent of their energy. Since the energy of a photon is inversely proportional to its wavelength, the quantum scale becomes more sensitive, relative to the radiometric scale, at longer wavelengths since it takes more photons to carry the same amount of energy. The quantum scale is useful for computation of photochemical reactions where the flux of photons over a certain energy threshold is required and it is increasingly used in photosynthesis studies where McCree (1972) has shown that it has some advantage over the radiometric system. A convenient quantum unit is the Einstein (E) which is equal to N quanta, where N is Avogadro's number (6.02×10^{23}).

The photometric scale of measurement is based on the spectral sensitivity of the light-adapted human eye. The eye's response to light is a bell-shaped function of wavelength with peak sensitivity at 555 nm and the bandwidth at half the maximum value is 100 nm (Arnold, 1975). The eye thus sees only a narrow waveband of light and its response is non-uniform within that band so that photometric measurements

are not generally comparable with quantum or radiometric measurements. The photometric analogue of radiant power (Watts) is luminous flux (Lumen). Photometry finds its proper use in Illumination Engineering and improper use in many other fields.

It would be useful to have a set of conversion factors between the different measurement systems in common currency. This is in principle possible only when the radiation has a known spectral distribution. In the case of photometric measurements the radiation spectrum should also fall within the range of sensitivity of the human eye. This does not occur with solar radiation measurements, but empirical relationships may be valid if the solar radiation spectrum does not vary. The spectrum of global radiation is relatively constant, but the same is not true of the diffuse. Walsh (1961) reviewed the data on solar radiation and recommended a mean ratio of 108 Lumen per Watt for global radiation; the factor increased with solar altitude. For direct radiation the ratio was about 5% lower. It would be unwise to apply a mean conversion factor for diffuse radiation where the spectrum may vary considerably.

For quantum measurements of photosynthetically active radiation, McCree (1972) found that the ratio of quantum to energy flux in the waveband 400 - 700 nm was 4.57 μ E s^{-1} W^{-1} for global radiation and 4.24 μ E s^{-1} W^{-1} for sky radiation. McCartney (1975), making measurements at Sutton Bonington found that the ratio in this waveband was 4.54 μ E s^{-1} W^{-1} for global radiation under both cloudless and overcast skies. For direct radiation the ratio was a linear function of direct irradiance.

1.4 Diffuse Radiation

There are essentially two types of diffuse radiation with different spectral and geometric characteristics. The diffuse radiation from clear blue skies is due to atmospheric scattering and is discussed in some detail in Chapter II. Scattering of radiation by clouds is spectrally less selective but may be geometrically more complex. Below partially cloudy skies both types of scattered radiation are present. Where spectral or geometric differences are important it may be necessary to treat the two types of diffuse radiation separately. In Britain, the diffuse radiation is predominantly of the cloudy type. Since diffuse radiation is about 60% of the average global radiation and blue sky radiation is 15 to 35% of the global on clear days, the blue sky diffuse radiation can account for only about 15% of annual receipts.

Where diffuse radiation is not measured on a routine basis it becomes necessary to estimate it from other parameters. Bener (1963) attempted to define relationships between the diffuse irradiance of a horizontal surface, D and solar height as a function of cloud type during overcast conditions. Several methods have been proposed to estimate D from the global irradiance G . Liu and Jordan (1960), Page (1976) and Ruth and Chant (1976) suggested a relationship between monthly mean values of D/G and G/G_e where G_e is the extra-terrestrial irradiance (on a horizontal surface). Page expressed the relationship in the form

$$\frac{D}{G} = c + d\,\frac{G}{G_e} \qquad 1.1$$

where c and d were regression coefficients with mean values of 1.00 and -1.13 respectively, based on data from a large number of

stations. Anderson (1970) adopted an empirical relationship of the form

$$D = a\,G^{b} \qquad 1.2$$

where a and b were empirical constants. Kalma and Fleming (1972) found better results by normalising the radiation terms in Eq. 1.2 with respect to G_e. They also suggested that D can be expressed approximately as a constant fraction k of the attenuation of the direct component of global radiation, B .

$$D = k\{G_e - B\} \qquad 1.3$$

Values of k vary with site.

Estimations by these methods may be regarded as reliable for monthly means. Liu and Jordan claimed that their method could be used to estimate daily diffuse radiation to an average accuracy of ±5%. Their measurements however show that individual values could be in error by a much larger factor. For shorter periods than a month therefore, independent measurements of D should be made.

1.5 Solar Irradiation of Slopes

Standard measurements of radiation are almost invariably made on a horizontal surface. Whenever the irradiance of a tilted surface is required it becomes necessary either to measure the irradiance directly or to adapt measured horizontal values to the surface in question. It is frequently impractical to perform the direct measurements and much effort has been put into the problem of estimating slope irradiance from the standard horizontal measurements. None of the methods presently used is generally satisfactory.

The solar irradiance of slopes is a complex problem due to the

different geometries of direct and diffuse radiation. Two approaches have generally been adopted: In the component approach the solar radiation is separated into direct radiation, diffuse radiation from the sky and reflected radiation from the surrounding surfaces and each component is treated separately; in the integral approach the total slope irradiance is treated as one entity. The first stage in the component process has in many places already been done because diffuse and global irradiance are measured individually on a horizontal surface. Both approaches usually separate sky conditions into clear, partly cloudy and overcast. Partly cloudy conditions are the least well studied due to measurement difficulties.

In the integral approach the slope irradiance is measured and compared with horizontal irradiance. Relative values are defined for different conditions of the sky and of surface to sun geometry. Kondratyev and Manalova (1960) and Kondratyev (1969) did this for clear sky conditions and compared measured values with those deduced from the component approach. Kondratyev and Fedorova (1976) extended this work and some of their results are discussed in Chapter III. Temps and Coulson (1977) used similar measurements to produce flux diagrams for slopes of any angle, Fig. 1.1, and similar results are presented by Valko (1976). Curves by these authors define the relative global irradiance in terms of slope angle, azimuth and solar height. Similar data is available from Heywood (1966).

Most other studies consider only a few surfaces. Liu and Jordan (1961) tabulated monthly averages of irradiance of a S facing wall. Threlkeld (1963) considered vertical surfaces facing N, S, E and W on clear days. Norris (1966) analysed results from a N facing,60 degree

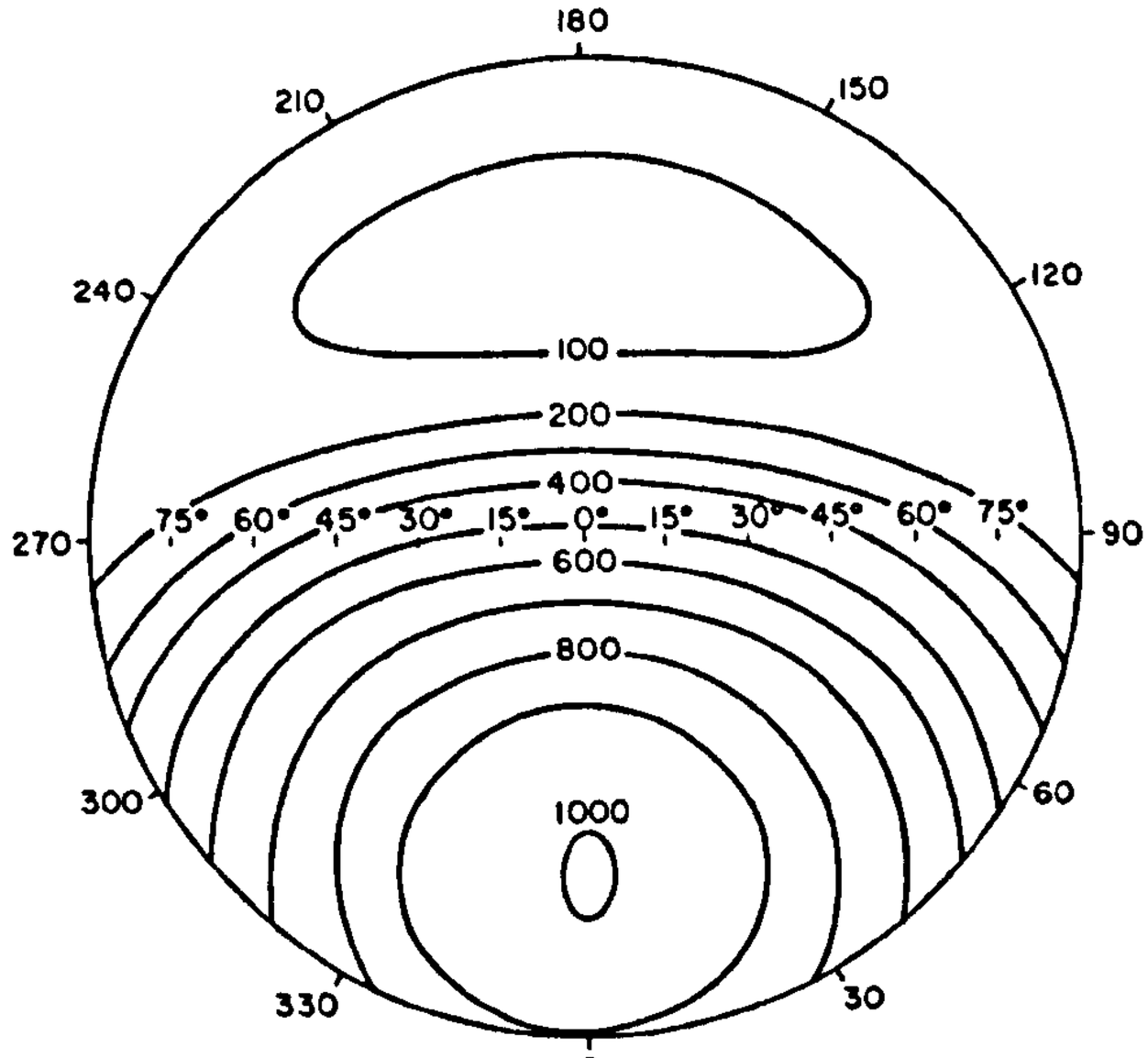

Fig. 1.1 Global solar irradiance (W m^{-2}) of a tilted pyranometer as a function of angle of tilt (plotted radially) and azimuth relative to the sun. The measurements were made with clear skies and a solar elevation of 34^{o}. (From Temps and Coulson, 1977).

slope and Heywood (1970) extended part of his earlier work to general sky conditions with a more limited set of surfaces. For clear skies, the results of Valko (1975) are very comprehensive and are discussed further in Chapter III. It should be noted that the results of different authors are frequently not comparable due to different reflection coefficients of the neighbouring ground and to poorly specified sky conditions. Current experimental programmes include routine observations by the Meteorological Office of N, S, E and W vertical irradiance at Bracknell (Collingbourne, 1975) and measurements of irradiance of planes in 77 different orientations by Valko (1976).

In the component approach to the radiation balance the direct, diffuse and reflected radiation on the surface are considered separately. The direct irradiance B may be found from the perpendicular beam irradiance I by defining the trigonometrical relationship of the slope to the sun, e.g. Garnier and Ohmura (1968). Petherbridge (1965) described a graphical method. The calculations have in some cases been applied to situations of real topography (Garnier and Ohmura, 1970). Ohmura (1970) and LeCarpentier (1974) also take account of shading of slopes from the direct beam by surrounding topographic features. The transmission of the direct beam through the atmosphere is a well known function of the concentrations of absorbing and scattering gases in the atmosphere and the effect of dust may be accounted for by means of a coefficient of turbidity (Unsworth and Monteith, 1972).

The radiation R reflected from horizontal ground is a component of the radiation budget which becomes more important with increasing slope. The reflected radiation is generally assumed to be isotropic in which case on a slope of tilt α it is

$$R(\alpha) = \rho G \{1 - \cos \alpha\}/2 \qquad 1.4$$

where ρ is the reflection coefficient of the ground. Kondratyev and Manalova (1960) showed that the isotropic assumption is not always accurate, even for uniform surfaces, but that the error is appreciable only for steep slopes ($\alpha > 75^\circ$), where it can amount to 30% when the sun is low.

To estimate the diffuse irradiance of slopes from horizontal measurements of D, the assumption is frequently made that the diffuse radiation is isotropic across the sky. The diffuse irradiance of a slope of tilt α is then given by

$$D(\alpha) = D \{1 + \cos \alpha\}/2 \qquad 1.5$$

and the global irradiance of the slope becomes

$$G(\alpha) = I \cos \eta + D \{1 + \cos \alpha\}/2 + \rho G \{1 - \cos \alpha\}/2 \qquad 1.6$$

where η is the angle between the sun and the normal to the slope. Norris (1966) concluded that the isotropic assumption was reasonable for monthly averages of diffuse radiation. However it is certainly not a good assumption for cloudless skies. The results of Kondratyev and Manalova indicated that the diffuse irradiance of a slope may be as much as twice the amount indicated by the isotropic assumption. The isotropic assumption is also of doubtful value for overcast skies which become darker towards the horizon, e.g. Dines and Dines (1927). Thus the problem of estimating the diffuse irradiance of a slope has again had two approaches. One is to measure $D(\alpha)$ and compare it with D; the other is to measure the distribution of radiance across the sky.

In the first category the clear sky irradiance of sloping surfaces of all aspects was measured by Valko (1976) and Temps and Coulson (1977).

Their data are however limited to a few individual occasions. Parmalee (1954) and Valko (1969, 1970, 1975) analysed clear sky diffuse irradiance of vertical surfaces as a function of turbidity, solar height and wall solar azimuth. Some of these results are discussed in Chapter III.

Measurements of the diffuse radiance of skies were reported by Dines and Dines (1927) for clear and overcast skies. Their measurements were limited to the E facing plane however and are insufficient to describe the complete radiance distribution. Kondratyev and Manalova (1960) measured clear sky radiance distributions and integrated the results to determine $D(\alpha)$ for a variety of slopes and solar elevations. Kondratyev (1969) gave angular distribution diagrams plotted from measurement data. Kondratyev and Manalova stated that "... the isotropic assumption proves to be satisfactory for the conditions of overcast sky (dense cloudiness)". They appear however to have confused isotropy with azimuthal symmetry which is a necessary but not a sufficient condition. Radiance distributions for cloudless skies with values normalised with respect to the zenith were produced by Tonne and Normann (1960). They derived a standard distribution by averaging and smoothing the distributions measured on a large number of occasions. Unfortunately some, and perhaps all of the measurements were of luminance rather than radiance. The spectral composition of diffuse radiation is knownto vary across the sky (Kondratyev, 1969) and in view of the remarks in Section 1.3, luminance distributions cannot be applied as radiance distributions.

For overcast skies the spectral composition of diffuse radiation is not a function of angle and Kondratyev showed that the difference between relative luminance and relative radiance is minimal. An

empirical formula for the luminance distribution of the 'Standard Overcast Sky' proposed by Moon and Spencer (1942) has sometimes been applied for the radiance distribution, Monteith (1973). The radiance N at a zenith angle of θ in the sky is given by

$$N(\theta) = N(o)\{1 + 2\cos\theta\}/3 \qquad 1.7$$

There is some evidence to suggest that the overcast sky rarely in fact conforms to a standard, but Eq. 1.7 may represent a mean (Grace, 1971). The standard overcast sky formula allows for the lower radiance towards the horizon and slope irradiance values are lower than those estimated by the isotropic assumption, Fig. 1.2. Walsh (1961) suggested that

$$N(\theta) = N(o)\{2 + 3\cos\theta\}/5 \qquad 1.8$$

might be a more accurate representation of the mean overcast sky. In conditions of light overcast the situation becomes more complicated as the distribution is then influenced by the position of the sun.

Very few measurements have been made of diffuse radiation from partially cloudy skies but various authors have developed models. Kondratyev and Manalova (1960) suggested that the relative global irradiance of a slope $G(\alpha)/G$ could be treated as a linear function of cloud amount n between known values for cloudless skies $(n = 0)$ and overcast skies $(n = 1)$. Tonne and Normann (1960) interpreted the geometric distribution of diffuse radiation between cloudless and overcast conditions to define a standard distribution for 50% cloud cover. There is no evidence to support either model and there is an inherent disadvantage in using n as a parameter because cloudiness

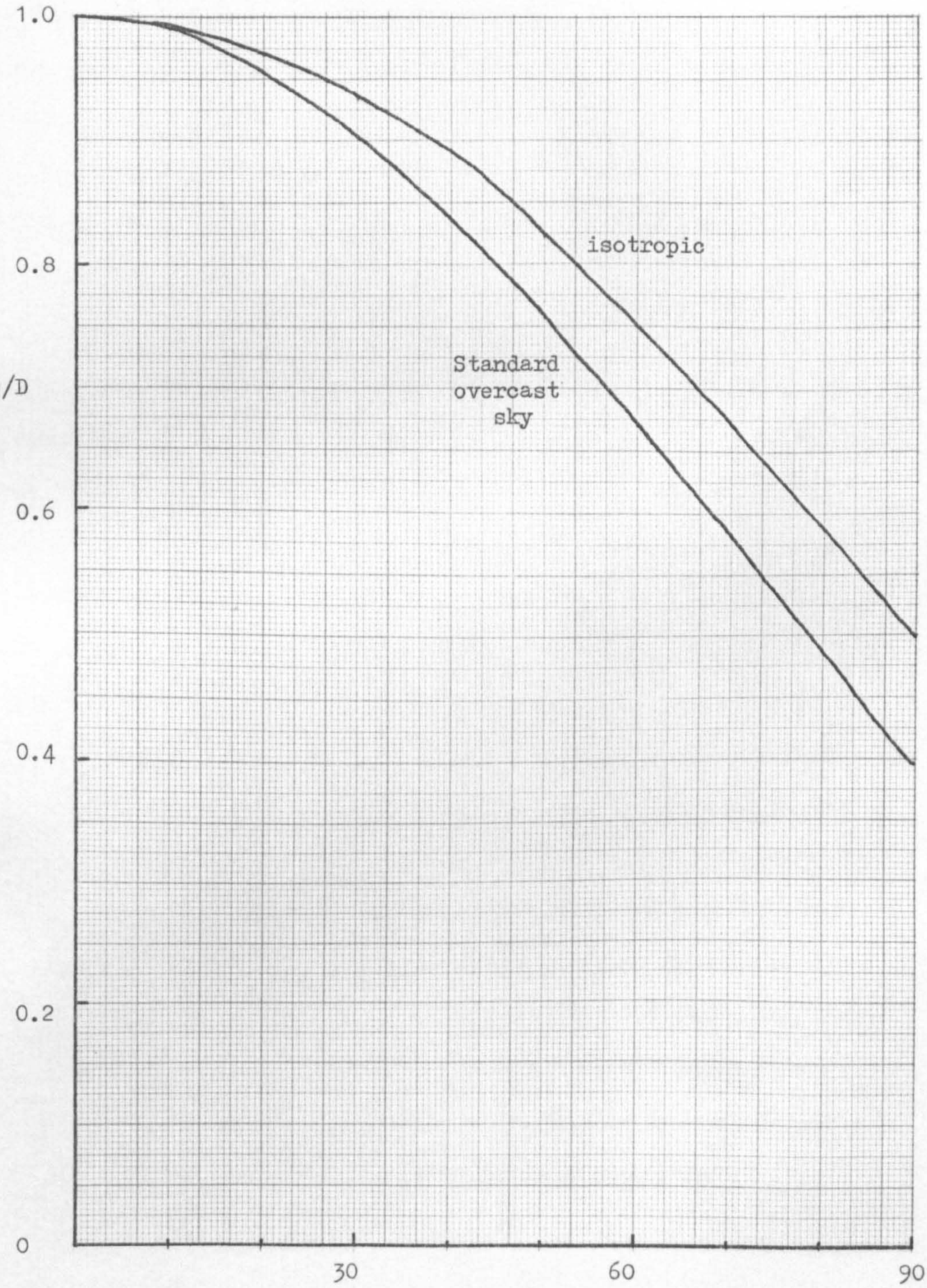

Fig. 1.2 Diffuse irradiance of slopes, relative to unit horizontal irradiance, for isotropic and standard overcast skies.

is difficult to measure objectively. Furthermore the models would seem to assume that D is a linear function of n, whereas in reality the relationship is more complex, Stagg (1947). As an alternative model, Robinson (1966) suggested that the blue part of the sky could be separated from the cloudy part and different geometric factors applied to each. Some results using a similar model are discussed in Chapter VI .

The best approach to the estimation of solar irradiation of slopes depends on the information available. The integral approach is appropriate where only G is measured as standard practice, because of the additional uncertainties in the breakdown of global radiation into direct and diffuse. Basic data on the irradiance of vertical surfaces under all weather conditions are quite widely available, but information for other surfaces is more limited. Where D is measured separately from G however, the component approach allows a more accurate determination of irradiance from the geometry of the surface and the radiation. This thesis presents improved information on the geometry of diffuse radiation and attempts to synthesise this into a model of solar irradiation of slopes: Chapters II and III are concerned with clear skies; Chapter IV describes a radiation instrument used in the study of partially cloudy and overcast skies; Chapter V presents the results of measurements with this instrument; and Chapter VI presents the results of a solar radiation model.

II.* CLOUDLESS SKIES : THE GEOMETRY OF DISTRIBUTION

2.1 Atmospheric Scattering Processes

The processes of radiation scattering in the atmosphere depend very strongly on the scale length r of the scattering elements and on the wavelength λ of the radiation. When $r \ll \lambda$ the oscillating electric field associated with the radiation striking the scatterers can be approximately treated as homogeneous. If the scattering material is dielectric then the scatterer acts as a dipole and the resulting radiation field was described by Rayleigh (1871, 1899). The scatterers in Rayleigh's theory were shown by Smolokhovsky and separately by Einstein (Kondratyev, 1969) to be microscopic fluctuations in air density rather than the air molecules as Rayleigh thought, but this does not affect the basic conclusions. The Rayleigh scattering function, which determines the amount of energy scattered in each direction, is the product of a scattering cross section which is strongly dependent on λ and an angular distribution function which is independent of r and λ. This implies that some wavelengths are scattered more than others, but the proportion of energy scattered in each direction is the same for all wavelengths. The scattering cross section is in fact proportional to $\lambda^{-4.05}$ (Robinson, 1966) so that shorter wavelengths are very much more susceptible to scattering. Rayleigh used this to explain the blue colour of the sky.

---

* The bulk of this Chapter has been previously published under the title 'Standard Distributionsof Clear Sky Radiance' (Steven, 1977).

When $r > 0.1\ \lambda$ the assumption of a homogeneous electric field does not hold and multipole fields of higher order have to be taken into account. The original theory due to Mie is described in some detail by Robinson (1966) and Kondratyev (1969). Both the scattering cross section and the angular scattering function depend on ρ_a where $\rho_a = 2\pi r/\lambda$. Figures2.1 and 2.2(b) show that the wavelength dependence of the cross section tends to decrease and the forward component of scattering increases with increasing ρ_a . Figures 2.2(a) and (b) also show that the angular distribution is much more strongly directional than with Rayleigh scattering. The scatterers in this case are dust particles and the behaviour of the overall atmospheric scattering function depends both on the particle density and the size distribution of aerosol in the atmosphere (McCartney, 1975). Since these are variable quantities, both the total amount of scattered radiation and its angular distribution depend on the atmospheric conditions.

The wavelength dependence of scattering by aerosol also depends on the size distribution of the particles. Kondratyev (1969) suggested that the scattering is proportional to λ^{-b} where b is a constant. He gave values of b ranging from 0.2 to 2.6 for various artificial aerosols. In the atmosphere, calculations by McCartney (1975) and measurements in the solar aureole by Piaskowska-Fesenkova (Kondratyev, 1969) suggest that values between 1.0 and 2.0 are more appropriate. Because Mie (aerosol) scattering has a weaker wavelength dependence, Rayleigh scattering is always important at shorter wavelengths ($\lambda < 500$ nm), (Bullrich, 1964). In Britain however the results of Unsworth and Monteith (1972) show that there is always enough aerosol in the atmosphere for Mie scattering to be significant in the overall energy flux.

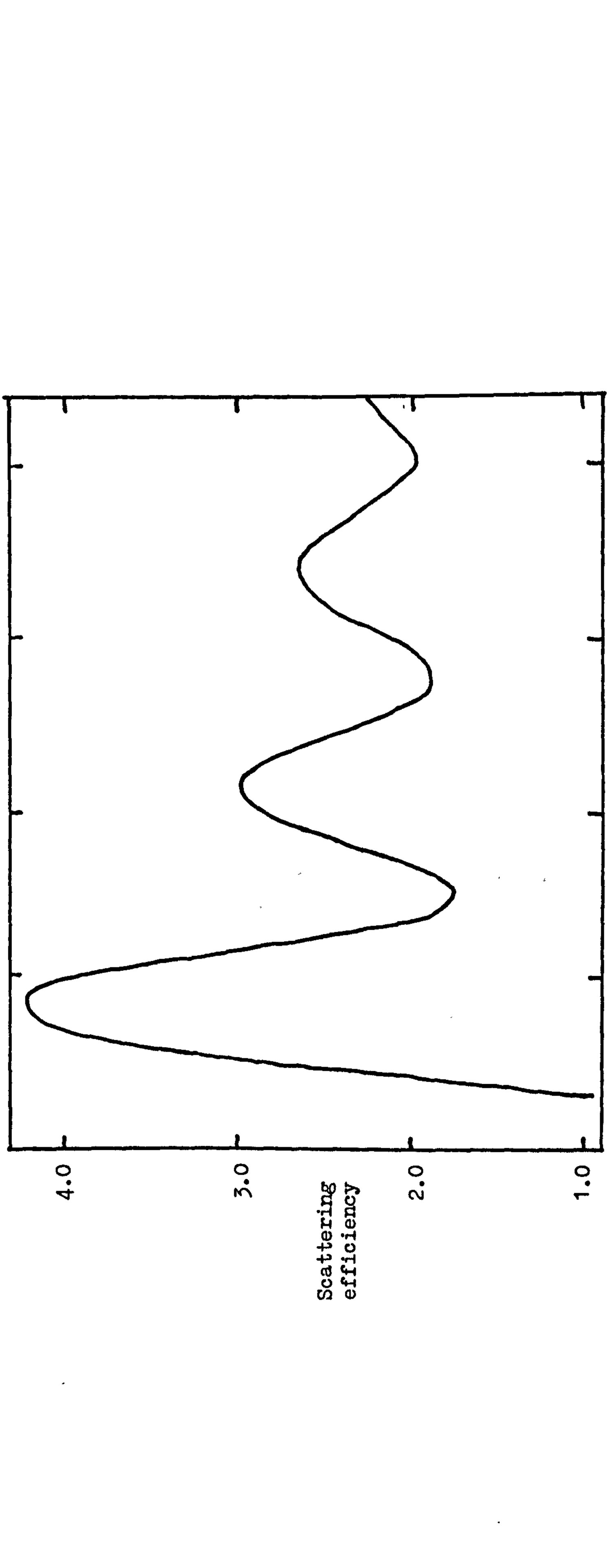

Scattering Efficiency on ρ_a for particles of the
efficiency is the ratio of
The dependence of Mie Scattering
refractive index 1.5. The scatte
scattering cross section to πr^2.

Fig. 2.1

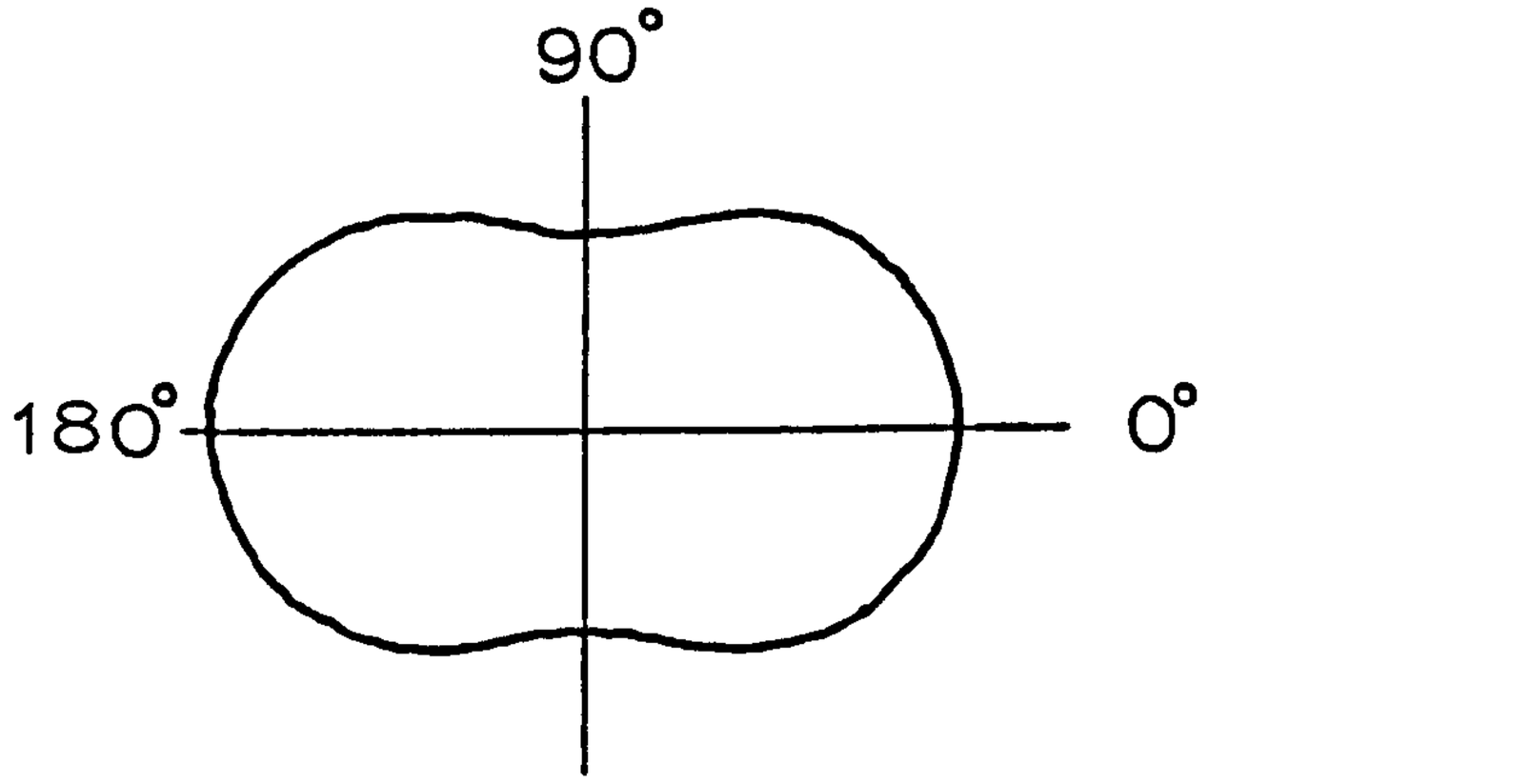

(a)

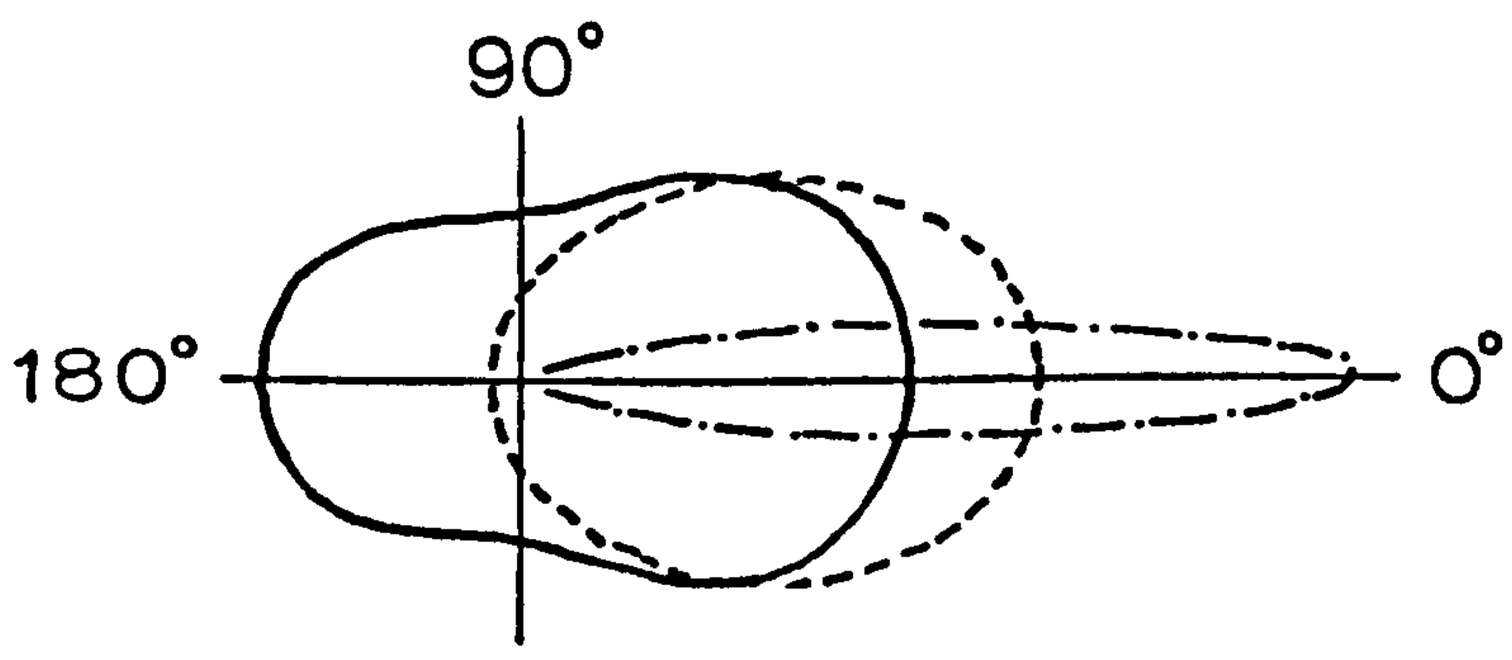

(b)

Fig. 2.2 Polar diagrams of the angular distribution of (a) Rayleigh and (b) Mie scattering for unpolarised green light (λ = 500 nm).

——— r = 50 nm

– – – – r = 100 nm

—·— r = 500 nm

The effect of atmospheric aerosol on solar radiation may be described by the aerosol turbidity coefficient τ. Following Unsworth and Monteith (1972) τ is defined by

$$I = I' \exp(-\tau m) \qquad 2.1$$

or

$$\tau = m^{-1} \ln(I'/I)$$

where I is the measured irradiance of the perpendicular beam, I' the calculated irradiance under a clean moist atmosphere and m is the air mass number. I' takes into account all the depletion of the direct beam due to Rayleigh scattering and absorption by water vapour and other gaseous constituents. τ thus separates out the effect of atmospheric dust from that of other causes of turbidity. Unsworth and Monteith showed that values of τ in Britain range from 0.05 for the cleanest air to 0.55 for the most polluted, more typical values being 0.1 to 0.4. Their calculations of the effect of τ on diffuse solar radiation D are shown in Fig. 2.3. The bottom curve with $\tau = 0.0$ is the result of pure Rayleigh scattering and the difference between this curve and the curves corresponding to other values of τ represents the contribution of Mie scattering.

The angular distribution of diffuse radiation therefore depends on the relative importance of Rayleigh and Mie scattering and on the size of the aerosol scatterers. For $\tau < 0.1$ the scattering regime is predominantly Rayleigh whereas at higher turbidities Mie scattering tends to dominate (Fig. 2.3). Bullrich (1964) showed theoretically that the fractional contribution of Rayleigh scattering to the diffuse radiation depends on the scattering angle as well as turbidity and

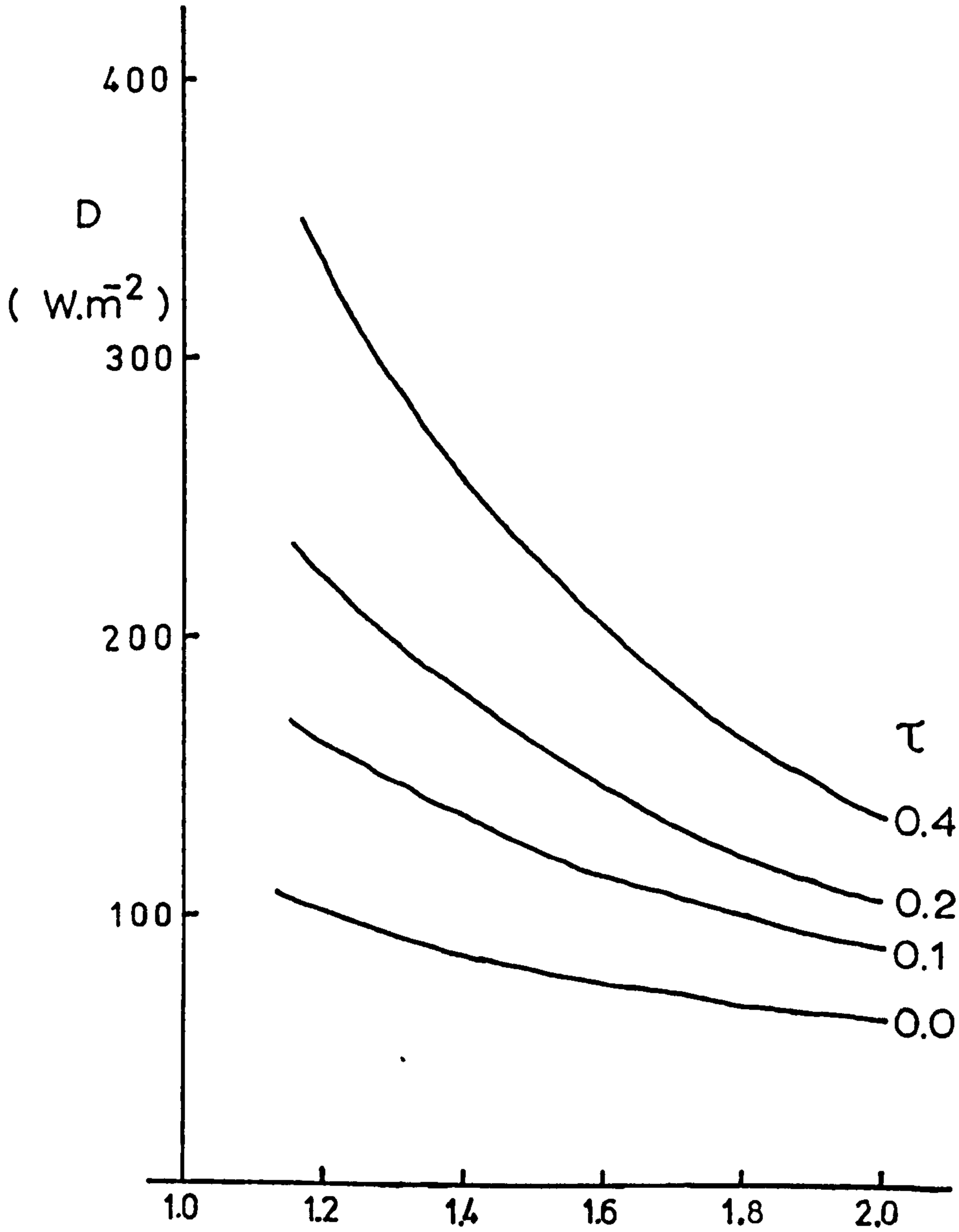

Fig. 2.3 Diffuse radiation as a function of aerosol turbidity.

wavelength. Rayleigh scattering is most effective at shorter wavelengths and at larger scattering angles, having its maximum effect at 130°. Higher turbidities reduce the fractional Rayleigh contribution, particularly at longer wavelengths. A further complication of high turbidity is the possibility of multiple scattering. Multiple scattering would tend to diffuse the directional character of the Mie regime. However Piaskowska-Fesenkova (Kondratyev, 1969) found that the effect of multiple scattering on measured scattering functions was practically insignificant.

Two principal factors thus affect the angular distribution of scattered radiation in a clear sky: the transition from a Rayleigh to a Mie scattering regime with increasing turbidity; and the effect of aerosol size distribution on Mie scattering. McCartney (1975) deduced from measurements of turbidity and spectral irradiance that the aerosol size distribution over central England in summer was fairly constant. Angular distributions of clear sky radiance can therefore be expected to be functions of turbidity and solar height.

2.2 Previous Measurements

Measurements of the photometric or luminance distribution of a clear sky were reported by Kimball and Hand (1921, 1922), Peyre (1927), Hopkinson (1954), Dogniaux (1954), Tonne and Normann (1960), Dorno (Robinson, 1966) and Kondratyev (1969). Most of these published results represent only one or two positions of the sun in the sky on a few individual occasions but the distribution of diffuse radiation is strongly dependent on the solar zenith distance and varies to some extent with atmospheric turbidity. Furthermore, photometric units are based

on the spectral sensitivity of the human eye and have no general applicability (Chapter I, section 1.3). Kondratyev (1969) compared the photometric and radiometric distribution of diffuse radiation in a clear sky and pointed out that while they were qualitatively similar they did not correspond quantitively. When described relative to the zenith value the relative radiance at some points differed by a factor of 3 from the relative luminance. For solar energy applications it would be useful to define standard radiance distributions based on many measurements made over a wide range of solar angles and atmospheric turbidities.

2.3 Measurements of Clear Sky Radiance

Over a long series of cloudless days* between June 1975 and May 1976 the radiance distribution of clear skies was measured on 67 occasions. On each occasion a Linke-Feussner actinometer was used to scan the sky, measuring the radiance N at 34 points in the hemisphere, and to make auxiliary measurements of the direct solar beam. Each complete scan took about 40 minutes and the order of measurements was varied to reduce biasing due to trends over this period. The instrument received radiation from a cone of half angle $5^{\circ}6'$ and thus each point measurement is in fact an average over a solid angle of 0.025 steradians. For convenience N was expressed in watts per square metre per π steradians which makes it an 'equivalent flux density', (Unsworth and Monteith, 1975). This choice of units implies that in an isotropic sky N would be numerically equal to the horizontal diffuse irradiance D.

*listed in appendix G

The radiance of a point in the sky depends both on its position relative to the sun and on its air mass number m , the former being more important close to the sun and the latter near the horizon. For this reason the measurements of radiance in each scan were of two types. One consisted of measurements at the zenith and at zenith angles of 30°, 60° and 75° in planes angled $\pm 45^{\circ}$, $\pm 90^{\circ}$, $\pm 135^{\circ}$ and 180° to the solar plane, allowance being made for the azimuthal motion of the sun during the period of the scan. A further set of circumsolar measurements to record the bright region about the sun was taken, in the solar plane at intervals of 10° above and below the sun's zenith angle z , and in planes of azimuth 20° to either side of the solar plane at zenith angles z and $z \pm 10^{\circ}$. In these measurements both the azimuth and zenith angles were determined from the contemporary position of the sun. This system was a compromise allowing an almost instantaneous picture to be built up over the period of the scan and enabling a more flexible pooling of data.

To confirm the accuracy of the radiance distribution, measurements of the horizontal diffuse irradiance D using a Kipp solarimeter with a shade ring, were compared with estimates of D derived by integrating the radiance values according to the relation

$$D = \frac{1}{\pi} \int_{o}^{2\pi} d\phi \int_{o}^{\pi/2} d\theta \; N(\theta , \phi) \cdot \sin \theta \cdot \cos \theta \qquad 2.2$$

where θ and ϕ are zenith and azimuth angles respectively. The values were 98% correlated and the integrated values were on average some 6% larger than those measured directly, the best agreement generally being

found at larger irradiance. The systematic differences can be accounted for by the different calibrations of the instruments, error in the empirical shade ring correction and the fact that the measurements could not be absolutely simultaneous. Some uncertainty also exists in the extrapolation of radiance, particularly in the circumsolar region. The circumsolar radiation has been measured to within 10^{o} of the sun which leaves a zone about the sun containing a solid angle of about 0.1 steradians. Due to the increasing brightness towards the sun, N is ill-defined by the surrounding points and a possible error of 25% in the estimation of N could result in a 3% error in D .

When normalised with respect to the horizontal diffuse irradiance D , the clear sky distribution of relative radiance for a particular solar height was remarkably constant. The distribution of N/D was thus independent of D over a large range of values. Possible reasons for this phenomenon are discussed in section 2.6.

Due to the positioning of measurements relative to the sun it proved possible to pool data from different scans over a range of values of z . Table 1 presents mean values denoted $\overline{N/D}$ made over 10 degree ranges of z . Since N was given in $W\,m^{-2}.\pi\,sr^{-1}$, the units of N/D are $(\pi \text{ steradians})^{-1}$. A few individual measurements which departed greatly from the mean were rejected and the mean and standard deviation recalculated. All points thus deleted were more than 3.4 new standard deviations from the new mean, and the editing process eliminated no more than $1\frac{1}{2}$ per cent of all the data. N/D values at points symmetric in the solar plane were averaged together to balance the distribution. The coefficient of variation was calculated for each point and appears to be roughly constant over the whole sky. The means of these coefficients are

Table 2.1 Mean values $\bar{N}/\bar{D}$ of normalised sky radiance data

Range of z	30° to 39°	40° to 49°	50° to 59°	60° to 69°
Mean z	35°	45°	55°	65°
Number of data sets	11	12	12	13

Zenith angle θ°	Azimuth φ°	Zone	Relative radiance $(\pi\ st)^{-1}$			
z - 10	0	C	3.12	3.54	4.04	4.93
z + 10	0	C	3.25	3.93	4.72	6.44
z	±20	C	3.14	3.04	3.25	3.65
z - 10	±20	C	2.51	2.55	2.58	2.87
z + 10	±20	C	2.53	2.84	3.17	3.87
z + 20	0		2.49	2.98	3.83	
z + 30	0		1.98	2.52		
z + 40	0		1.57			
z - 20	0		1.86	1.92	2.05	2.46
z - 30	0			1.21	1.26	1.36
z - 40	0				0.82	0.88
30	180	U,A	0.41	0.35	0.36	0.31
60	180	A	0.40	0.44	0.48	0.49
75	180	L,A	0.54	0.58	0.66	0.71
30	±90	U,P	0.69	0.66	0.54	0.43
60	±90	P	0.60	0.67	0.63	0.58
75	±90	L,P	0.68	0.76	0.76	0.76
30	±45	U	1.61	1.30	0.93	0.71
60	±45		1.20	1.37	1.44	1.33
75	±45	L	1.15	1.41	1.60	1.74
30	±135	U,A	0.45	0.43	0.38	0.32
60	±135	A	0.44	0.46	0.49	0.47
75	±135	L,A	0.54	0.58	0.64	0.64
0		U	0.84	0.69	0.55	0.41
Mean coefficient of variation			0.105	0.12	0.13	0.14
Mean turbidity	τ		0.38	0.32	0.30	0.22

Note: The zone symbols in column 3 refer to groupings of the data for statistical analysis in Section 2.4.

given at the bottom of Table 2.1. Because of their constancy the 95% confidence limits for $\overline{N/D}$ can be given as about 0.08 of the mean for each point.

Table 2.1 can be used to draw diagrams of standard distributions of $\overline{N/D}$ for solar zenith angles 35° to 65°. Figure 2.4 shows distributions drawn by hand from the means in Table 2.1. Distributions for intermediate values of z can be drawn by interpolating between columns of Table 1. In this case the position of the derived circumsolar values should depend both in θ and ϕ on the location of the sun whereas for the planar values only ϕ should depend on the sun's position.

2.4 Statistical Analysis

2.4(a) Variation with z

In an attempt to explain some of the residual variation in $\overline{N/D}$ the values of N/D in each scan were averaged over zones in the sky to remove some of the spatial variability. This reduced the coefficients of variation from about 0.12 to 0.09. Five zones were examined. The Circumsolar zone marked C in Table 2.1 is made up of point measurements around the sun. The other zones examined were the Perpendicular zone, marked P, consisting of points in the 90° plane, the Antisolar zone A of points with azimuth greater than 90°, the Upper zone U and the Lower zone L. The P and A zones represent azimuthal regions, i,e, they are averaged over all zenith angles. The U and L zones are averaged over azimuth and represent the upper and lower portions of the sky generally. The P and A zones consequently overlap with the U and L zones to some extent. The zonal values for each scan, denoted (N/D) were regressed against z to assess the validity of pooling data

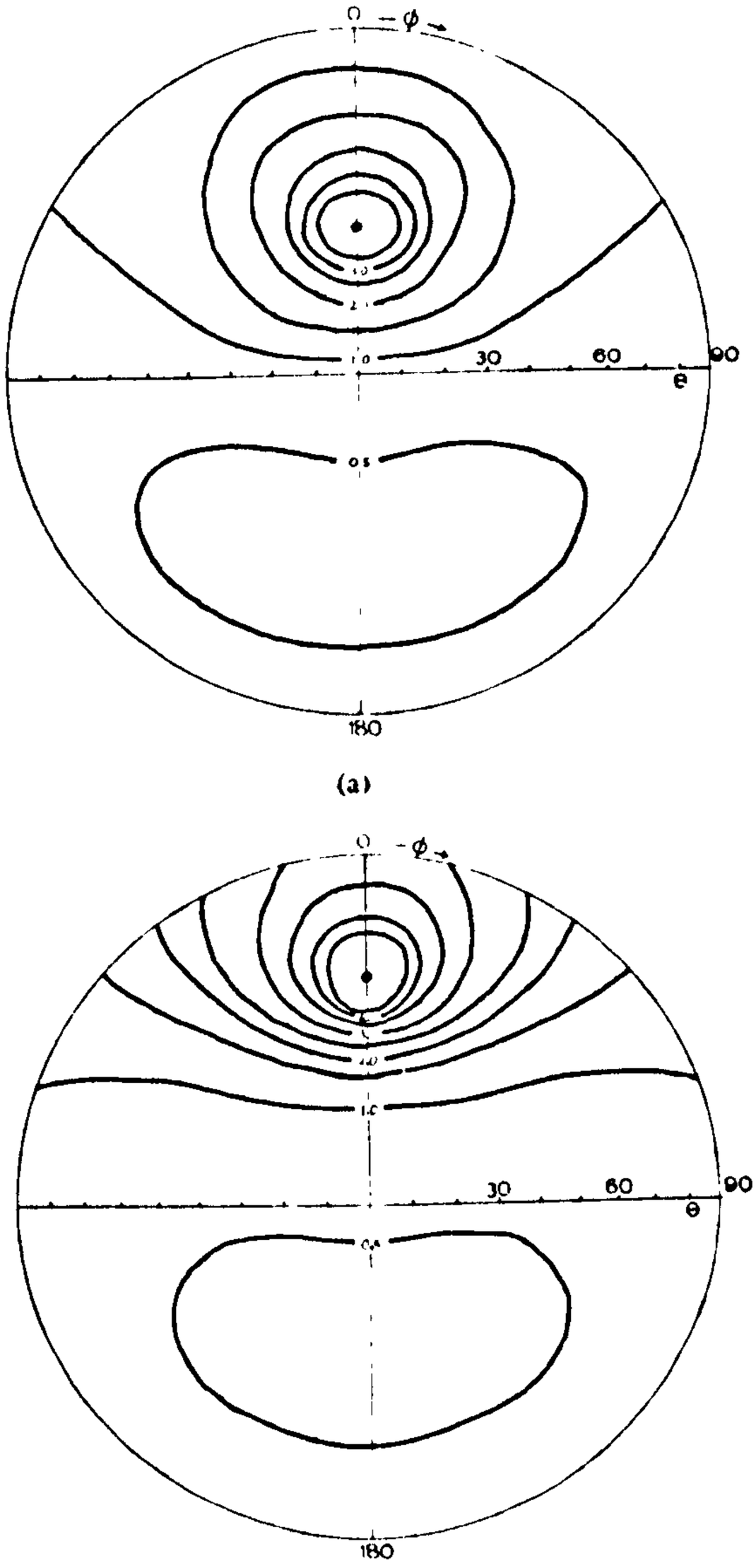

Fig. 2.4 Standard distributions of normalised sky radiance N/D : (a) for $z = 35^{\circ}$; (b) for $z = 55^{\circ}$. The contours are of the ratio of 'equivalent flux density' to horizontal diffuse irradiance. The plot is on a 'Lambert' projection so that equal solid angles are represented by equal area. The radial scale is consequently proportional to $(1-\cos\theta)^{\frac{1}{2}}$.

by 10 degree intervals of z. Figure 2.5 shows the regression for the circumsolar zone which was statistically significant at the 0.1% level. The regression value of (N/D) increases by a factor of 1.7 when z is increased from 30° to 70°. However, when only data within a 10 degree range of z were considered, e.g. between 30° and 40° in Figure 2.5, none of the regressions of (N/D) on z were significant even at the 10% level. In other words the trend over this range is not large compared with the local variation in (N/D) due to other sources. Other zones examined exhibited the same behaviour. Pooling the data over this range of z is therefore satisfactory.

2.4(b) Variation with turbidity

To determine the effect of atmospheric turbidity on the distributions, the values of (N/D) were taken in 10 degree ranges of z to reduce the variation due to solar zenith angle, and regressed on τ. It was found that in the Perpendicular and Antisolar zones (N/D) was not significantly related to τ in any range of z values. The other zones all showed significant regressions though not always in all ranges of z. The results are summarised in Table 2.2, all the regressions being significant at better than 5%. Multiplying the slope of the regression by the range of τ values experienced, the change in (N/D) due to turbidity can be calculated. These show that up to about 15 per cent departure from the means given in Table 2.1 can be expected due to variation in turbidity, but the departure due to a more typical range of turbidities of 0.1 to 0.5 (Unsworth and Monteith, 1972) would be about 5 to 10 per cent.

Figure 2.6 shows a typical example of the dependence of (N/D) on τ for the Upper zone. Some of the very large values of τ were

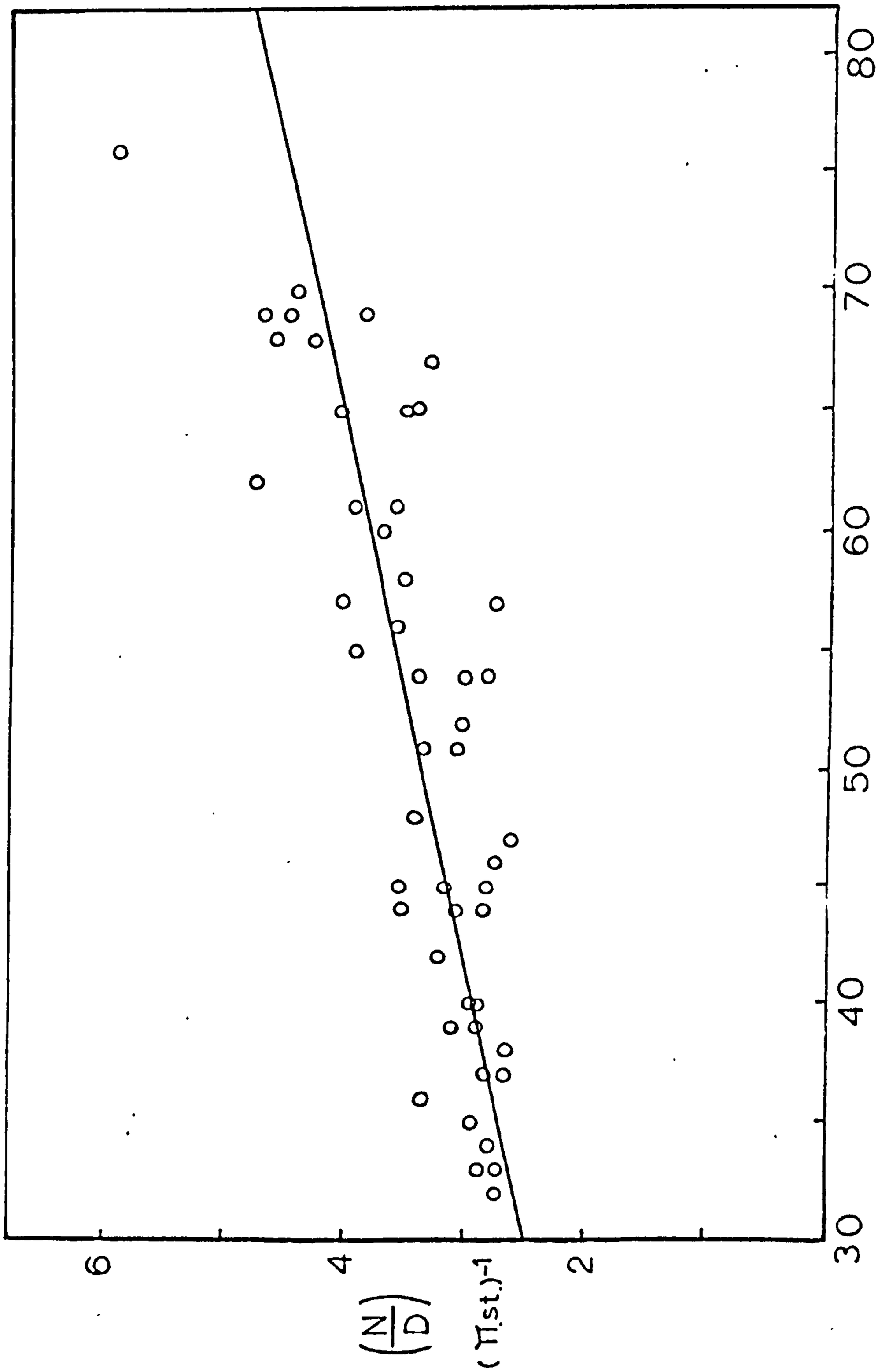

Fig. 2.5 Zonal mean relative radiance as a function of solar zenith angle for the circumsolar zone.

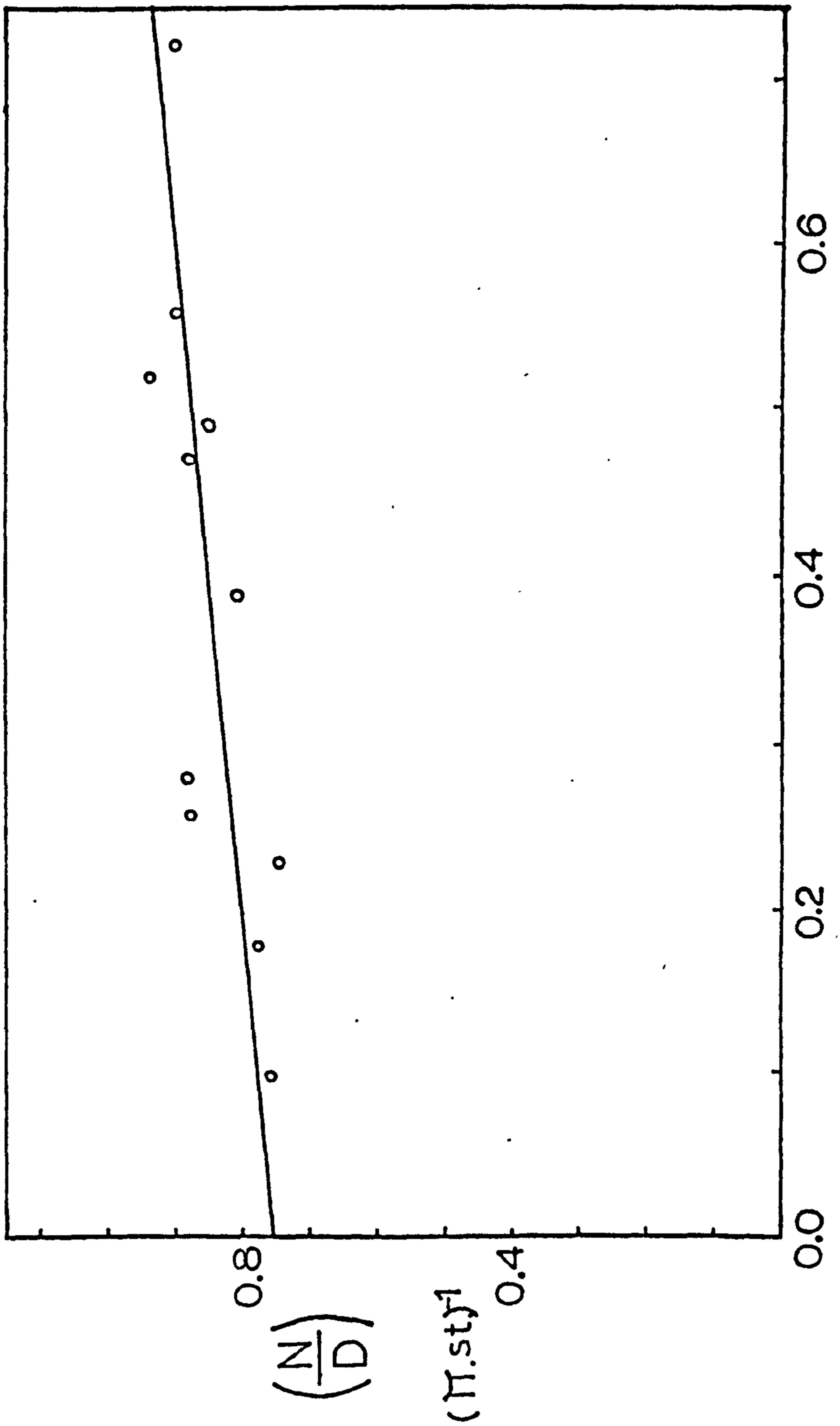

Fig. 2.6 Zonal mean relative radiance as a function of turbidity for the upper zone, with solar zenith angles 30° to 39°

Table 2.2 Regressions of zonal (N/D) on turbidity

Zone	Range of z	$\overline{N/D}$	Range of τ	Regression slope
Perpendicular	All ranges			not significant
Antisolar	All ranges			not significant
Circumsolar	30° to 39°	2.86	0.10 to 0.72	-0.75
	40° to 49°	3.06	0.11 to 0.81	-1.07
	50° to 59°	3.34	0.14 to 0.71	-1.55
	60° to 69°	4.01	0.14 to 0.38	-3.56
Upper	30° to 39°	0.85	0.10 to 0.72	0.25
	40° to 49°	0.74	0.11 to 0.81	0.24
	50° to 59°	0.58	0.14 to 0.71	0.35
	60° to 69°	0.46	0.14 to 0.38	0.65
Lower	30° to 39°	0.76	0.10 to 0.72	-0.33
	40° to 49°	0.87	0.11 to 0.81	-0.26
	50° to 59°	0.95	0.14 to 0.71	-0.31
	60° to 69°			not significant

probably due to a thin layer of cloud rather than dust but there is no evidence that this extra factor distorts the trend. The effect of larger turbidities generally is to reduce N/D in the circumsolar region and to increase relatively the radiance of the upper part of the sky at the expense of the lower part, while increasing the overall diffuse radiation from all regions of the sky, as shown by Unsworth and Monteith (1972). The first can be explained qualitatively as the effect of multiple scattering weakening the large forward scattering component of a single scattering regime. Also since the attenuation of radiation is proportional to $\exp(-\tau m)$, an increase of turbidity will have a greater effect at large air mass. The scattering probability depends on the air mass traversed by the direct beam and hence is the same for all points in the sky. The scattered radiation however is attenuated over an air

mass dependent on its perceived direction, and hence the lower regions of the sky appear depleted relative to the higher regions.

In conclusion, these results show that the effects of turbidity on the distribution of diffuse radiation are significant but small. The information in Table 2.1 should be regarded as referring to mean turbidities τ of about 0.2 to 0.4. It would be possible to include corrections to the mean distributions in Table 2.1, using the data in Table 2.2, and bearing in mind that since the radiance values are normalised it is necessary to balance any positive adjustment in one region with a negative one in another. It is doubtful however, whether such a procedure would be justified either statistically or in practice. The distribution of N/D remains very constant over a wide range of D and the deviation due to turbidity is very much a second order effect.

2.5 Analytic Approximations

The distribution of clear sky diffuse radiation was first explained theoretically by Lord Rayleigh (1871). Since than a number of attempts have been made to fit the theory to the observed distributions. Pokrowski (1929), as cited by Walsh (1961) proposed the formula

$$N(\theta,\xi) = a_1 \left\{ \frac{1 + \cos^2 \xi}{1 - \cos \xi} + a_3 \right\} \left\{ 1 - \exp (a_2 \sec \theta) \right\} \qquad 2.3$$

where ξ is the scattering angle, the angle which the radiation makes with the sun, a_1 is a scaling factor, a_2 is a scattering coefficient and a_3 an empirical constant to allow for multiple scattering. Pokrowski proposed the values 0.32 and 5 for a_2 and a_3 respectively. Hopkinson (1954) however found better agreement with measured luminance distributions with the arbitrary constant omitted, with $a_3 = 0$ and

$a_2 = 0.32$. A similar formula was proposed by Dogniaux (1975) as follows :

$$N(\theta,\xi) = N(o)\left\{\frac{b_1 + b_2 \exp(b_3\xi) + b_4 \cos^2 \xi}{b_1 + b_2 \exp(b_3 z) + b_4 \cos^2 z}\right\}\left\{\frac{1 - \exp(b_5 \sec \theta)}{1 - \exp(b_5)}\right\} \qquad 2.4$$

where $N(o)$ is the radiance at the zenith and the values of b_i were given as 0.91, 10, -3, 0.45 and -0.32 for $i = 1$ to 5 respectively.

The formulae, Eqs. 2.3 and 2.4 were tested by substituting the measured (normalised) values of N from Table 2.1 and using the FORTRAN function fitting routine E04GAF (NAG, 1975) to find the best values of the parameters a_i and b_i. The routine worked iteratively to minimise the sum of squares at all the measured points of the function $F = (N - N')/N$ where N' is the analytic approximation. This formulation, using relative rather than absolute differences, prevents excessive weight being placed on the circumsolar region.

Using the distribution data for $z = 35^o$, the values of a_1, a_2 and a_3 at the best fit of Eq. 2.3 were 0.49, 0.92 and 11.7 respectively. The fit was not particularly good however and relatively insensitive to changes of 10 or 20% in the values of the parameter a_1. The residual standard deviation of the relative differences was 0.24 which indicates that the departure of the fitted function from the measured values was, on average, about 24%. Some individual fitted values were in error by over 40%. For comparison the standard deviations of the measured values were only 11% of the means, (Table 2.1) and hence Pokrowski's formula was not regarded as satisfactory.

When the Dogniaux formula (Eq. 2.4) was applied to measurement data from all ranges of z, the residual standard deviation was 0.12 and the largest individual errors of fitted values were 25%. In addition to

being too inaccurate for practical use, Eq. 2.4 was found to be particularly unsatisfactory for function fitting. The parameters b_i were not independent and the values of several of the parameters at the best fit were not significantly different from zero.

The Dogniaux formula was also applied in each range of z separately, for which purpose it was modified to the form

$$N(\theta,\xi) = \{c_1 + c_2 \exp(c_3 \xi) + c_4 \cos^2 \xi\} \{1 - \exp(c_5 \sec \theta)\} \qquad 2.5$$

With Eq. 2.5 the agreement between fitted and measured values was considerably better, the residual standard deviation being reduced to 0.04. The maximum error in any individual value was about 10%. The best values of the coefficients c_i together with their standard error are tabulated in Appendix A. Figure 2.7 shows relative radiance values in a cross section through the solar plane, and the fitted formulae of Pokrowski (eq. 2.3) and Dogniaux (Eq. 2.5) may be compared with the measured values.

Slightly better results with the fitting routine were obtained using a series of orthogonal functions of θ and ϕ, based on spherical harmonics, plus an exponential function of ξ to approximate the circumsolar radiation. The form of this approximation is

$$N(\theta,\phi) = \sum_{i=1}^{10} d_i f_i(\theta,\phi) + d_{11} \exp(- d_{12} \sin \xi) \qquad 2.6$$

where the functions f_i and the values of the coefficients d_i at the best fit are given in Appendix A. The residual standard deviation was again about 0.04 but the maximum error of any individual fitted value was 8%, which is well within the uncertainties of the measured data.

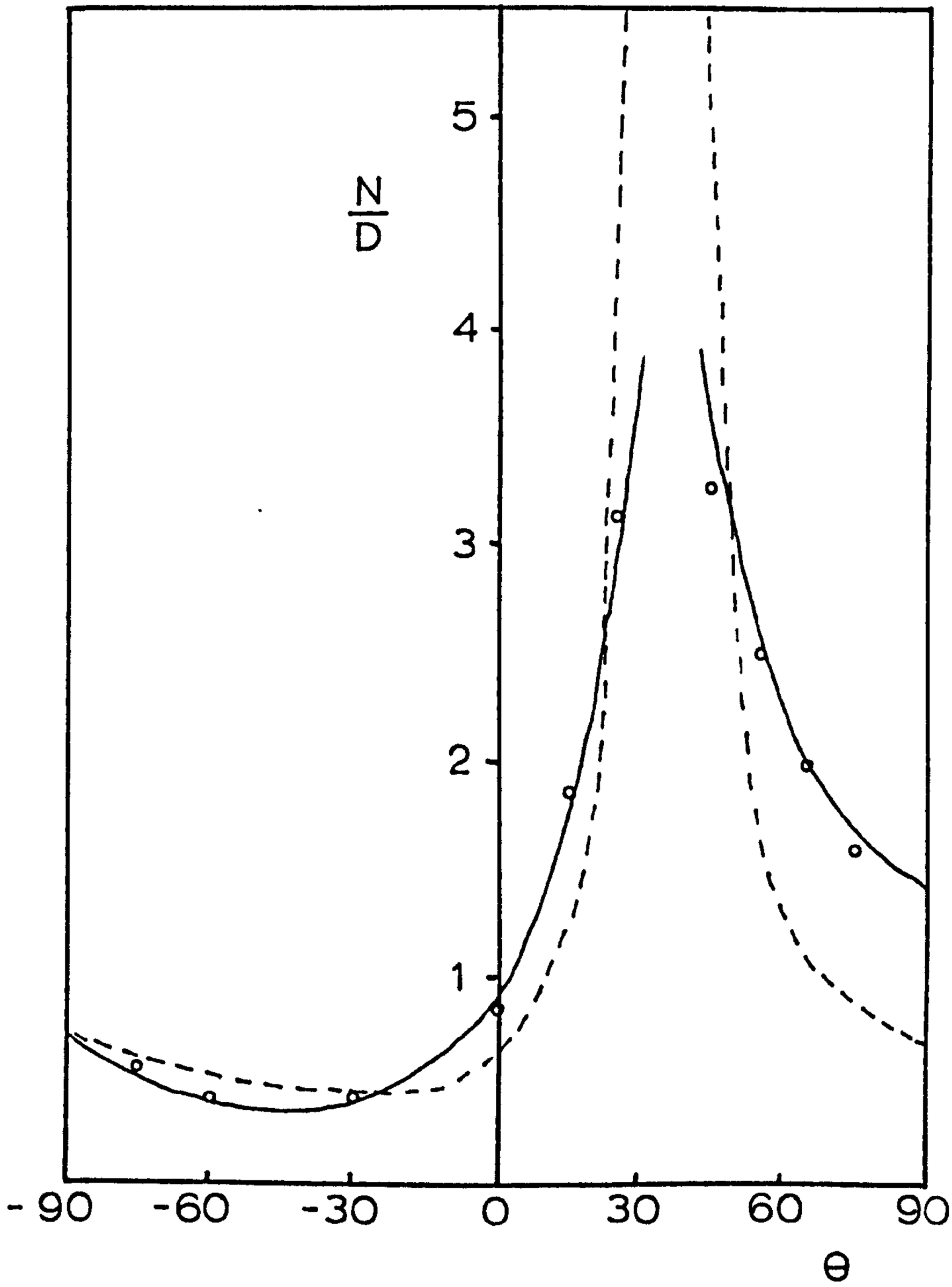

Fig. 2.7 Relative radiance values for $z = 35^\circ$, in a cross section through the solar meridian.

o Measured values

——— Fit of Dogniaux' formula (Eq. 2.5)

- — - — Fit of Pokrowski's formula (Eq. 2.3)

2.6 Conclusions

The measurements presented in this chapter define standard distributions of clear sky radiance which are, to a first approximation, independent of turbidity. Since higher turbidity must result in a Mie scattering regime whereas at lower turbidities Rayleigh scattering is still dominant, this result is somewhat surprising. These measurements however, were made at relatively high turbidities where Mie scattering is already dominant. Moreover the angular distributions of Mie and Rayleigh scattering regimes may not in practice be very different. Integration over ρ_a and λ reduces much of the disparity when actual distributions of aerosol size are considered. The strongly directional Mie scattering at higher turbidities may be partly compensated by increased multiple scattering which tends to diffuse the distribution, and the forward scattering due to very large particles ($\rho_a > 10$) is probably not measured as diffuse radiation anyway as most of the radiation is scattered into the solar aureole and may for all practical purposes be regarded as part of the direct beam.

The standard distributions of Table 2.1 therefore represent means which can be used to a useful degree of accuracy over a wide range of turbidities. Due to their relative independence of τ they should remain valid regardless of geographical location or season except at high altitude or in very dusty regions. The analytic formulae of Pokrowski (Eq. 2.3) and Dogniaux (Eq. 2.4) do not fit the data well enough to be useful, but the modified Dogniaux formula (Eq. 2.5) and the spherical harmonic representation (Eq. 2.6) with their coefficients given in Appendix A, are sufficiently accurate for most practical

purposes. The spherical harmonic representation is used in Chapter III to calculate the relative diffuse irradiance of plane surfaces. Turbidity should have little effect on this procedure since the calculation of surface irradiance involves integrating over a large area of sky, a fact which should smooth out errors due to inaccuracies in the distribution.

III. CLOUDLESS SKIES : THE GEOMETRY OF INTERCEPTION

3.1 Integration of Radiance Distributions

In Chapter II, measurements of the radiance of clear skies were described. It was found that when the radiance N at a point in the sky was normalised with respect to the horizontal diffuse irradiance D, the relative radiance values were largely independent of turbidity and mean distributions of N/D were given as a function of solar zenith angle, z in Table 2.1. These distributions may be used to estimate the diffuse irradiance of sloping surfaces.

The diffuse irradiance $D(\alpha , \psi)$ of a slope of tilt α and azimuth ψ may be calculated from N by integrating over the sky with the appropriate weighting function. The integral is

$$D(\alpha , \psi) = 1/\pi \iint N(\theta , \phi)\ \vec{A} \cdot d\vec{\Omega} \qquad 3.1$$

where N is given as a function of zenith angle θ and azimuth ϕ. $\vec{A}$ is the unit vector normal to the slope and $d\vec{\Omega}$ is the solid angle of an element of the sky, the vector part denoting the direction of the element. The angular relationships are shown in Fig. 3.1 The vectors are given by

$$\vec{A} = \begin{pmatrix} \sin\alpha \cos\psi \\ \sin\alpha \sin\psi \\ \cos\alpha \end{pmatrix} \quad \text{and} \quad d\vec{\Omega} = \begin{pmatrix} \sin\theta \cos\phi \\ \sin\theta \sin\phi \\ \cos\theta \end{pmatrix} \sin\phi \, d\theta \, d\phi$$

and $\vec{A} \cdot d\vec{\Omega}$ is their scalar product. Eq. 3.1 can therefore be expanded to the form

$$D(\alpha,\psi) = 1/\pi \iint N(\theta,\phi) \left\{ \sin\alpha \sin\theta \cos(\psi - \phi) + \cos\alpha \cos\theta \right\} \sin\theta \, d\theta \, d\phi \qquad 3.1(a)$$

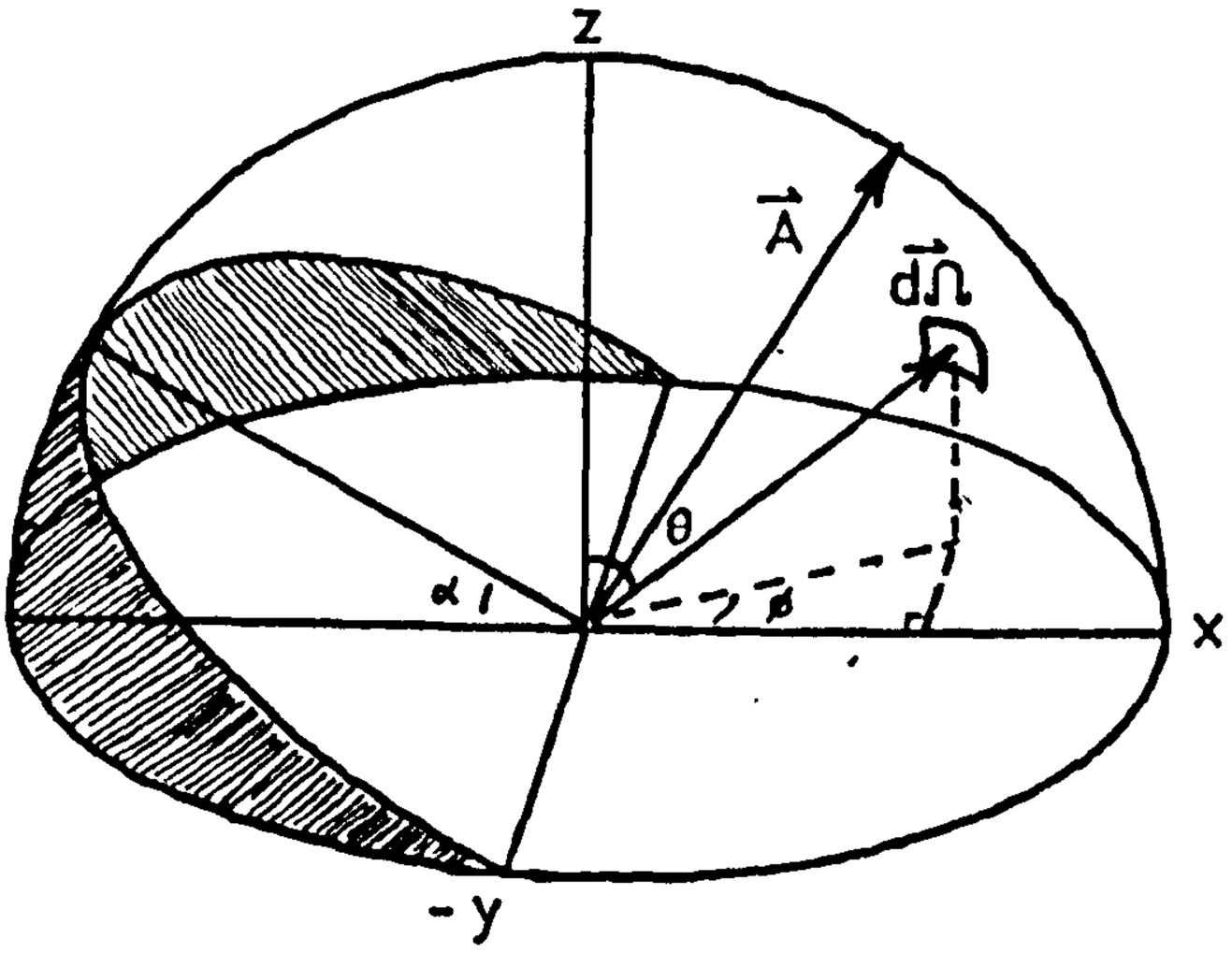

Fig. 3.1 Angular relationships of slope to sky. The shaded area of sky is hidden from the slope.

and the integration is performed over the region of sky that is exposed to the slope, see Fig. 3.1. The limits are $0 \leqslant \theta \leqslant \pi/2$ for $\psi - \pi/2 \leqslant \phi \leqslant \psi + \pi/2$ and $0 \leqslant \theta \leqslant \theta_1$ for $\pi/2 + \psi < \phi < 3\pi/2 + \psi$. The limit θ_1 is the zenith angle at the skyline and can be found by solving the equation $\vec{A} \cdot d\vec{\Omega} = 0$.

The spherical harmonic approximations to the mean radiance distributions (Eq. 2.6 and Appendix A), were substituted for N in equation 3.1 and the integrations were performed numerically using the FORTRAN routine D01DAF (NAG, 1975). Integrations were also done on horizontal planes as a check on the normalisation of N and the fitted functions. The integrated D values were 1.015, 1.044 0.996 and 0.926 for z values of 35°, 45°, 55° and 65° respectively and the integrated irradiances of slopes were renormalised with respect to these values. Tables 3.1 to 3.4 thus show integrated values of $D(\alpha, \psi)$ relative to unit horizontal diffuse irradiance, for every 30° of azimuth and 15° of tilt. The four tables correspond to the mean radiance distribution at four solar zenith angles given in Chapter II.

The absolute accuracy of the integration procedure was given as $\pm$ 0.001 and this was checked by splitting the integral into two parts and comparing results. In all cases tried the agreement was better than $\pm$ 0.0003. The major uncertainties in the integrated values therefore depend on the uncertainties in the radiance measurements and on the fitting procedures used to obtain the analytic approximations of N. As a check on the latter, integrations were also performed using different approximations for N. The same series of functions (Eq. 2.6) were used, but the coefficients were derived by a

Table 3.1 Relative diffuse irradiance of tilted planes for $z = 35^{\circ}$.

α°	15	30	45	60	75	90
ψ°	$D(\alpha, \psi)/D$					
0	1.12	1.19	1.19	1.12	0.98	0.79
30	1.10	1.15	1.14	1.06	0.92	0.73
60	1.05	1.05	1.00	0.90	0.75	0.58
90	0.98	0.92	0.83	0.70	0.56	0.42
120	0.92	0.80	0.66	0.53	0.41	0.32
150	0.87	0.71	0.56	0.43	0.34	0.28
180	0.85	0.68	0.52	0.40	0.32	0.27

Table 3.2 Relative diffuse irradiance of tilted planes for $z = 45^{\circ}$.

α°	15	30	45	60	75	90
ψ°	$D(\alpha, \psi)/D$					
0	1.16	1.25	1.28	1.23	1.12	0.94
30	1.13	1.21	1.22	1.16	1.04	0.86
60	1.07	1.09	1.05	0.96	0.83	0.66
90	0.98	0.93	0.84	0.72	0.58	0.44
120	0.90	0.78	0.65	0.52	0.41	0.32
150	0.84	0.68	0.54	0.42	0.34	0.27
180	0.82	0.64	0.50	0.40	0.32	0.26

Table 3.3 Relative diffuse irradiance of tilted planes for $z = 55^{\circ}$.

α°	15	30	45	60	75	90
ψ°	$D(\alpha, \psi)/D$					
0	1.20	1.33	1.40	1.39	1.29	1.12
30	1.17	1.28	1.32	1.29	1.19	1.02
60	1.09	1.13	1.11	1.04	0.92	0.76
90	0.98	0.93	0.85	0.74	0.61	0.48
120	0.88	0.76	0.63	0.52	0.42	0.34
150	0.81	0.65	0.52	0.43	0.36	0.29
180	0.79	0.61	0.49	0.41	0.35	0.28

Table 3.4 Relative diffuse irradiance of tilted planes for $z = 65^{\circ}$.

α°	15	30	45	60	75	90
ψ°	$D(\alpha, \psi)/D$					
0	1.26	1.46	1.58	1.60	1.54	1.38
30	1.22	1.39	1.48	1.48	1.40	1.24
60	1.12	1.19	1.21	1.17	1.06	0.90
90	0.99	0.95	0.88	0 78	0.66	0.53
120	0.86	0.74	0.63	0.53	0.45	0.37
150	0.78	0.62	0.52	0.45	0.39	0.32
180	0.75	0.58	0.49	0.43	0.38	0.31

fitting procedure which minimised the sum of squares of absolute rather than relative differences. There were slight differences in the coefficients and in the accuracy of fit to the radiance distribution at different points in the sky. The integrated values were also slightly different but these differences were typically 1% of $D(\alpha , \psi)$. The maximum disparity, about 2%, occurred on planes facing away from the sun and at the largest solar zenith angle, 65^{o}. The values in Tables 3.1 to 3.4 are calculated from the approximations of N with the minimum relative error.

There is also some uncertainty due to the departure of the horizontal integrations from unity. If this departure is due to an isotropic error function, i.e. one that is proportionally the same in all directions, then all the planar integrations are affected equally and the renormalisation makes an exact correction. The accuracy of the integrated values may then be estimated as $\pm$ 2% from the comparison of the two approximations of N. The error however need not be isotropic and the renormalisation may introduce a systematic error. This error will be a minimum on gradual slopes since $D(\alpha , \psi)$ must be 1 when $\alpha = 0$. If the renormalisation were not made the integrated values would differ from those tabulated by up to 7.4% in the case where $z = 65^{o}$ and when added to the other estimates of error this gives an overall estimate of 10% in the worst possible case. In the 35^{o}, 45^{o} and 55^{o} ranges of z the estimatesof worst possible error are only 4%, 7% and 3% respectively. Any remaining uncertainty is due to uncertainties in the angular distribution of radiance.

3.2 Comparison with other studies

Several authors have published values for the irradiance of vertical or sloping surfaces below cloudless skies. Dogniaux (1975) derived the diffuse irradiance of vertical surfaces D(90) by integrations of Eq. 2.4. Parmalee (1954) and Valko (1975) measured the diffuse irradiance of vertical surfaces directly, but included a component of reflected radiation from the ground. All three studies provided auxiliary data on the direct and diffuse components of horizontal irradiance as functions of turbidity, τ . In order to make a comparison with the present results, values of vertical irradiance were selected where the corresponding value of beam irradiance at normal incidence, I was equal to the mean from the present set of measurements; consequently the values of τ should roughly correspond. With the results of Parmalee and Valko the reflected component was subtracted from the diffuse irradiance, using data provided by the authors. The values of D(90) were normalised with respect to D and the resulting values of D(90)/D were plotted as a function of ψ (Figs. 3.2 and 3.3).

With $z = 35^{\circ}$ the present results agree well with those of Valko when ψ is close to 0° or 180°, but they tend to be lower for ψ between 40° and 140°. The results of Dogniaux agree well with the present results when ψ is small but tend to be larger as ψ approaches 180°. The values from Parmalee are consistently lower than the others. With $z = 55^{\circ}$ the disparities between the present work and Valko's results are greater but the same general relationships hold, both here and with $z = 45^{\circ}$ and 65° which are not shown.

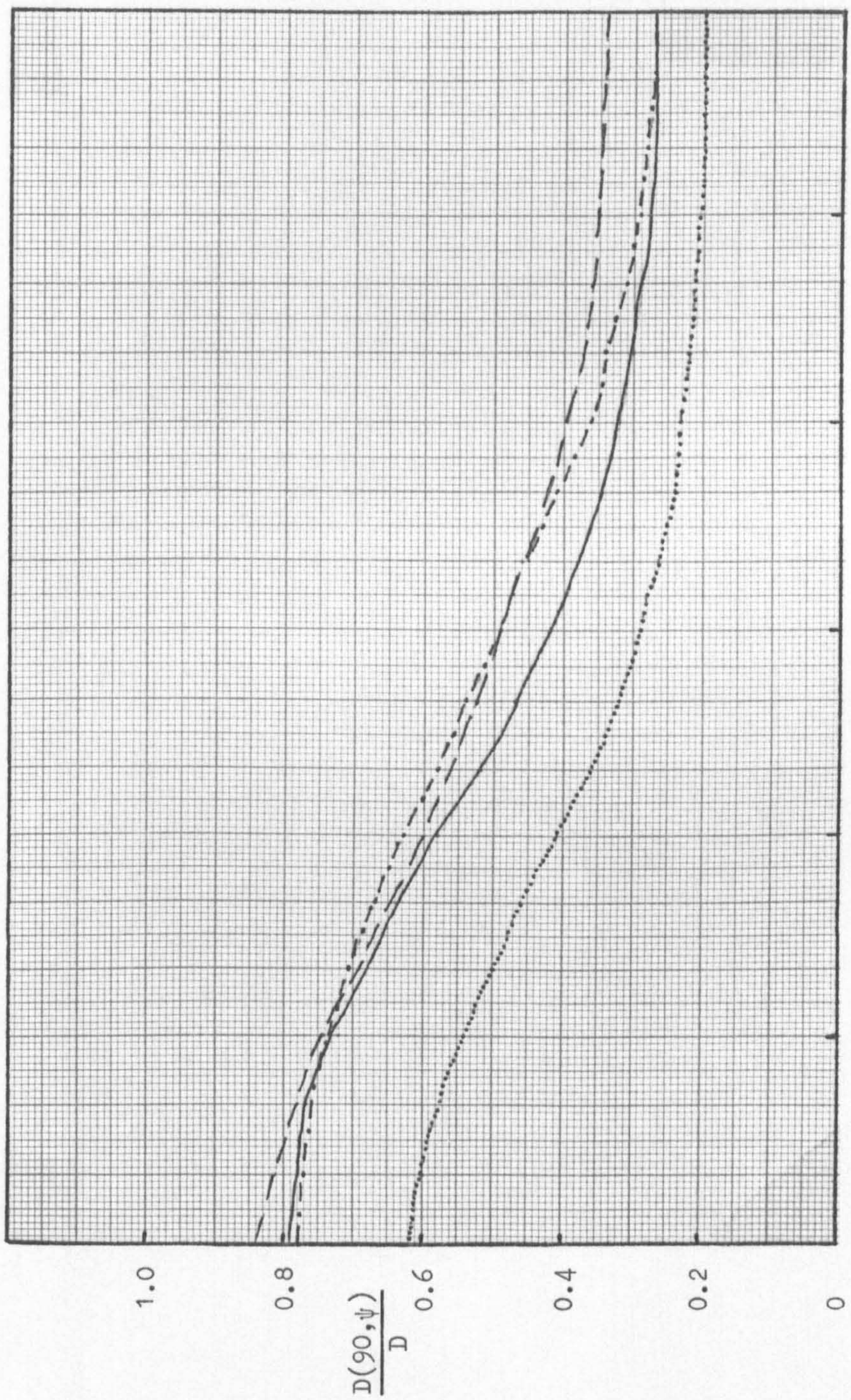

Fig. 3.2 Comparison of the diffuse irradiance of vertical surfaces under clear skies for $z = 35^{o}$, according to various authors.

—— Steven —·—·— Valko – – – – Dogniaux ..... Parmalee

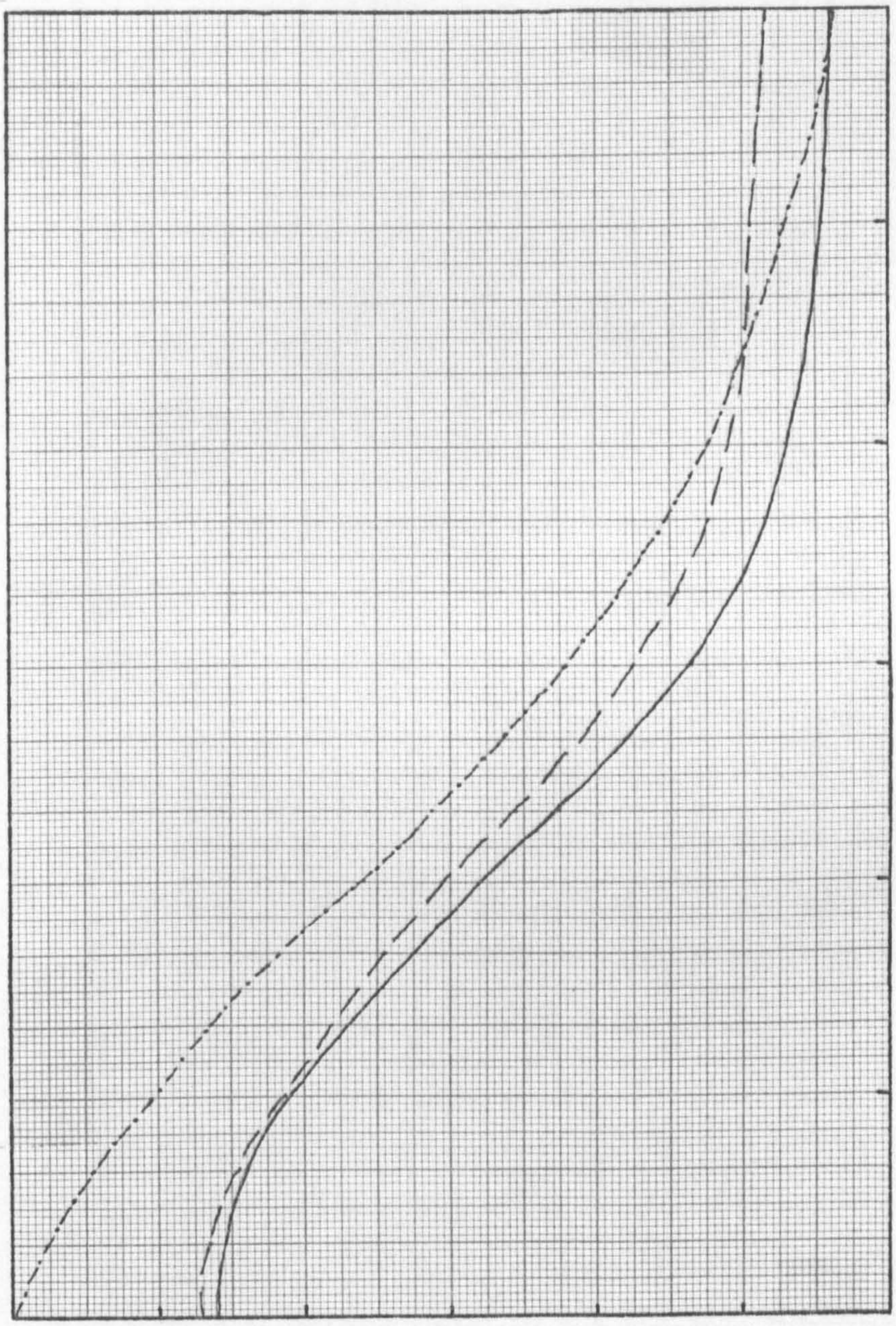

Fig. 3.3 Comparison of the diffuse irradiance of vertical surfaces under clear skies for $z = 55^{o}$, according to various authors.

Valko also made measurements at other turbidities and some of the results at higher turbidity match up more closely with the present work as shown in Fig. 3.4, although the discrepancy at angles between 40^{o} and 140^{o} is still evident. The relative irradiance values derived from Valko's measurements however appear to have an irregular relationship with turbidity.

Kondratyev and Fedorova (1976) tabulated measurements of the diffuse irradiance of slopes of different tilt and azimuth, made on a number of occasions. Their data for $z = 42^{o}$ when τ was about 0.25, are compared in Fig. 3.5 with linear interpolations of the integrated values from Tables 3.1 and 3.2. The figure shows that Kondratyev and Fedorova's slope irradiance values are on average 11% less than the integrated values.

There are several factors which could explain the differences between the results of different workers :

(i) The present results are based on radiance distributions that have been averaged over a range of turbidities, whereas the irradiance values of other workers are based on a smaller number of measurements at particular turbidities. With Kondratyev and Fedorova's results the turbidity was lower than the mean of the present measurements. With the other results used for comparison the beam irradiance at normal incidence was chosen to agree. Since I is not a linear function of τ however, the turbidity corresponding to the mean value of I is not the same as the mean turbidity and hence the irradiance figures selected for comparison may be inappropriate.

(ii) If the diffuse radiance at a point in the sky is a non-linear function of turbidity there may be a bias introduced into the mean

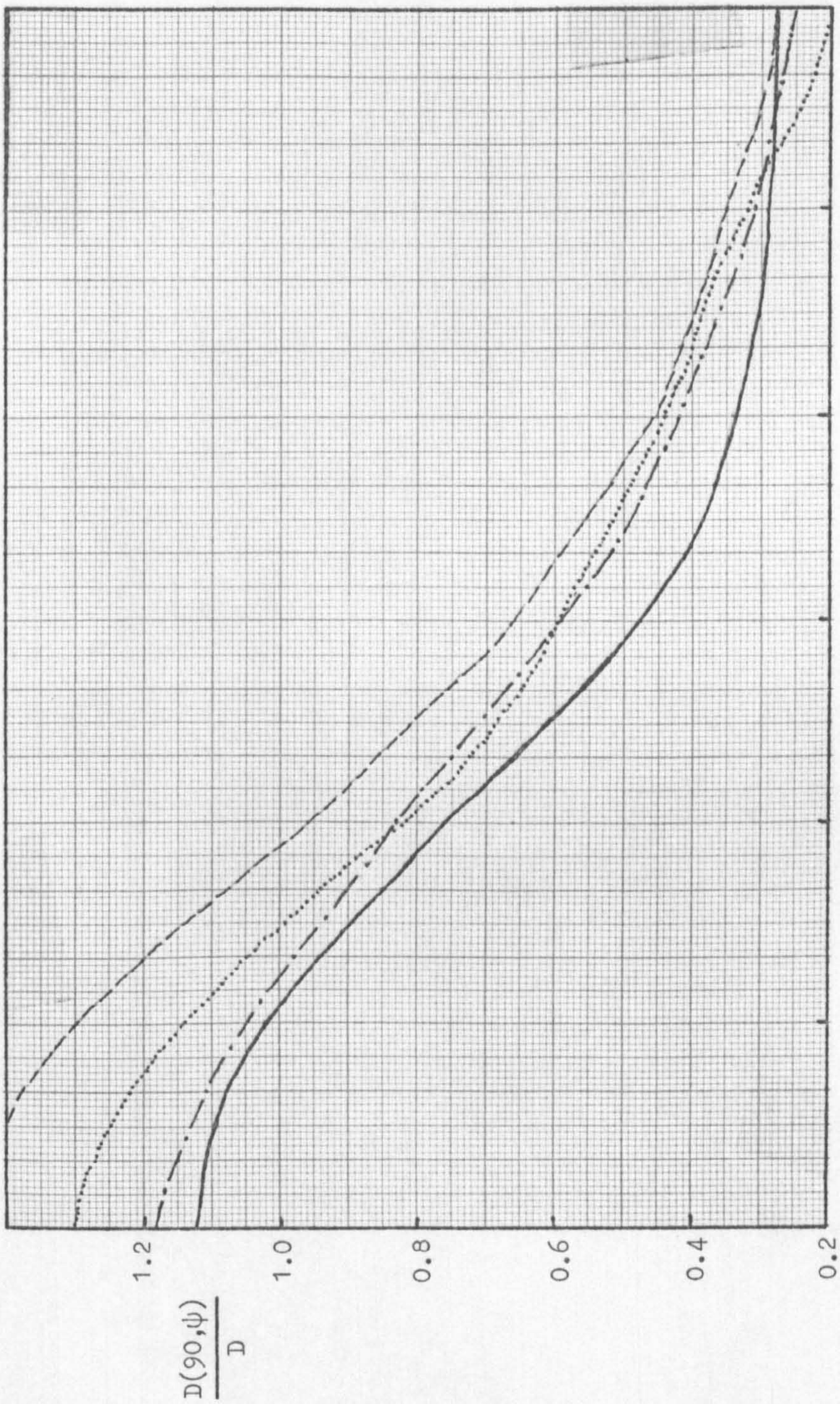
$\frac{D(90,\psi)}{D}$
1.2
1.0
0.8
0.6
0.4
0.2
0
30
60
90
120
150
180
ψ
Comparison of the diffuse irradiance on vertical surfaces under clear skies for z = 55°.
..... τ = 0.1 Valko
– – – – τ = 0.25
—·— τ = 0.45
——— Steven

Fig. 3.4

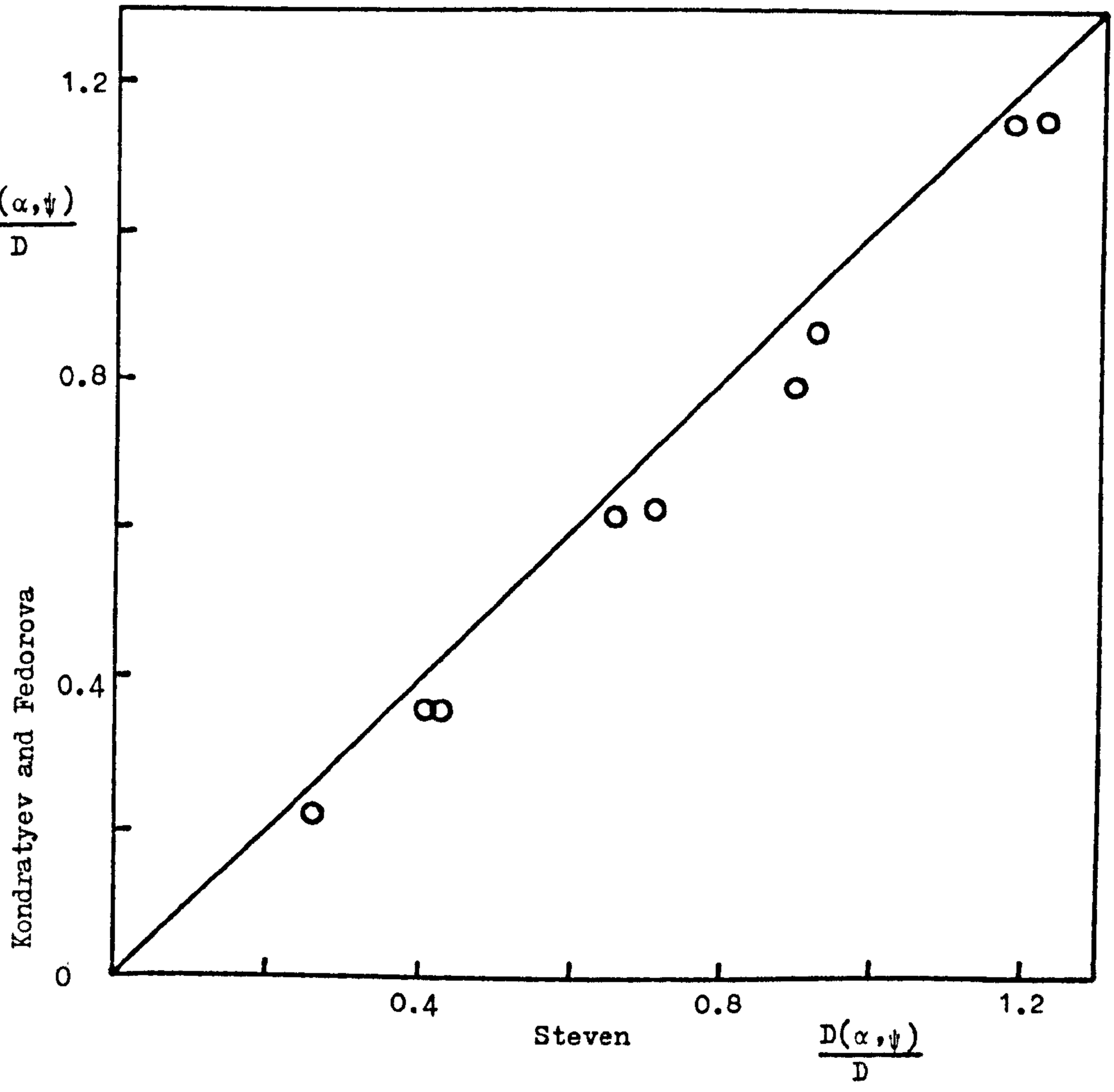

Fig. 3.5 Comparison of the diffuse irradiance of slopes under clear skies.

distribution which could affect integrated irradiance values. The error here should be small however as the coefficient of variation of N/D values was only about 10% due to all causes.

(iii) In order to compare D(90) values from Parmalee and Valko, a component of ground reflected radiation had to be subtracted using the isotropic assumption. Any small errors in the values may be magnified in this process. It is also very likely that the ground reflection was not isotropic. Since reflected radiation from the ground can be a very large component of slope irradiance, particularly on vertical surfaces at low turbidities, the errors introduced may have been quite large. This could explain the curious relationship with ψ and τ of the D(90)/D curves derived from Valko's data as shown in Fig. 3.4.

(iv) Scattering regimes may be different in the different parts of the world where measurements were taken, even at similar turbidities, due to differences in the aerosol size distribution. This explanation seems unlikely however as summer turbidities in Britain are typical of continental aerosol (McCartney, 1975) and in any case such an effect should be small.

(v) There is uncertainty in the radiance function used. The departures of the fitted functions from the measurement data were examined closely and were not found to be systematic. No measurements however were taken at angles θ greater than 75° and the fitted functions were extrapolated there. While this region does not affect horizontal irradiance very much, it has its maximum effect on vertical surfaces. This could be the explanation for the disparity in the irradiance figures for ψ between 40° and 140°.

(vi) Diffuse radiation measurements by different authors may include different amounts of circumsolar radiation owing to the different shade rings and corrections used. This problem is considered in Section 3.3.

3.3 Shade Ring Corrections

Routine measurements of diffuse radiation D on a horizontal surface are usually made with a pyranometer which is shielded from direct radiation by a shade ring. The shade ring obscures the entire diurnal path of the sun and is adjusted every few days for changes in solar declination. Since the ring also intercepts a part D^* of D, the measurements are multiplied by a correction factor K (Blackwell, 1954; Drummond, 1956) where $K = D/\{D - D^*\}$. Knowledge of the angular distribution of diffuse radiation for anisotropic skies enables D^* to be calculated and thus values of K can be determined.

Drummond expressed the correction factor K as the product of a geometric correction g and an anisotropy correction h where $g = D/\{D - D_o^*\}$ and h was determined empirically. D_o^* is the irradiance that would be intercepted by the ring if the sky were isotropic, and in such conditions g is the only correction required. Since $K = gh$, h is given by $\{D - D_o^*\}/\{D - D^*\}$. It can be shown by algebraic manipulation that the shade ring corrections can be written as

$$g = 1/\{1 - f\} \qquad \text{where } f = D_o^*/D \qquad 3.2$$

and

$$h = \{1 - f\}/\{1 - q\,f\} \qquad 3.3$$

where $q = D^*/D_o^*$. The ratio f is simply the horizontal view factor of the shade ring, calculated from $\iint \sin\theta \cos\theta \, d\theta \, d\phi$, where the double integral is performed over the area of the shade ring. The

factor q is the ratio of the irradiance of a horizontal surface from the obscured section of sky to the corresponding irradiance from an isotropic sky. An advantage of this formulation is that q is largely independent of shade ring width.

When the radiance distribution $N(\theta,\phi)$ is known, D* may be calculated from Eq. 3.1 where $\vec{A}.d\vec{\Omega}$ for a horizontal surface is $\sin\theta \cos\theta \, d\theta \, d\phi$, and the limits of integration are defined by the angular extent of the shade ring. With the Drummond design of shade ring, as used in most parts of the world, the surface integral may be approximated by a line integral along the sun's path (Drummond, 1956), thus

$$D^* = \frac{b}{r} \cos^3\delta \int_{-t_o}^{t_o} N(\theta(t), \phi(t)) \{\sin L \sin \delta + \cos L \cos\delta \cos t\} \, dt \qquad 3.4$$

in which b = ring width, r = ring radius, t_o = hour angle of sunset from solar noon, δ = solar declination and L = latitude. The parameter t is used here as a dummy variable, the sun's angular position being fixed. Schmid (1976) used Eq. 3.4 to calculate shade ring corrections with theoretical distributions of N. For the particular case of the isotropic sky, Drummond (1956) integrated Eq. 3.4 analytically to derive

$$f = \frac{2b}{\pi r} \cos^3\delta \{\sin L \sin \delta \, t_o + \cos L \cos \delta \sin t_o\} \qquad 3.5$$

Schmid however, pointed out that the line integral approximation is only valid when $b/r < 0.2$ and when the sensing element is small compared to b. For $b/r > 0.2$, Eq. 3.1 must be applied.

The radiance distribution functions of Chapter II were integrated numerically using the NAG (1975) FORTRAN routines D01DAF to perform the two dimensional integration (Eq. 3.1) and D01AGF to evaluate the one dimensional approximation (Eq. 3.4). Results of the two dimensional integration are shown in Table 3.5 for the 15th day of each month. The data are for Sutton Bonington: $\lambda = 52.7^{\circ}$ N; b/r = 0.2. Figure 3.6 compares the two methods of integration for an isotropic sky and shows that Eq. 3.4 is inaccurate in the summer, even for the geometric correction alone.

Measurements of the direct beam at normal incidence I , always include a component of circumsolar diffuse radiation, and for all practical purposes this radiation should be treated geometrically as part of I although to be rigorous, it is scattered radiation. The shade ring integrations for Sutton Bonington were therefore repeated with a 10 degree diameter zone around the sun excluded, and the resulting values of h are shown in Table 3.6. These 'practical' shade ring corrections are considerably lower than the values in Table 3.5 and their magnitudes are more in accord with the empirical estimations of Drummond (1956) and Schmid (1976). Schmid (1976) adopted a similar procedure using a zone of diameter 6 degrees but I have chosen 10 degrees because this corresponds closely with the angular width of the shade ring used at Sutton Bonington.

Shade ring corrections with the circumsolar radiation excluded were also performed using the one dimensional approximation (Eq. 3.4) to evaluate q for different dates and latitudes. The results are tabulated in Appendix B and can be used to calculate corrections for narrow shade rings (b/r < 0.2) using Eqs. 3.3 and 3.5.

Table 3.5 Shade ring correction factors for Sutton Bonington, including circumsolar radiation.

z^o		65	55	45	35
Date	g	h	h	h	h
15/1	1.02				
15/2	1.04				
15/3	1.07	1.12			
15/4	1.09	1.09	1.09	1.07	
15/5	1.09	1.08	1.07	1.06	1.06
15/6	1.09	1.08	1.07	1.05	1.05
15/7	1.09	1.08	1.07	1.05	1.05
15/8	1.09	1.09	1.08	1.06	
15/9	1.08	1.11	1.10		
15/10	1.05	1.13			
15/11	1.03				
15/12	1.02				

Table 3.6 Shade ring anisotropy correction for Sutton Bonington, excluding circumsolar radiation.

z^o	65	55	45	35
Date		h		
15/3	1.07			
15/4	1.06	1.05	1.05	
15/5	1.05	1.04	1.03	1.04
15/6	1.04	1.04	1.03	1.03
15/7	1.04	1.04	1.03	1.03
15/8	1.05	1.05	1.04	
15/9	1.06	1.06		
15/10	1.09			

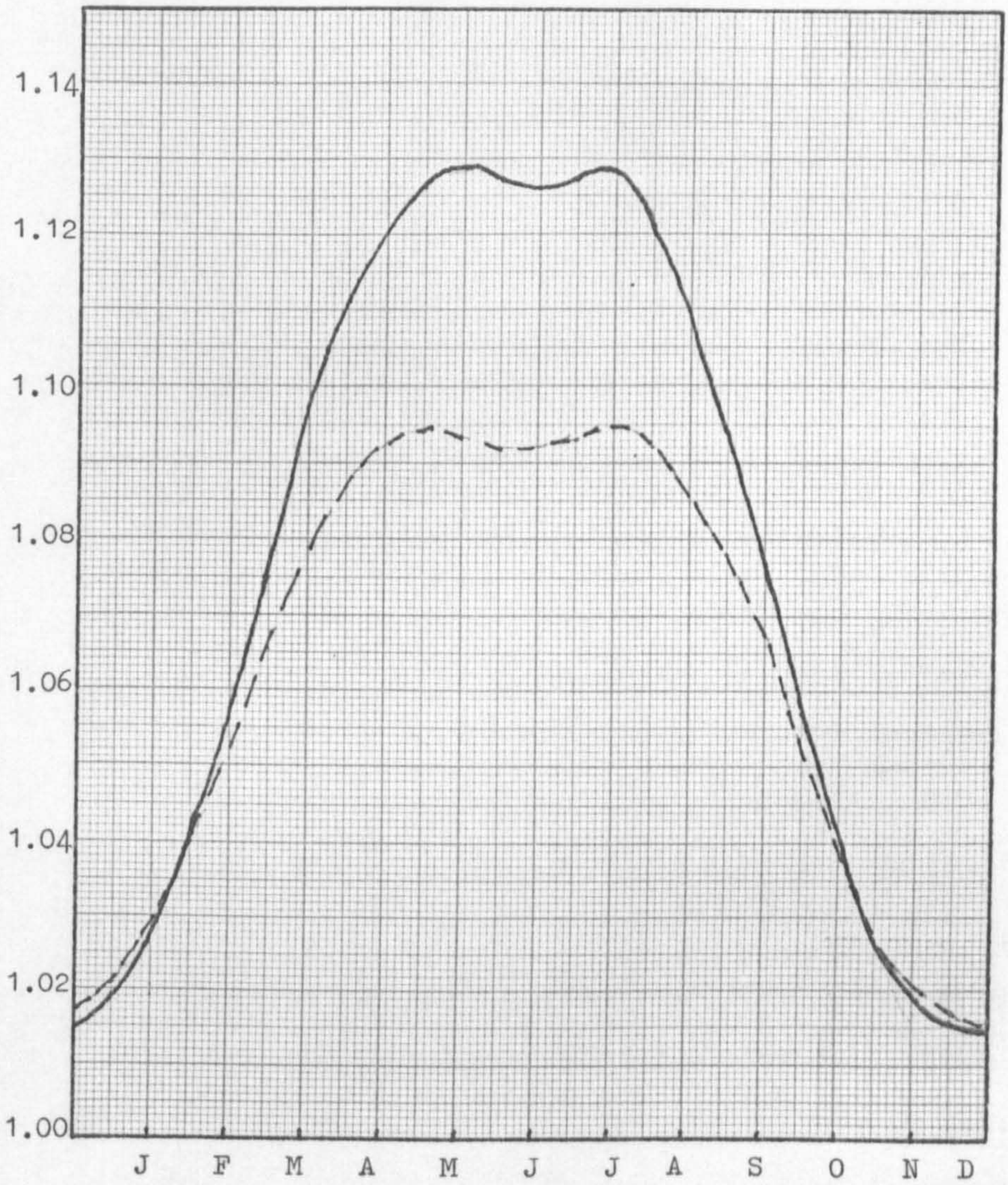

Fig. 3.6 Monthly variation of the geometric shade ring correction at Sutton Bonington.

——— Drummond approximation (Eq. 3.5)

– – – – by 2 dimensional integration (Eq. 3.1)

The present results show that the correction for the anisotropy of cloudless skies varies both seasonally and diurnally, although the diurnal variation is rarely more than 1% and can safely be ignored. The total correction K is less seasonally variable than either g or h , which vary in opposite directions. The seasonal variation in h was attributed by Drummond (1956) to changes in turbidity. Equation 3.3 however shows that h depends on f and q , both of which vary seasonally for geometrical reasons. Turbidity may indeed influence the results, but it is more likely to affect the values of Table 3.5 where the circumsolar radiation is included, than the 'practical' correction values of Table 3.6.

The procedure currently employed at Sutton Bonington to correct the diffuse radiation measured under cloudless skies uses the Drummond formula (Eq. 3.5) to calculate g and a value of 1.07 for h . This gives a value of K at midsummer of about 1.20 whereas according to the present results (Fig. 3.6 and Table 3.6), a better value is 1.13 . Thus when D is taken to exclude the circumsolar radiation from a zone of diameter 10^{o}, the standard procedure at Sutton Bonington will over-estimate D by as much as 7%, the error being contributed equally by g and h . Values of D at Sutton Bonington were measured by Unsworth (private communication) on a clear day in June 1971, using a shade ring and a shading disc of angular diameter 10^{o}. Values of K ranged from 1.12 to 1.16 which are very close to the present results.

3.4 Modelling of Diffuse Radiation from Cloudless Skies

Many attempts have been made to model the effect of cloudless sky anisotropy on the diffuse irradiance of slopes. Fitted functions that

approximate the radiance distribution can be integrated as in Section 3.1, but for many purposes this procedure is too complex. Loudon (1965) and Robinson (1966) noted that much of the clear sky diffuse radiation comes from a narrow region close to the sun and so they attempted to treat the diffuse radiation as the sum of a background isotropic component D' and a circumsolar component D_c which is treated geometrically as if it came from the sun. The diffuse irradiance of a tilted plane is then

$$D(\alpha,\psi) = D_c \cos \eta/\cos z + D' \left\{1 + \cos \alpha\right\}/2 \qquad 3.6$$

where η is the angle between the sun and the normal to the slope. The first term in Eq. 3.6 drops out when $\eta > 90^\circ$. Robinson suggested that D_c could be expressed as sD with $s = 0.25$. Loudon on the other hand claimed that the background diffuse radiation D', was virtually independent of turbidity and could be treated simply as a function of z. The sum $B + D_c$ is equal to $G - D'$ and measurements of D are in theory, unnecessary. His data show considerable scatter however in the determination of D', and as they are based on vertical irradiance measurements only, their applicability is limited.

Robinson's hypothesis was tested by substituting the integrated irradiance values (Tables 3.1 to 3.4) in Eq. 3.6 and using the function fitting routine E04GAF (NAG, 1975) to find the best value of s. The best value of s was about 0.5 but the fitted values were almost all lower than the integrated values, by as much as 30% in some cases. In order to improve the relationship the isotropic assumption for the background radiation was replaced by a form of the radiance distribution which was linear in $\cos \theta$,

$$N'(\theta) = \left\{\frac{1 + \beta \cos \theta}{1 + \beta}\right\} \quad N'(0) \qquad 3.7$$

The standard overcast sky (Eq. 1.7) has this distribution with $\beta = 2$.

Moon and Spencer (1942) showed that this distribution can be integrated analytically to give the diffuse irradiance of any tilted plane under a standard overcast sky. For the general case where β can take on any value the relative background diffuse irradiance is

$$D'(\alpha)/D = \{1 + \cos\alpha\}/2 + \frac{2\beta}{\pi[3 + 2\beta]}\{\sin\alpha - \alpha\cos\alpha - \pi[1 - \cos\alpha]/2\} \quad 3.8$$

When $\beta = 0$ this reduces the isotropic formula and when $\beta = 2$ it is identical with the standard overcast sky formula of Moon and Spencer.

When both s and β were allowed to vary in the function fitting routine the results improved considerably. The model was fitted to the irradiance data in two ways: in one, data from all solar zenith angles were taken together; in the other they were separated into four groups according to z. The results are summarised in Table 3.7, where the 90% confidence limits on the values of s and β are $\pm$ 0.02 and $\pm$ 0.07 respectively. The errors in fitting were typically 0.06 of D but the differences between the fitted and the integrated values were systematic, the largest values occurring on planes facing away from the sun. This disagreement is inevitable because the model allows no azimuthal dependence of irradiance for planes which are not exposed to direct radiation, whereas in reality the azimuthal dependence is quite marked, see Figs 3.2 and 3.3 and Tables 3.1 to 3.4. When the data were treated in four separate groups according to z rather than all together, the improvement in fitting accuracy was largely confined to planes facing towards the sun. For practical purposes a model with fixed s and β is more amenable and the accuracy of the model in which all solar zenith angles were taken together is considered sufficient for most purposes.

The integrated irradiance values on which this model is based were calculated from radiance distributions which cover the whole sky and hence include the circumsolar radiation. Standard measurements of D however are subject to shade ring corrections which usually exclude some of the circumsolar radiation and allot it to the direct beam component B. In using this model with measured values of D the circumsolar radiation must not be added to B twice, and s must be reduced to account for the circumsolar radiation already included in B. For Sutton Bonington this may be done by comparing the shade ring correction value K used to obtain D, with a value K^* based on Table 3.5, which accounts for the whole shade ring. The corrected value of s is then

$$s' = K^* s/K + 1 - K^*/K \qquad 3.9$$

For example if Table 3.6 were used to correct D, then $K^*/K \approx 1.03$ and $s' = 0.48$. In other places where different shade rings and different types of correction may be in use, it is necessary to ascertain what proportion of the diffuse radiation is included in measurements of the direct beam.

Table 3.7 Results of model of diffuse irradiance of slopes

z^o	s	β	Residual standard deviation	Maximum error
All z	0.51	- 0.87	0.06	0.16
35	0.63	- 1.04	0.04	0.08
45	0.60	- 1.00	0.04	0.10
55	0.53	- 0.90	0.05	0.11
65	0.46	- 0.85	0.06	0.13

IV. INSTRUMENTATION

4.1 Design Principles

The following factors have to be considered in the design of solar radiation instruments :

i) Linearity
ii) Spectral selectivity
iii) Zero drift and stability
iv) Sensitivity
v) Response to thermal radiation
vi) Temperature dependence of calibration
vii) Time dependence of calibration
viii) Angular response characteristics
ix) Dependence of calibration upon inclination
x) Time constant

In addition, instruments must be sufficiently robust for normal use. In the present study the instruments were for measuring the distribution of diffuse radiation and a narrow angle of view was required. The design is therefore comparable with that of the Linke-Feussner actinometer which was described in some detail by Kondratyev (1969). There are however significant differences in the purpose of the two instruments. The Linke-Feussner is mainly intended for measurements of the direct solar beam, although diffuse solar and thermal radiation are also sometimes measured. In particular it is designed for manual operation. The new instrument was required only to measure diffuse solar radiation and to be operated unattended, recording automatically on a data-logger every few minutes. Consequently, critical factors were sensitivity and zero drift as well as weather proofing.

To meet these criteria as closely as possible it was decided to build an instrument with a thermopile sensor. Although this gives a lower sensitivity than photoelectric or photographic methods, it has the advantages of being relatively free from spectral selectivity and of having a very linear response.

The zero drift of a thermopile instrument is partly due to long wave radiative exchanges between the thermopile junctions and the body of the instrument. As the temperature of the instrument changes with the environment, the junctions lag behind because they are thermally insulated from the body of the instrument. Long wave radiative exchanges result in a zero offset if the hot and cold junctions are exposed to different thermal environments. This effect is quite noticeable in the Moll thermopile (Moll, 1923) as used in the Linke-Feussner instrument, where the cold junctions are in good thermal contact with the instrument and the hot junctions are suspended in air. The zero offset of the Linke-Feussner actinometer may be measured by blocking the aperture, and at times a zero signal as large as 20 μV may occur. Typical signals when measuring diffuse radiation are 50 μV in the Linke-Feussner and 100 μV in the new instrument. It is impractical to monitor the zero offset of an automatic instrument and therefore particular attention must be paid to minimising its drift. The thermopile of the new instrument had both sets of junctions on the upper surface with equal amounts of thermal insulation. Thus both sets of junctions should be in the same radiative and thermal environment.

4.2 The Thermopile Sensor

The thermopile consisted of 100 to 120 pairs of copper-constantan

junctions produced by winding a constantan wire around a Tufnol former and electroplating selected areas with copper. The specifications of the thermopile and details of the construction are given in Appendix C. The form of the thermopile is shown in Fig. 4.1. Both the hot and the cold junctions are on the upper surface of the thermopile, the hot junctions under black paint and the cold junctions under white. The paints were chosen for their optical and thermal properties (Appendix C) and they also had a good reputation for weathering so the instrument calibration should not change much with time. The arrangement of the hot and cold junctions is in the form of a 2 by 2 chequer board to reduce the azimuthal dependence of the sensor. Apart from the geometrical arrangement, this design of thermopile is similar to the thermopile described by Monteith (1959).

The linearity of response to solar radiation depends on the variation of thermoelectric potentials with temperature and on how the absorbed radiative energy is dissipated. Over the temperature range -20 to +50°C, the thermoelectric potential of copper-constantan thermocouples is effectively a linear function of temperature difference, the departure from linearity being less than 0.15% (Ebert, 1967). Studies by Anderson (1967) have shown that the heat transfer coefficients are a much more serious source of non-linearity in thermopile instruments. Heat is dissipated from the thermopile by conduction, both through the former and along the plated wires, by long wave radiative exchange and by convection. The conduction terms are strictly proportional to the temperature difference δT . The long wave radiative exchange between two black bodies at temperatures T_1 and T is $\sigma \{T_1^4 - T^4\}$ where σ is the Stefan-Boltzmann constant (5.67×10^{-8} W m^{-2} K^{-4}). When the

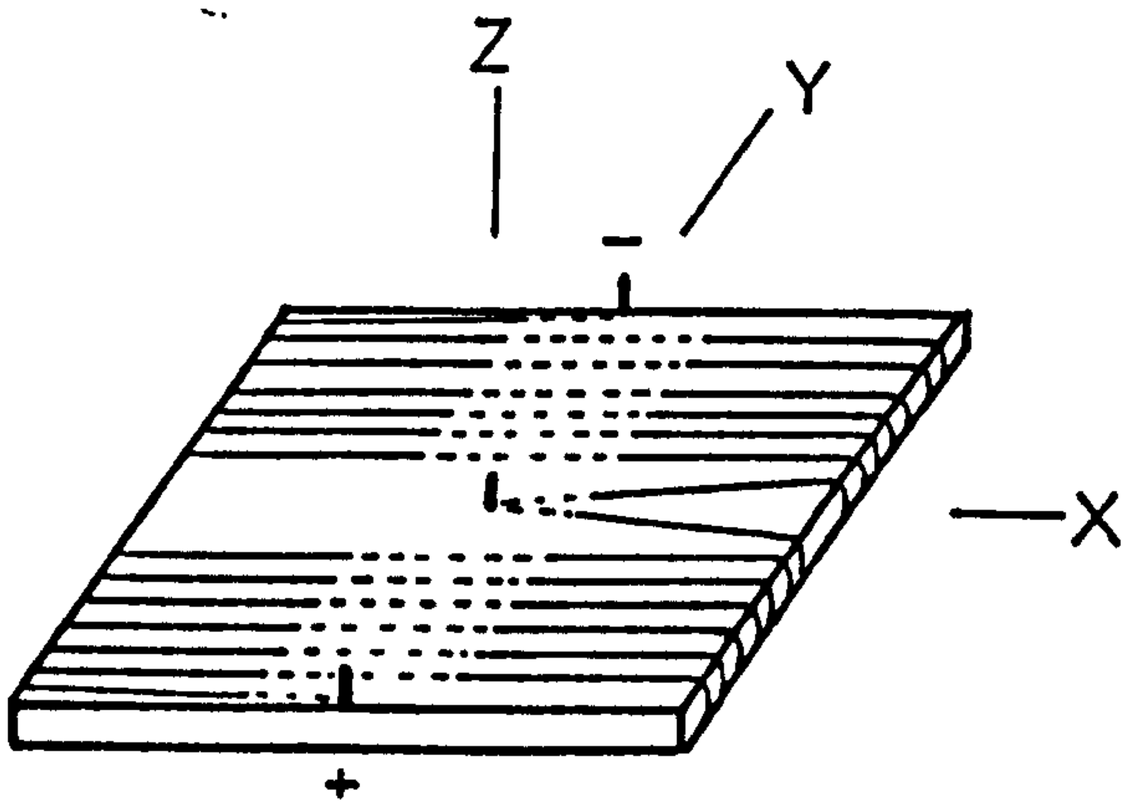

(a)

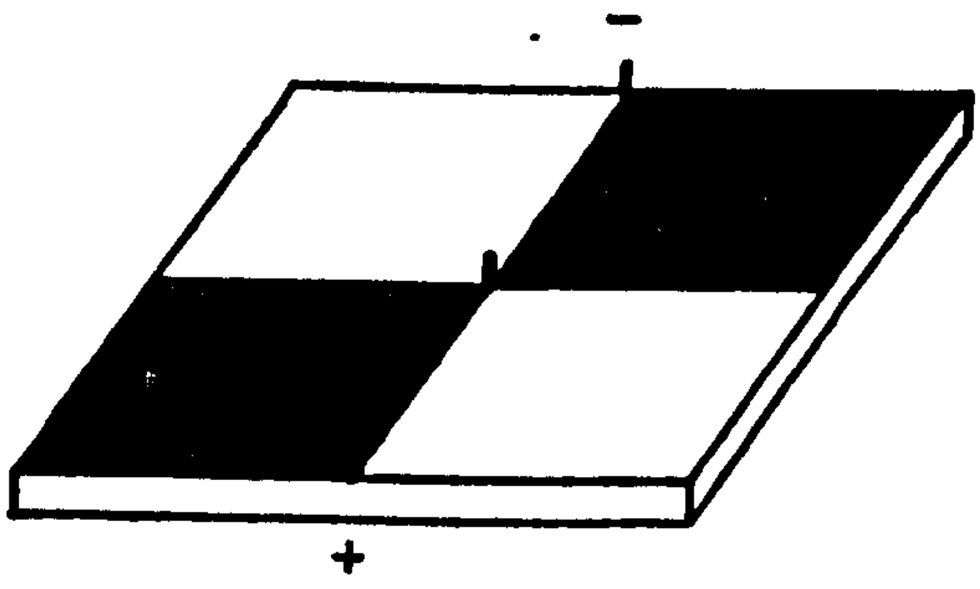

(b)

Fig. 4.1 The thermopile sensor.
(a) The constantan windings : dashed lines - bare constantan; solid lines - constantan with copper plating.
(b) The completed thermopile with black and white painted surface.

temperature difference δT is small, the exchange can be approximated by $4\sigma T^3 \delta T$ and hence this term is also nearly linear in δT. The convective heat loss is proportional to Nu δT where Nu is the Nusselt number. For free convection Nu is proportional to $\delta T^{0.25}$. However the convective term is small compared to the others. For a temperature difference of 0.05°C, typical of the thermopile under diffuse radiation, a preliminary analysis based on data in Appendix C gave the partition of heat loss shown in Table 4.1.

Table 4.1 Dissipation of heat in the thermopile

Conduction through Tufnol	60 $W m^{-2} K^{-1}$
Conduction along wires	< 6 $W m^{-2} K^{-1}$
Long wave exchange	6 $W m^{-2} K^{-1}$
Convection	2 $W m^{-2} K^{-1}$

Table 4.1 indicates that conduction through the Tufnol is the dominant term in the heat transfer and non-linearity of the thermopile response should therefore be a minimum. The temperature dependence of the calibration factor is $-0.2\% K^{-1}$ in the Linke Feussner actinometer (manufacturer's data) and is of a similar magnitude in other thermopile instruments (Anderson, 1967; Fuquay and Buettner, 1957). Since the temperature dependence of the transfer coefficient for conduction is much less than for convection and long wave radiation (Monteith, 1959), the calibration factor of the new instrument should have a relatively weak dependence on temperature.

In instruments which are not mounted horizontally the dependence of calibration on the tilt of the instrument is an important factor.

In the Eppley pyrheliometer the change in calibration with tilt can be more than 5% (Fuquay and Buettner, 1957). However, the only heat transfer term that depends on gravity is convection. Convection is of minor importance in the new instrument, and therefore the tilt of the instrument should not present a problem.

The thermopile has a relatively long time constant - about one minute to equilibrium - due to the low thermal diffusivity of the Tufnol former. This helps to filter out short term instability of the signal, and by effectively integrating over a period of time helps to reduce some of the scatter inherent in spot readings.

4.3 Energy Budget of a Monteith-type Thermopile

The design criteria in constructing a thermopile of the Monteith type, can best be examined by considering the energy budget. Consider an element of the thermopile surface (Fig. 4.2). The element is symmetric about one of the wires and has length δx in the direction of winding, width δy and sufficient depth to include both wire and paint. The origin of the x axis is at the junction of the black and white surfaces with the black surface in the positive direction. The net radiation balance $R_n(x)$ of the element is given by

$$R_n(x) = \left\{\gamma S + \varepsilon \sigma \left[T_i^4 - T(x)^4\right]\right\} \delta x \, \delta y \qquad 4.1$$

where γ is the surface absorptivity, ε the infra-red emissivity, S the incident solar radiation, T_i the radiative temperature of the instrument and $T(x)$ the mean surface temperature of the element. The net radiation balance is dissipated by convection, conduction through the Tufnol former and conduction down the wires, hence

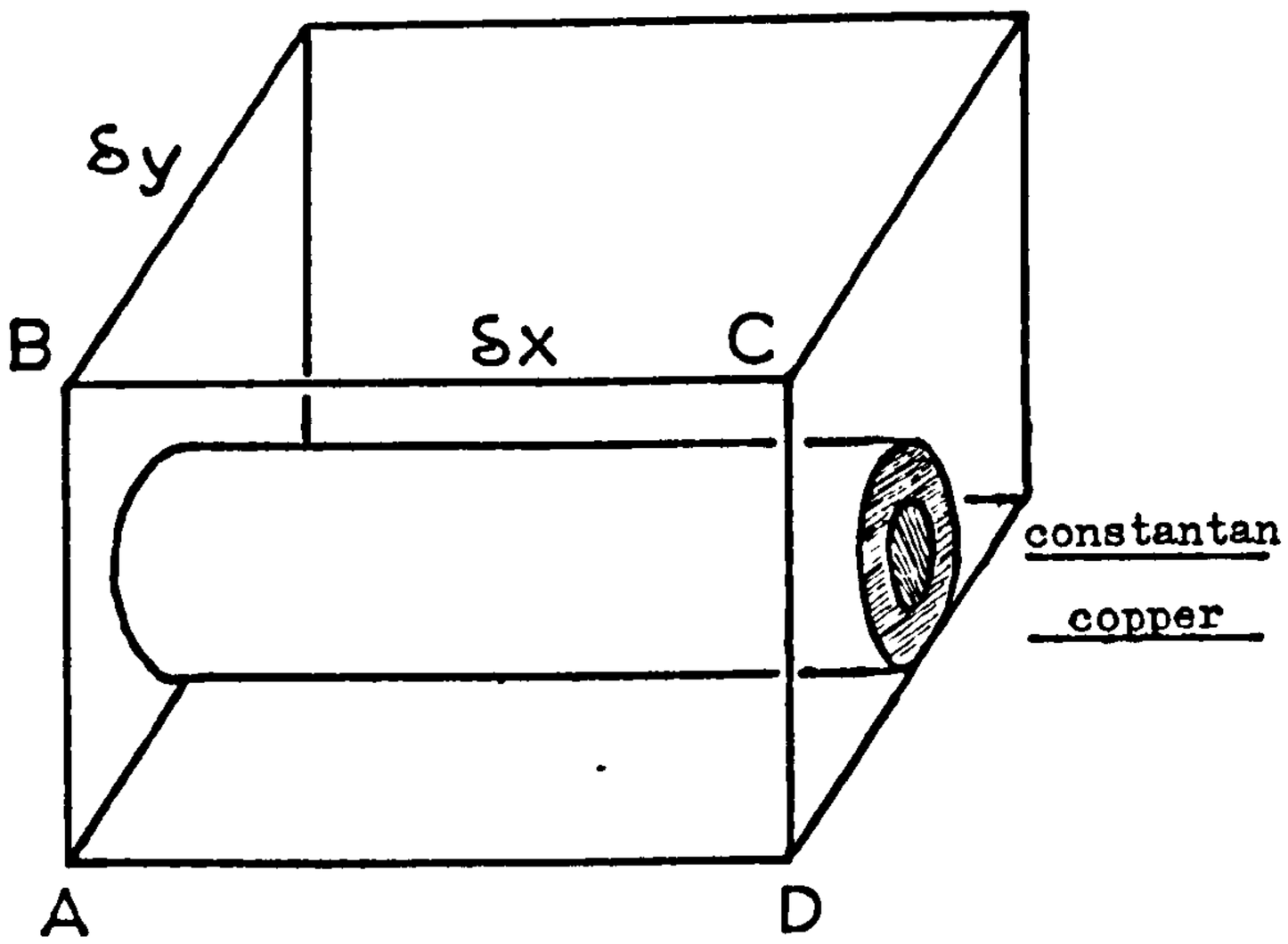

Fig. 4.2 An element of the thermopile surface.

$$R_n(x) = \frac{Nu\ k_4}{l} \{T(x) - T_a\}\ \delta x\ \delta y + \frac{k_1}{d} \{T(x) - T_b\}\ \delta x\ \delta y$$
$$- \delta x \frac{d^2}{dx^2} T(x) \{k_2 A_2 + k_3 A_3\} \qquad 4.2$$

where T_a and T_b are the temperatures of the air and of the instrument base; l is the characteristic dimension for convection and d is the thickness of the Tufnol. The terms k are thermal conductivities and the terms A are cross sectional areas, where the suffices refer to : 1 - Tufnol, 2 - constantan, 3 - copper and 4 - air.

The output of the thermopile depends on the difference in the radiation balance of the black and white surfaces. Thus writing a similar equation to 4.2 for the corresponding white element at $-x$ and subtracting gives

$$\{\gamma_n S - \sigma [T(x)^4 - T^4(-x)]\}\ \delta x\ \delta y =$$
$$\frac{Nu\ k_4}{l} \{T(x) - T(-x)\}\ \delta x\ \delta y + \frac{k_1}{d} \{T(x) - T(-x)\}\ \delta x\ \delta y \qquad 4.3$$
$$- \{k_2 A_2 + k_3 A_3\} \frac{d^2}{dx^2} (T(x) - T(-x)).\ \delta x$$

where γ_n is the difference in absorptivity between the two paints. All the temperatures except $T(x)$ and $T(-x)$ have disappeared. Denoting $T(x) - T(-x)$ by $\Delta(x)$ and assuming that Δ is small yields the approximate expression

$$\gamma_n S - \left\{4 \sigma T^3 + \frac{k_1}{d} + \frac{Nu\ k_4}{l}\right\} \Delta(x) + \left\{\frac{k_2 A_2 + k_3 A_3}{\delta y}\right\} \frac{d^2}{dx^2} \Delta(x) = 0 \qquad 4.4$$

Eq. 4.4 is an ordinary differential equation of the form

$$E - F \Delta + W \Delta'' = 0 \qquad 4.4(a)$$

A solution with the appropriate boundary conditions may be used to maximise instrument sensitivity in terms of the variables in the design.

To solve Eq. 4.4 it was necessary to assume that F is independent of Δ, an assumption that is justified in the present instrument because the conduction term k_1/d is dominant as shown in Table 4.1. A further implicit assumption is that the temperature does not vary in the y direction. The error introduced by this simplification depends on the value assigned to δy which may be interpreted as the width of surface over which the wires act as an effective heat sink. If the paint distributes heat uniformly in the y direction then δy is the average spacing of the wires. If the paint conducts heat very poorly then δy is not much larger than the diameter of the wires themselves. The truth probably lies somewhere between these extremes. It is also assumed that the wires alone conduct heat in the x direction as their conductivity is much larger than that of Tufnol or paint.

Subject to the limitations imposed by these assumptions, Eq. 4.4 has the general solution

$$\Delta(x) = E/F + g_1 \cosh \sqrt{F/W}\, x + g_2 \sinh \sqrt{F/W}\, x \qquad 4.5$$

where g_1 and g_2 are constants. Since the thermopile wires were plated with copper over only part of their length, the parameter W has two values and the solution must be found separately in the regions $0 \leqslant x \leqslant x_1$ where there is no copper and $x_1 \leqslant x \leqslant x_2$, where x_2 is the edge of the thermopile. The solutions are then matched at the thermojunction x_1. Denoting the regional solutions as Δ_1 and Δ_2 respectively, the boundary conditions are :

$\Delta_1(0) = 0$, since $\Delta_1(0) = T(0) - T(-0)$;

$\Delta_2(x_2) = 0$, since both ends of the thermopile are in good contact with the instrument base;

$\Delta_1(x_1) = \Delta_2(x_1)$ to match the solutions at the thermojunction;

$W_1 \Delta_1'(x_1) = W_2 \Delta_2'(x_1)$ to ensure that the heat conduction along the wires at x_1 is the same in both solutions. W_1 and W_2 are the values of W in the two regions.

Substitution of the boundary conditions into the general solution Eq. 4.5 gives equations for the relative temperature distribution over the thermopile. The particular solution required is the temperature difference δT at the junction. This is $\Delta(x_j)$ and is given by

$$\delta T = \frac{E}{F} \left\{ 1 - \frac{\sinh u_2[x_2 - x_1] + w \sinh u_1 x_1}{\cosh u_1 x_1 \sinh u_2[x_2 - x_1] + w \sinh u_1 x_1 \cosh u_2[x_2 - x_1]} \right\} \quad 4.6$$

where $w = \sqrt{W_2/W_1}$ and $u_i = \sqrt{F/W_i}$. Bener (1950) derived a similar expression for the Moll thermopile.

4.4 Sensitivity of the Thermopile

The voltage output V of the thermopile is proportional to the mean temperature difference between the junctions, thus

$$V = n_j \nu \delta T \quad 4.7$$

where n_j is the number of thermopile pairs and ν is the thermoelectric potential for the copper-constantan junctions. Denoting the term in curly brackets in Eq. 4.6 by χ , and rewriting $E = \gamma_n S$, Eq. 4.7 then becomes

$$V = n_j \nu \gamma_n S \chi / F \quad 4.8$$

and the sensitivity V/S of the instruments to solar radiation may be calculated from the design data.

The appropriate values for $F = 4\sigma T^3 + \frac{k_1}{d} + \frac{Nu\, k_4}{l}$ are given in Table 4.1. Hence $F = 68$ W m^{-2} K^{-1}. The value of γ_n was 0.77 from the manufacturers data (Appendix C) and n_j was usually 120. The thermoelectric potential of copper-constantan thermocouples over the temperature range 0 to 20°C is given as 38 μV C^{-1} by Ebert (1967) but when thermocouples are made by electroplating, the constantan core of the plated section of wire carries a reverse current which lowers the measured voltage, (Wilson and Epps, 1920). The reduction factor is the ratio of the resistance of the plated section of wire to the resistance of the copper sheath alone and therefore depends on the plating thickness. The relative cross sectional area of copper plating to constantan was typically 0.6 and ν must be reduced by a factor of 0.95 .

The value of χ is not easy to determine because u_1 and u_2 depend on δy which is not known. However, putting in a maximum value for δy of 0.25 mm (the spacing between windings) gives a value of χ of 0.985 . With a minimum value for δy of 0.05 mm (approximately the diameter of a plated wire), the value of χ obtained is 0.79 . The overall result is thus relatively insensitive to the value of δy and it is possible to use an approximate solution to improve the estimate of δy and to approach the solution by iteration. Assume that the temperature of the wire under the black paint is $T + E\chi/F$ and the temperature of a point in the paint well away from the wire is $T + E/F$. The mean of these two temperatures, $T + E\{1 + \chi\}/2F$ occurs somewhere in between. Assume that this occurs at a point on the side ABCD of the element of thermopile in Fig. 4.1, at a distance $\delta y/2$ from the wire.

Assume also that the heat conduction from this point is partitioned equally between conduction to the wire and conduction to the instrument base. The conduction to the wire is then

$$\frac{2k_5}{\delta y}\left\{\frac{E}{2F}[1+\chi] - \frac{E}{F}\chi\right\} = \frac{E}{F}\frac{k_5}{\delta y}\{1-\chi\}$$

where k_5 is the thermal conductivity of the paint. The conduction to the base is $\frac{E}{F}\frac{k_1}{d}\{1+\chi\}/2$. Setting these expressions equal gives

$$\delta y = 2\frac{k_5}{k_1}\left\{\frac{1-\chi}{1+\chi}\right\}d \qquad 4.9$$

Successive approximations to δy by resubstitition of δy from Eq. 4.9 into χ give an estimate of δy of 0.17 mm and the corresponding value of χ as 0.97. Although the assumptions used to obtain these figures were crude and the value of δy may be considerably in error, this will not seriously affect the value of χ.

Estimates of all the parameters of Eq. 4.8 are given in Table 4.2. Using these values the calculated sensitivity of the present design of thermopile is 50 $\mu V/W\ m^{-2}$.

Table 4.2 Thermopile design parameters for calculation of sensitivity (Eq. 4.8).

n_j	120
ν	36 $\mu V/W\ m^{-2}$
γ'	0.77
χ	0.97
F	68 $W\ m^{-2}\ K^{-1}$

To compare the theoretical sensitivity with measured sensitivities of the instruments it was necessary to increase the measured values by 17% to allow for the attenuation of S by two layers of glass. The sensitivities thus derived from the calibration data (Appendix E) lay between 20 and 30 $\mu V/W\ m^{-2}$. Although there are substantial uncertainties, perhaps up to 25% in F and 10% each in γ_n and χ in Eq. 4.8, and although in many of the thermopiles there were effectively fewer windings due to accidental crossing of wires, these factors are insufficient to account for the large difference between the theoretical and the measured values. A possible source of the discrepancy may be the value of ν. Copper plating has a fine crystalline structure as shown in Fig. 4.3, and due to the plating process the electrical properties may not be isotropic as in a sample of annealed metal. In addition the patchy quality of plating in evidence in many places may decrease the electrical conductivity of the plating. The leakage current through the constantan core would then be larger and a significant reduction of the e.m.f. could result.

The analysis of the thermopile energy budget and the approximate solution in Eq. 4.6 provide a useful insight into the working of the thermopile and the relative importance of many factors in the design. The fact that the value of χ is very close to 1 indicates that conduction down the wires is relatively unimportant and therefore that changes in, for example, plating thickness or x_1 and x_2 will have little effect on the sensitivity of the instrument. It is normally assumed that increasing the number of windings will increase the sensitivity in direct proportion. There is however a limit to this increase because the wires act as heat sinks over an area of painted

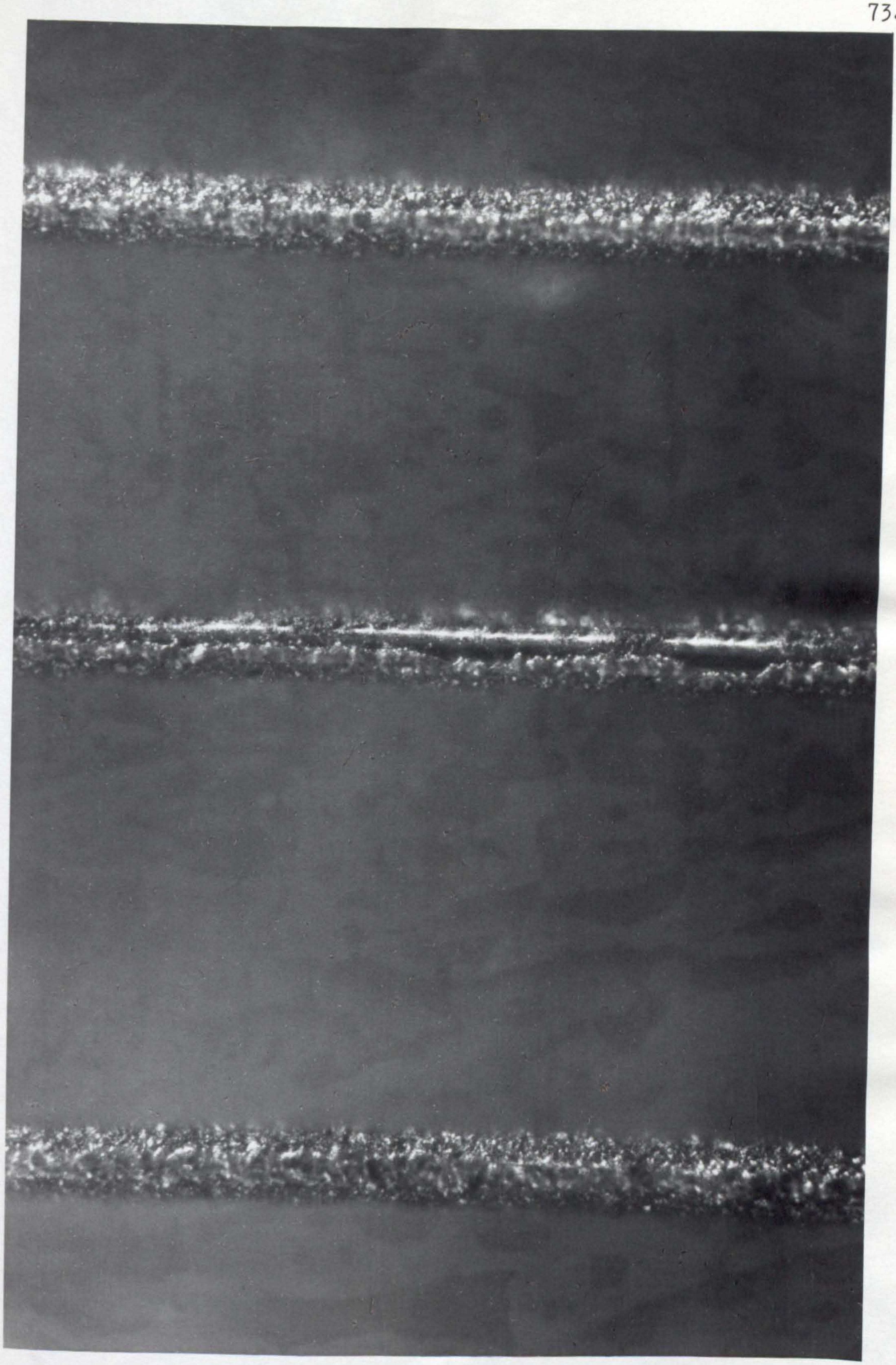

Fig. 4.3 Photomicrograph of copper plating on 50 swg constantan wire (X100 approx.).

surface. There would be little advantage in having a density of windings greater than $1/\delta y$, in this case 6 per mm. With a density of 4 per mm, the sensitivity of the present thermopile already approaches the point of diminishing returns. To provide absolute values of sensitivity however, a more rigorous analysis coupled with better knowledge of the physical properties of the thermopile seems necessary.

4.5 The Instrument Body

The thermopile is mounted on an aluminium base which screws into a 160 mm tube (Fig. D.1, Appendix D). Clear glass filters which are mounted on the base about 10 mm above the thermopile surface and at the upper end of the tube, shield the thermopile from external sources of thermal radiation. The outer glass filter also serves to keep rain out of the tube and to isolate the inner filter and the thermopile beneath from the external environment. The inner filter minimises effects of temperature differences between the top and the bottom of the tube on the radiation balance of the thermopile, and in addition limits convection over the thermopile which helps to prevent fluctuations of the signal. Shielding of the thermopile from temperature differences is intended to reduce thermal zero drift. For the same reason the instrument was insulated with polystyrene foam and covered with reflective foil to slow down temperature changes and hence to reduce internal temperature differences. Details of the design specifications and the materials used are given in Appendix D.

To achieve suitable sensitivity the angle of view of the instrument was made relatively large, about 10^{o} half-angle compared with 5^{o} in the

Linke-Feussner. By measuring over a wider angle, rapid changes in radiance due to travelling clouds are reduced and some stability is gained. However, a disadvantage is that in field operation the instrument 'sees' the sun directly more often. It also becomes more difficult to eliminate the influence on the sensor of stray reflections within the instrument of the direct solar beam. The inner surfaces of the tube were sprayed with 'Nextel velvet' matt black paint to minimise reflection of radiation. In practice however the paint had a significant specular reflection at low angles of incidence and owing to the relative brightness of sun to sky, a mere 0.1% of the direct beam reaching the sensor could introduce serious errors in measurements of radiance. This problem is discussed in more detail in section 4.6(c). An additional problem is that the paint may weather in sunlight and by increasing the reflection from the sides of the tube, effectively increase the instrument's angle of view with time. In the Linke-Feussner actinometer, reflections are prevented by a series of baffles so that the thermopile does not 'see' any directly illuminated surface within the instrument.

Finally the instruments were sealed in a dry atmosphere to prevent moisture and pressure fluctuation effects. Most of the instruments contained silica gel in case of leaks, and three of the ten instruments used in the field had a thermodiode inserted in the base to monitor changes of temperature.

4.6 Tests of Instrument Characteristics

(a) Calibration

The instruments were calibrated by comparison with a Linke-Feussner actinometer, once in February 1976 and again in July 1977. The instruments were all mounted facing vertically upwards and their signals were recorded on a data logger. The Linke-Feussner was read manually using a Comark microvoltmeter. The 1976 calibrations were performed under both overcast and cloudless sky conditions; the 1977 calibrations were performed under overcast conditions only. Although the Linke-Feussner has a narrower aperture and therefore was looking at the centre of the wider region seen by the new instruments, this should not affect the calibration in terms of energy per solid angle, as the radiance of the zones seen by the two types of instruments should not be significantly different. The zero offset of the Linke-Feussner was measured before and after each radiance measurement and a mean zero reading was subtracted from the result. The other instruments were given adequate time to reach thermal equilibrium, hence no corrections for zero offset were made.

To eliminate some of the scatter between different instruments and to provide a longer series of measurements for the comparison, the signals from the new actinometer were first compared with the sum of signals from all ten instruments. The sum of the ten signals was then compared with the zero-corrected Linke-Feussner signal over a shorter series of measurements. By this procedure the absolute calibrations all have standard errors $< 5\%$ but the relative calibrations have standard errors of 1 to 3%.

The calibration values from both occasions are given in Appendix E. Two of the thermopiles, (No. III and No. VI) were broken during the year but a comparison of the other eight instruments shows that the sensitivities decreased in every case, on average by 10%. In one instrument (No,II) the decrease was 27%, but fortunately this instrument was a spare which was not used for routine measurements, and when No.II is excluded the average decrease was only 7%. The calibration values adopted for the analysis of radiance measurements were the means of the two sets of calibrations, except for instrument Nos. II, III and VI. For the two instruments (III and VI) where a second calibration was not available the adopted values for measurements up to January 1977 were obtained by reducing the initial calibration by 3½%, which was the mean reduction for the other instruments. After January 1977, instrument No, III had a new thermopile and the 1977 calibration was used. The uncertainty of radiance measurements based on these calibrations is estimated as ± 10%.

(b) Thermal characteristics

The thermal behaviour of one of the instruments was measured in a temperature controlled room. No significant change of sensitivity with temperature could be detected within the accuracy of the experiment over the range 6 to 33°C, and this indicates that the change of sensitivity with temperature is less than 0.3% C^{-1}.

The zero offset of the instrument was monitored as the temperature of the room changed. Following a suggestion of G.J. Dalrymple (private communication) it was found that the zero offset was approximately proportional to the rate of increase of temperature. The constant of proportionality was 1 $\mu V/^{o}C\ hr^{-1}$ when instrument temperature was measured

by a diode in the base, or 0.75 $\mu V/^{o}C\ hr^{-1}$ when referred to ambient air temperature. Since changes of air temperature in the field rarely exceed 4 $^{o}C\ hr^{-1}$, this zero drift is small and easily accounted for. The maximum zero correction made on this basis in field tests was 7 μV, but more typical values were 0 to 3 μV.

(c) Angular response

Ideally the response of the instrument to radiation from a direction η degrees off axis would be uniform for $\eta \leqslant 10$ and zero for $\eta > 10$. In practice this is impossible to achieve and theoretical analysis shows that the response decreases for $\eta \geqslant 3$. There is also an azimuthal asymmetry due to the arrangement of thermocouples shown in Fig. 4.1. When η is measured in the XZ plane, perpendicular to the winding axis Y, the theoretical response is shown as the curve in Fig. 4.4(a); with η in the YZ plane the relationship is shown in Fig. 4.4(b). The curves are based on calculations of the number of thermocouples pairs irradiated from a direction η, assuming that there are no reflections in the tube or glass so that the outer filter acts as a simple aperture.

Measurements of the angular response were made using a 15 mW Helium-Neon continuous laser at the Physics department of Loughborough University. The laser was adjusted to give a parallel beam 85 mm in diameter and, to minimise the effect of lateral non-uniformity of the beam, the actinometer position was always adjusted to be in the centre of the beam for all angles. The results from measurements in the XZ and YZ planes are shown as plotted points in Figs 4.4(a) and (b). Bearing in mind possible errors due to non-uniformity of the beam and

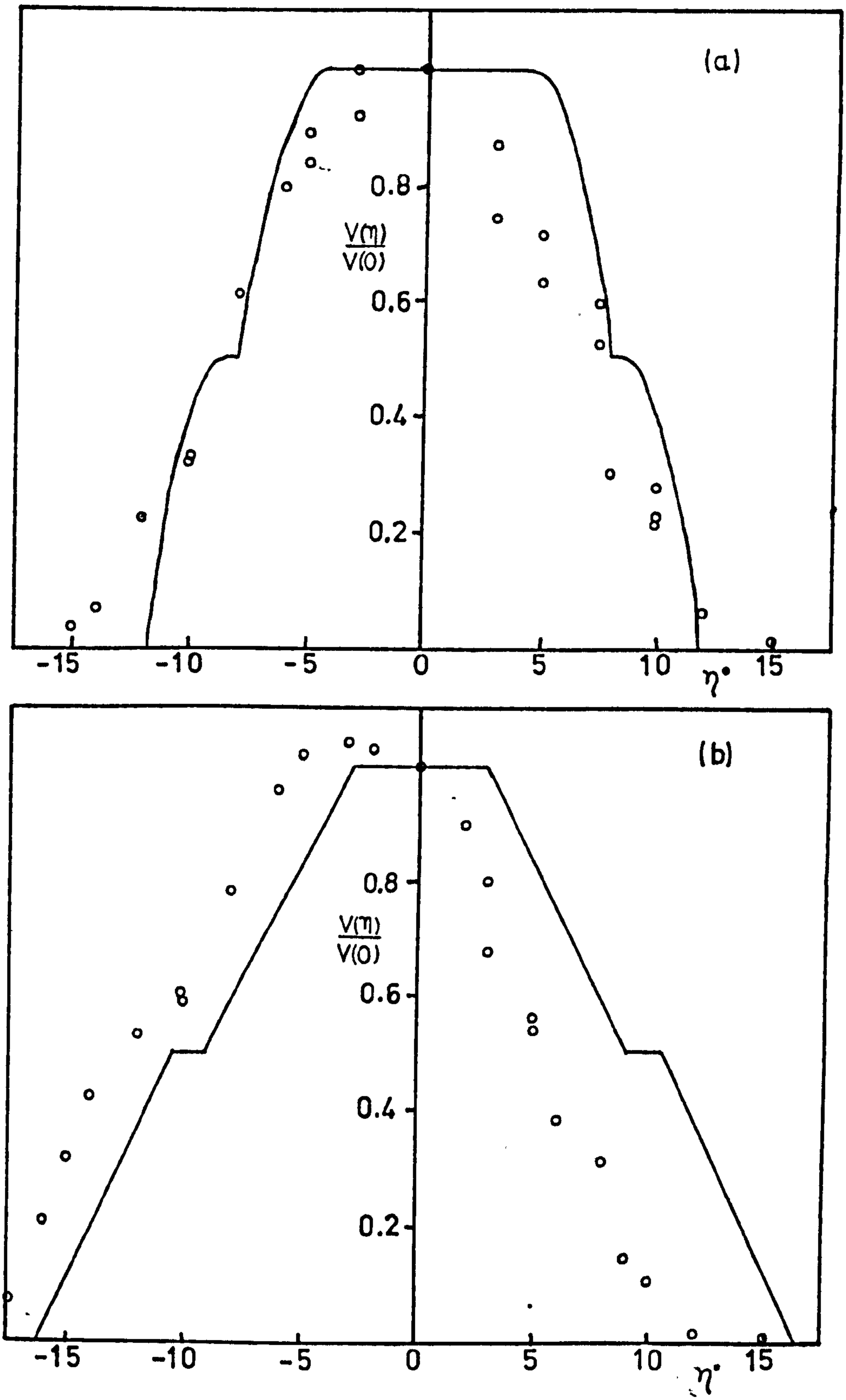

Fig. 4.4 Relative response of actinometer as a function of angle of incidence. (a) in the XZ plane; (b) in the YZ plane.

also that the angular zero was not strictly central, the agreement is reasonable except at larger angles where the measured response decreases less steeply than calculated. The laser was not sufficiently intense to give accurate readings when η was greater than 15^{o}. This region is important,not in terms of diffuse radiation, but because of errors that may be caused by reflection of the direct solar beam.

More accurate measurements for $\eta > 15^{o}$ were made in a similar experiment using a 2 kW theatrical lamp at about 1.5 m with its aperture narrowed to a bright spot subtending an angle of 2^{o} at the outer glass filter of the instrument. The experiment was performed outdoors at night to prevent the actinometer from seeing illuminated surfaces as the tolerable error was < 0.1%. The results are plotted logarithmically in Fig. 4.5 and show that 0.1% of the radiation still reached the sensor when the source was 50^{o} off axis. For angles η greater than 25^{o} the response, $V(\eta)$ fell off exponentially according to the formula :

$$\frac{V(\eta)}{V(0)} = a_1 \exp(-a_2 \eta) \qquad 4.10$$

as shown by the fitted line, where $a_1 = 0.074$ and $a_2 = 0.085$. This formula may be used to estimate approximately the contribution of the direct solar beam I to the radiance measurement when the direct beam is 25 to 60 degrees off axis. However uncertainties in such measurements are large: the output of the lamp varied by up to 5%; angles were measured with $\pm 1^{o}$ random error and $\pm 2^{o}$ systematic; the angular diameter of the source was larger than that of the sun; the angular response was measured in only one plane; there may have been residual errors due to reflections of stray light from the ground. The overall uncertainty in the estimation of $V(\eta)$ is taken from the graph as $\pm$ 30%.

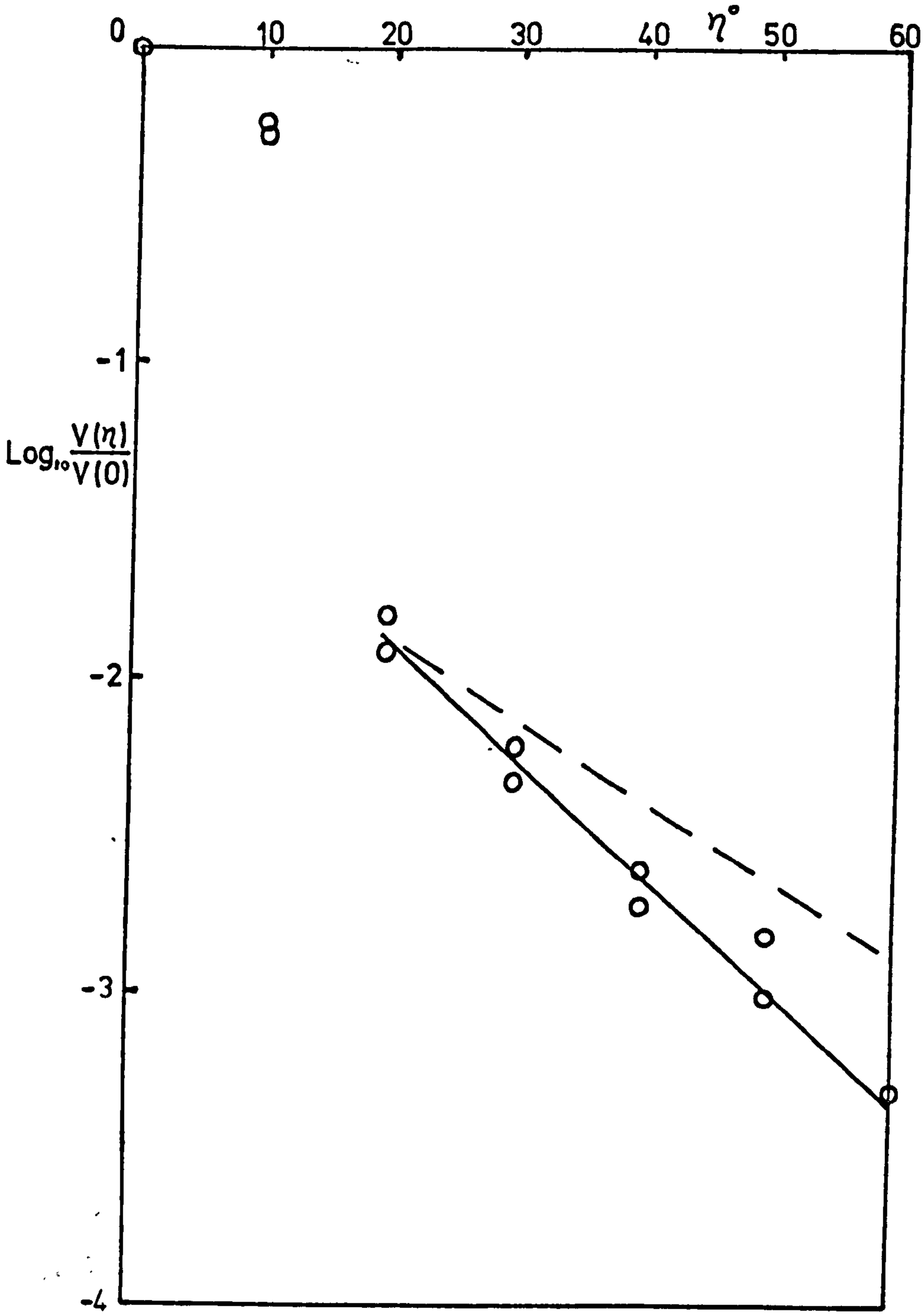

Fig. 4.5 Log_{10} of relative response of actinometer for angles of incidence up to 60^{o}; plotted points and solid line ——— lamp experiment; dashed line — — — field tests.

To study further the problem of the influence of I on radiance measurements, field comparisons were made with two actinometers facing in the same direction, one of which had an occluding annulus. The annulus, shown in Fig. 4.6 was designed to shield the outer glass filter of the instrument from radiation coming from more than 25° off axis, while still allowing the thermopile to be irradiated directly from angles up to 17°. This arrangement provided a separate field estimate of the coefficients a_1 and a_2 in Eq. 4.10 and defined the limits withinwhich a correction factor could be applied,

The measurements from the unshielded actinometer were corrected by using Eq. 4.10 with measured values of the direct solar beam to estimate the error. The corrected actinometer values were compared with measurements from the shielded actinometer and the values of the coefficients a_1 and a_2 in Eq. 4.10 were improved using the function fitting technique described in Chapter II. The values of a_1 and a_2 found were 0.043 and 0.058 respectively and the field estimate of the solar beam correction is plotted as the dashed line in Fig. 4.5. These results suggest that larger corrections for B are necessary, especially at large values of η , than were indicated by the lamp experiment. The uncertainties are still very large however, partly due to the uncertainties in the calibrations of the two actinometers, and the residual standard deviation of the corrected values was 28 W m^{-2} $(\pi\ st)^{-1}$. This was not a significant improvement on the comparison using the earlier correction based on the lamp experiment. It was concluded that this method of correction for the direct solar beam would not give reliable estimates of radiance when $\eta < 60^{o}$.

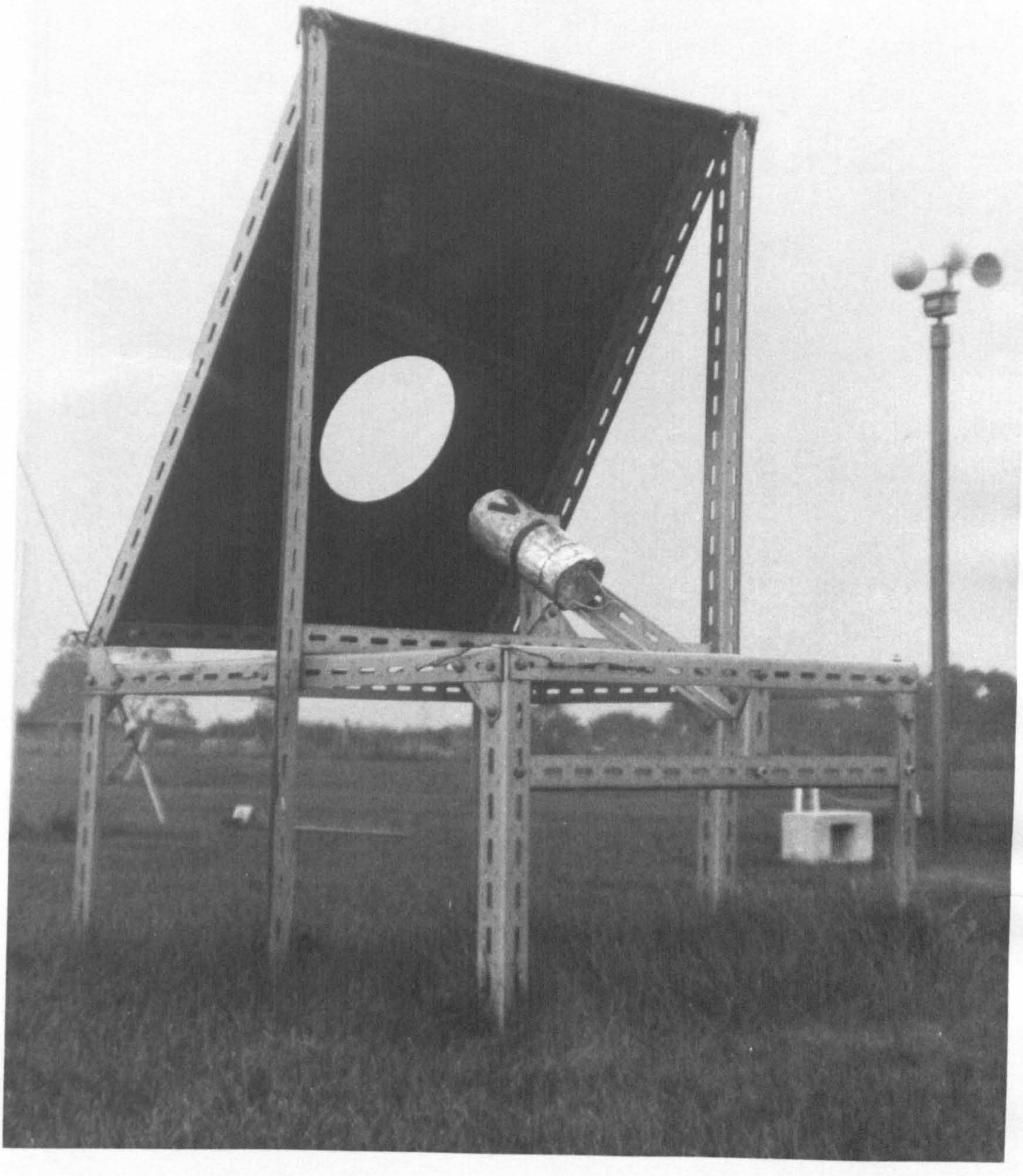

Fig. 4.6 Actinometer with occluding annulus.

The effective solid angle of view of the instrument, calculated by weighting each angular zone by its relative influence on the instrument, is 0.09 st when based on the theoretical calculations of the number of thermocouples irradiated. This is equivalent to an effective angle of view (with a square response) of 9.8^{o} and implies that the ratio of the direct calibration (in mV/W m^{-2}) to the diffuse calibration (in mV/W m^{-2} $(\pi$ st$)^{-1}$) is 34.5. When this ratio was measured on one of the instruments the ratio came to 27.2, equivalent to an effective angle of 11.2^{o} and an effective solid angle of 0.12 st. The larger field of view in practice is presumably due to the reflections off the sides of the instrument.

4.7 Field Operation

(a) The field site

The actinometers were mounted on a special stand in the Met. site as shown in Fig. 4.7. Eight instruments were arranged facing N , S , E and W at zenith angles of 30^{o} and 60^{o}, and a ninth instrument faced vertically upwards at 0^{o}. The orientations of the instruments are tabulated with their calibrations in Appendix E. A tenth instrument (No. II) was kept on the stand as a reserve and was used for part of the time with a shading annulus to evaluate corrections for the direct beam (Section 4.7(c). The actinometers and the temperature sensors in three of them were connected to a data logger. Two previously established Kipp pyranometers measured diffuse D and global radiation G on a horizontal surface, and a third Kipp pyranometer measured global radiation on a 45^{o} slope facing 47^{o} W of N as shown in Fig. 4.8. Their

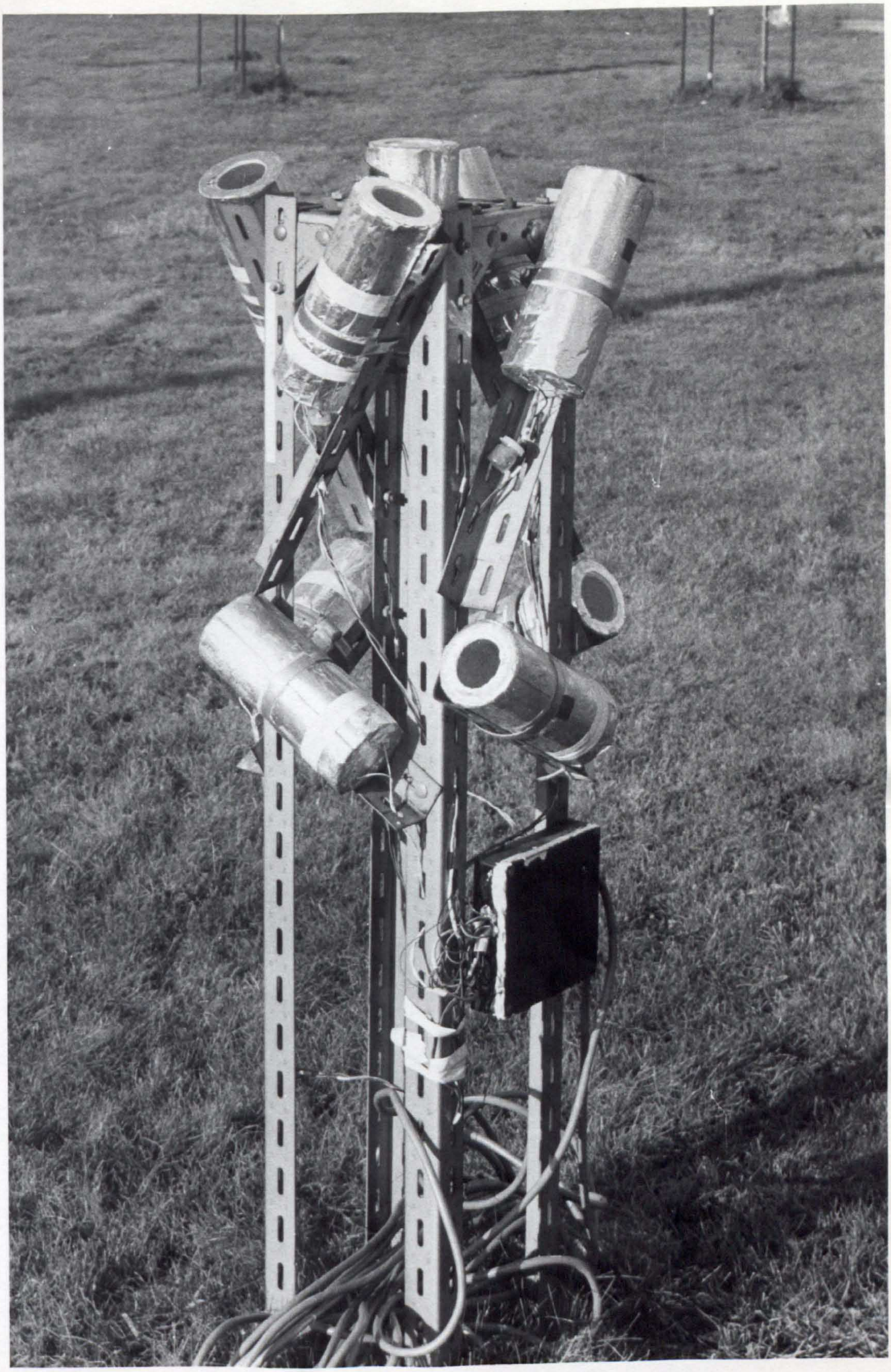

Fig. 4.7 The mounting of the actinometers in the field.

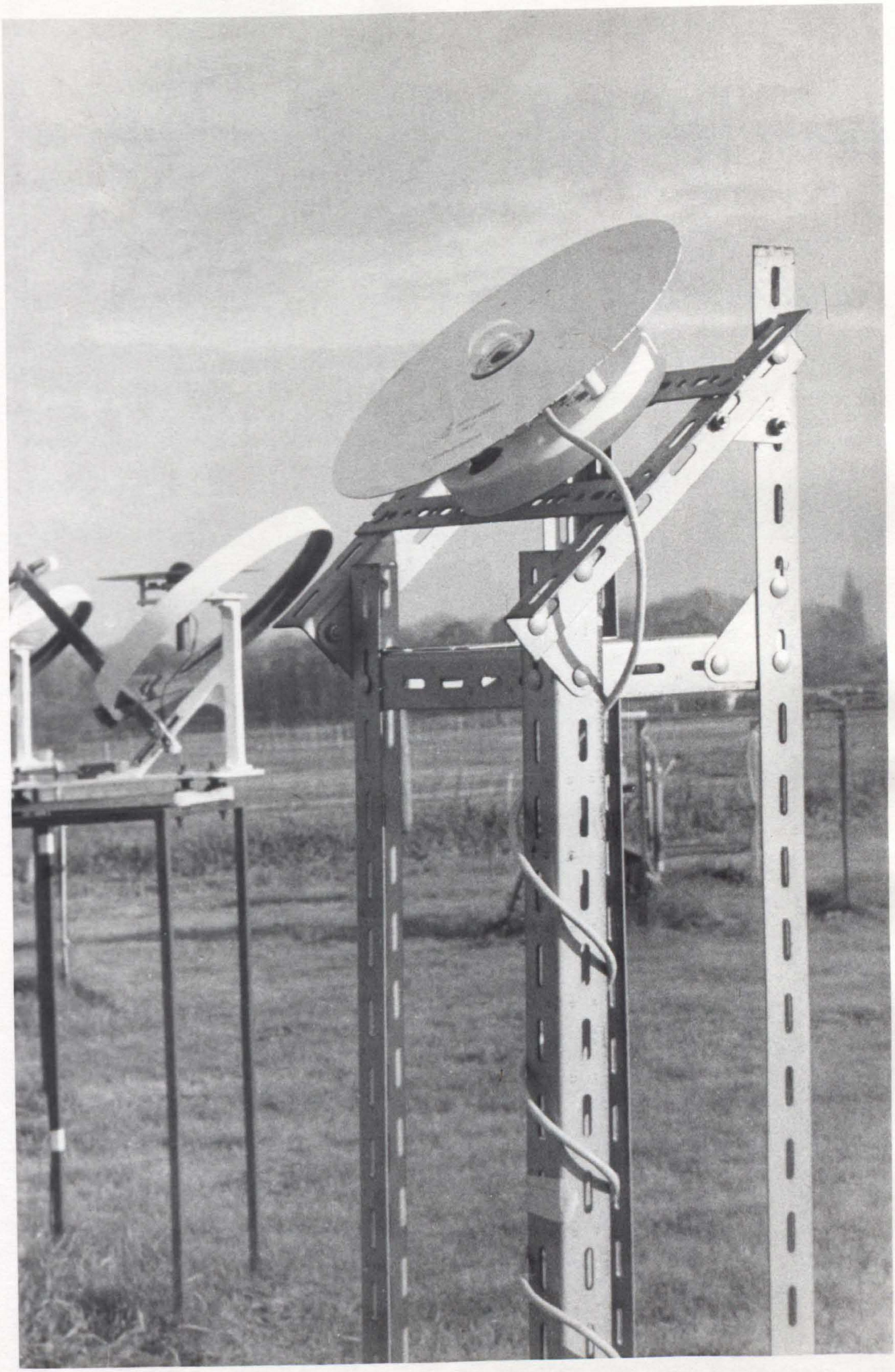

Fig. 4.8 A Kipp pyranometer mounted with a tilt of 45°.

calibration factors are given in Appendix E. The data logger monitored all the instruments at 10 minute intervals.

(b) Treatment of raw data

The paper tape records from the data logger were transferred to files in the computer which held half a month of ten minute readings for all the instruments. Two small corrections were applied to the raw data for zero offset of the actinometers. The thermal zero drift was predicted from the change in mean instrument temperature measured by the three diodes over each 10 minute intervals. A common figure was applied to all the actinometers. There were also zero offsets caused by other factors such as moisture in the cable connections. These were assumed to be long term effects and were assessed by averaging, for each instrument, the readings made at night between 2130 and 0230 when there was no measurable light. The calculated thermal zeros were subtracted from the night values before averaging and this reduced the night mean values somewhat. The average night values were typically ± 2 or 3 μV and tended to persist for several days. The night averages for each instrument were tested for significant departure from zero using Student's t-distribution at the 1% probability level. When a result was significant the night average was subtracted as a zero correction from the daytime readings in addition to the thermal zero correction.

Calibration factors were then applied to the corrected data using a separate program. A shade ring correction was applied to the diffuse radiation measurements using a Fourier series approximation to the Drummond geometric correction as a function of date, and an arbitrary empirical correction of 1.05 to allow for anisotropy of the sky.

Drummond (1956) analysed measurements of diffuse radiation in South Africa and suggested mean empirical corrections of 1.07 for clear skies, 1.03 for overcast skies and 1.05 for partially cloudy skies, with additional seasonal variations in the clear sky case. It was not possible to distinguish between these conditions on a 10 minute basis and so the factor 1.05 was chosen as a compromise. The results of Chapter III now indicate that Drummond's corrections are too large, overestimating D by up to 7% at midsummer.

A correction was also applied for the influence of the direct solar beam I, calculated as $\{G - D\}/\cos z$, on the diffuse radiance measurements. The direction of the sun was calculated for every 10 minutes and its angle η from the axis of each actinometer calculated. When $I > 0$ and $\eta < 25^\circ$ the actinometer reading was discarded. For angles η between 25° and 60° a correction was made using Eq. 4.10 and the method described in Section 4.7(c). The coefficients used with Eq. 4.10 were those derived from the lamp experiment. The estimated error of the correction was $\pm$ 30% and readings were discarded when the estimated error of the corrected value was more than 10%, i.e. when the correction was more than 1/3 of the corrected value.

The following Chapters present results from the analysis of the data from these instruments. Radiance distributions are defined for different atmospheric conditions, and their effect on the solar irradiance of slopes is studied.

V. DIFFUSE RADIATION FROM CLOUDY SKIES

5.1 Introduction

In Chapter IV an actinometer was described which was designed to measure sky radiance. A set of nine of these actinometers were used from May 1976 to May 1977 to measure the geometric distribution of sky radiance under all weather conditions. One actinometer was oriented vertically and the other eight were oriented at angles θ of 30^{o} and 60^{o} to the zenith, facing N , S , E and W , each instrument sampling a region of sky of about 0.1 steradians. The actinometer readings, together with measurements of the global irradiance G and diffuse irradiance D on a horizontal surface were recorded every ten minutes by a data logger and instrument calibrations were applied as described in Chapter IV. In this Chapter the analysis of these measurements is described and the relationship of the measured radiance distributions to sky conditions is considered. The effect of radiance distributions on the irradiance of inclined surfaces is evaluated.

5.2 Data Quality Control

The calibrated data were subjected to several tests to ensure that all the actinometers were working correctly. The calibration program automatically rejected readings that were over a set limit, defined to be about 10 times larger than the maximum observed radiance value of the sky. In addition radiance measurements which were influenced by the direct solar beam were corrected according to the procedure described in Chapter IV and where the uncertainty of this correction was too large the reading was rejected. Data selected for

analysis of radiance distributions consisted only of those scans where the readings of all the instruments were judged to be accurate. Cloudless skies were virtually eliminated by this procedure since one or other of the instruments was then nearly always affected critically by the direct solar beam, but cloudless sky conditions were examined in detail in the separate measurement program described in Chapters II and III.

For each instrument, the calibrated readings were corrected for the zero offset as described in Chapter IV Section 4.6. Part of this zero offset correction was calculated from an average of the instrument output at night. When the magnitude of the night average exceeded 10 μV (corresponding to an equivalent flux density of about 15 W m^{-2}), the actinometer readings were regarded as insufficiently accurate and radiance data from that day were rejected.

As an additional check on the data quality the radiance measurements of each actinometer were compared through each day with simultaneous measurements of D . The daily values of the correlation coefficients for each actinometer were usually greater than 0.9. Where correlation coefficients were less than 0.7 the readings were regarded as 'suspect'. In many cases values from these 'suspect' days were rejected for other reasons such as a large zero offset, but where a correlation coefficient was less than 0.6 the actinometer readings were regarded as unreliable and values for the day were rejected for this reason alone. Data that passed all the quality control tests were stored in computer files for further analysis.

5.3 The Effect of Sky Conditions on Radiance Distributions

(a) Representation of sky conditions.

Radiance distributions vary according to the sky conditions, in particular the degree of cloudiness of the sky. Cloudiness itself is difficult to measure objectively and three related 'sky parameters' were used to represent the sky conditions: the ratio D/G of diffuse to global radiation; sunshine hours as measured by a Campbell-Stokes recorder; and the relative frequency n_o/n_t with which the sun was obscured by cloud. n_o was the number of scans in which the measured value of D was equal to G, and n_t was the total number of scans during the time period considered. If cloud is distributed randomly over the sky and the cloud positions on different scans are not correlated, then n_o/n_t will, for sufficiently large n_t, approximate the fraction of sky covered by cloud as seen from the viewpoint of the instrument. This is in principle the same as 'cloud amount' as measured subjectively (Meteorological Office, 1956) by meteorological observers.

Cloud is not randomly distributed over short periods of time and may not be randomly distributed in the long term if there is a local source of preferential cloud formation. Both the radiance distributions and the sky parameters are thus subject to wide variation due to local effects of cloud, especially in the short term. In addition, since the measurements in this study were spot readings at 10 minute intervals there may be considerable statistical error in mean values of radiance or in values of D/G and n_o/n_t. Daily averages of the values were therefore used for analysis.

The sunshine measurements from the Campbell-Stokes recorder were divided by the length of the day (sunrise to sunset), calculated from standard astronomical formulae, to give relative sunshine hours h_s.

This term is sometimes known as 'percentage possible sunshine'. The mean values of h_s and D/G were based on the whole day but n_o and n_t were measured for only part of the day, when G was larger than 50 W m^{-2}. The daily values of D/G and n_o/n_t are closely related as shown in Fig. 5.1, but there is considerable scatter due to variation in turbidity and non-random distribution of cloud. Both D/G and n_o/n_t are negatively correlated with h_s. Linear regressions on h_s gave the slopes and intercepts shown in Table 5.1. The figures marked ± are the 95% confidence limits on the values. The time basis for averaging values of n_o/n_t was different from the other two parameters and this difference was greater in winter than in summer since G was less than 50 W m^{-2} for a greater part of the day. However the relationship between the parameters does not appear to vary significantly with the season (Fig. 5.1).

Table 5.1 Linear regressions of sky parameters D/G and n_o/n_t on h_s.

	Slope	Intercept
D/G	- 0.86 ± 0.06	0.99 ± 0.02
n_o/n_t	- 1.45 ± 0.16	0.84 ± 0.04

Page (1976) found the following relationships between G/G_e and h_s and between D/G and G/G_e, where G_e is the daily irradiation of an extraterrestrial horizontal surface :

$$G/G_e = 0.15 + 0.68\ h_s \qquad 5.1$$

$$D/G = 0{:}94 - 1.03\ G/G_e \qquad 5.2$$

Both relationships are based on data at Kew, 1947 to 1951. The derived

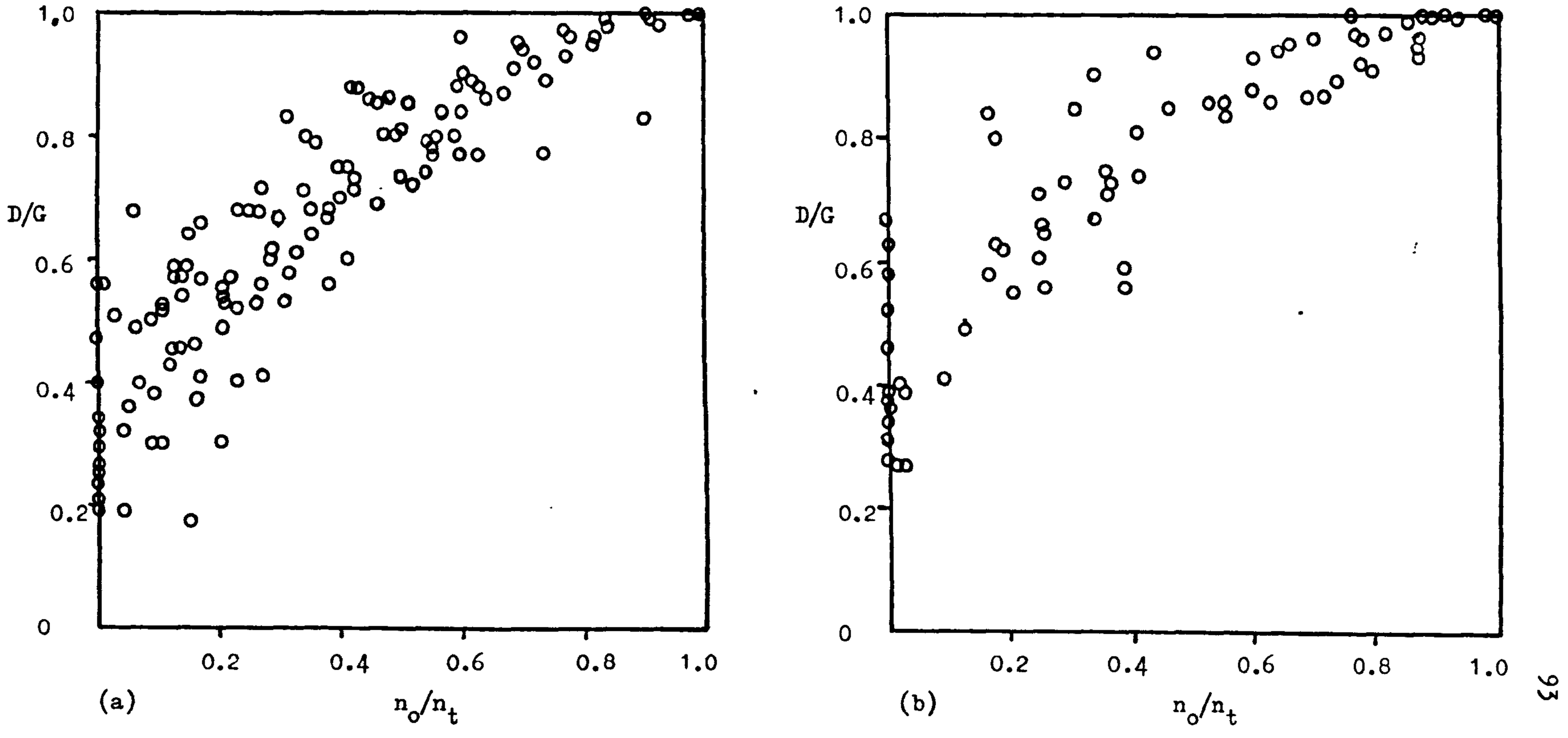

Fig. 5.1 The relationship between the sky parameters D/G and n_o/n_t.
(a) April - September (b) October - March

relationship between D/G and h_s is

$$D/G = 0.79 - 0.70\, h_s \qquad 5.3$$

Similar values were obtained from measurements at Cambridge. The slope and intercept found by direct comparison in the present study (Table 5.1) are physically more realistic than Eq. 5.3 however, since D/G must be 1 when there is no sunshine.

(b) Averaging procedures for radiance

Many of the radiance measurements in the files of calibrated data were corrected values where an estimated error in the measurement due to the direct solar beam had been subtracted as described in Chapter IV (Section 4.6). Since the correction procedure was subject to large uncertainties these corrected measurements may introduce a bias into the mean distributions of radiance. An unbiased set of radiance distributions was selected by taking only those occasions when the sun was obscured, so that the measured value of D was equal to G. Only those scans where $D > 50$ W m^{-2} were included as the actinometer signals were subject to serious errors at low values of irradiance. Although these files of 'sunless data' thus contained unbiased radiance distributions, the behaviour of these distributions with sky conditions may have been affected by the absence of data from times when the sun was shining. The files of 'corrected data' may also have suffered from this problem but the amount of missing data was considerably less. The 'sunless' data were probably more reliable for very cloudy skies.

The radiation data in each file were processed to give average values for each day. To reduce the introduction of bias due to missing

data, mean values for each instrument were evaluated every hour and the hourly values were averaged over the day. The daily means were rejected for further analysis when the number of hours included in the average was less than 2/3 of the length of the day (sunrise to sunset), * or when the mean number of scans used for the hourly averages were less than 3 out of the possible 6 . Due to this procedure no analysis could be done on days when cloud amount was small. Also, the average daily values derived from these sets of data should not be regarded as absolute since the 'sunless data' excluded all occasions when the sun was shining and the 'corrected data' excluded a large number of such occasions. For days of small cloud amount the mean values of D derived on this basis from the two files were considerably less than D values based on the whole day. The relative values of mean radiance however should be less susceptible to biasing by missing values, particularly on the cloudier days.

(c) Results

The daily values of radiance N were expressed relative to the mean value $\hat{N}$ from all 9 instruments and their variation with the sky parameters D/G , n_o/n_t and h_s was examined. Normalisation with respect to D was not used because there were additional uncertainties in the shade ring correction to D and furthermore the use of $\hat{N}$ eliminates the need for accurate absolute calibrations for the actinometers. The comparisons used 109 days from the 'corrected data' and 95 days from the 'sunless data' files. Sets of graphs were produced and linear regressions on the sky parameters were calculated. The relationship of $N/\hat{N}$ with cloudiness n_o/n_t for the vertical actinometer ($\theta = 0$) using the 'corrected data' is shown in Fig. 5.2. There is some tendency in

* The monthly distribution of selected days is given in Appendix G .

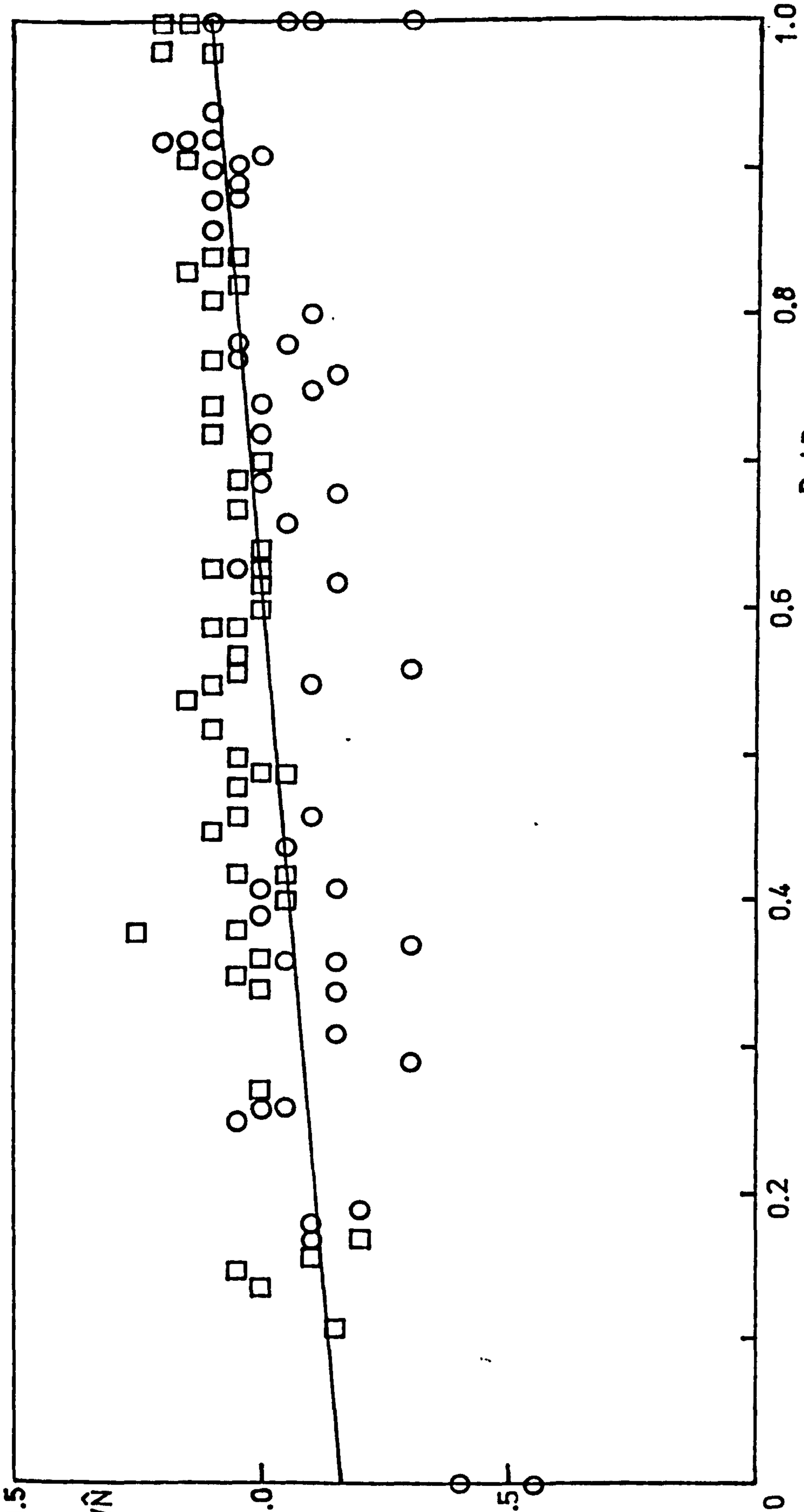

Fig. 5.2 $N/\hat{N}$ as a function of cloudiness n_o/n_t for the vertical actinometer.

the figure for the summer values (April to September) to be lower than the winter values (October to March) at small values of cloudiness. The greatest difference between summer and winter radiance ratios occurred with the actinometer facing S at $\theta = 60^{o}$, where the summer values were on average about 50% larger. Most actinometers however did not show a marked seasonal effect and the scatter in the values and uncertainties in the measurements are too large for a seasonal analysis to be useful. The regression line in Fig. 5.2 is based on all the values.

Linear regressions performed on the 'corrected data' were generally more significant than those performed on 'sunless data'. The corrected data contain a greater range of sky conditions and they probably represent the relationships of relative radiance with the sky parameters more accurately than the 'sunless data' which were more rigorously selected.

Tables 5.2 to 5.4 thus give the coefficients of linear regressions of $N/\hat{N}$ for the corrected data, on the various sky parameters X. The form of the regression equation is

$$N/\hat{N} = MX + Y_o \qquad 5.4$$

The standard errors of the slope M and the intercept Y_o are given and where the slope is significantly different from zero at the 99% probability level the value is marked **. The use of lower probability levels is not justified because with 9 instruments the probability of one achieving a higher significance level is too large. The regressions with n_o/h_t, Table 5.2 were marginally more significant than those with h_s or D/G.

Table 5.2 Linear regressions of $N/\hat{N}$ on n_o/n_t.

Zenith angle θ	Aspect	Slope	Standard error		Intercept	Standard error
0		0.26	0.04	**	0.84	0.03
30	S	0.03	0.03		1.11	0.02
60	S	- 0.90	0.16	**	1.77	0.11
30	E	0.21	0.04	**	0.91	0.03
60	E	- 0.16	0.06	**	1.07	0.04
30	W	0.19	0.04	**	0.90	0.03
60	W	- 0.12	0.05		1.00	0.03
30	N	0.38	0.03	**	0.66	0.02
60	N	0.10	0.02	**	0.74	0.02

Table 5.3 Linear regressions of $N/\hat{N}$ on D/G.

Zenith angle θ	Aspect	Slope	Standard error		Intercept	Standard error
0		0.30	0.08	**	0.75	0.07
30	S	0.06	0.06		1.08	0.05
60	S	- 1.10	0.32	**	2.16	0.28
30	E	0.28	0.09	**	0.80	0.07
60	E	- 0.24	0.11		1.18	0.10
30	W	0.18	0.08		0.86	0.07
60	W	- 0.31	0.09	**	1.19	0.08
30	N	0.61	0.06	**	0.37	0.05
60	N	0.23	0.04	**	0.61	0.04

Table 5.4 Linear regressions of $N/\hat{N}$ on h_s

Zenith angle θ	Aspect	Slope	Standard error		Intercept	Standard error
0		- 0.29	0.08	**	1.05	0.02
30	S	- 0.04	0.06		1.14	0.01
60	S	0.95	0.29	**	1.07	0.07
30	E	- 0.24	0.08	**	1.08	0.02
60	E	0.24	0.10		0.94	0.02
30	W	- 0.17	0.07		1.04	0.02
60	W	0.30	0.08	**	0.88	0.02
30	N	- 0.54	0.06	**	0.98	0.01
60	N	- 0.20	0.04	**	0.84	0.01

Distributions of radiance may be drawn up for different sky conditions using the regression equations. At low levels of cloudiness such distributions would be based on small numbers of measurements which would include a relatively large proportion of corrected values. Accepting that there may be systematic errors in the regression estimate of $N/\hat{N}$ due to the absence of much of the data when the sun was shining, the values in Tables 5.2 to 5.4 show that for small cloud amount the daily mean radiance distribution was brighter towards the S , and towards the E and W at large values of θ . With increasing cloudiness the brighter regions diminish and the darker regions are enhanced relative to the total. The radiance of the point facing S at $\theta = 30^{\circ}$ remains roughly constant relative to the sky as a whole. The behaviour of the radiance distribution with sky conditions is consistent with common observation.

In the 'sunless' radiation data there were no corrections that could bias the radiance distribution and the trends with cloudiness were less steep. These data were used to define a mean radiance distribution for partly cloudy skies. The mean values of $N/\hat{N}$ for each actinometer for all days using the 'sunless' data are given in Table 5.5. The values correspond to a mean cloud amount n_o/n_t of 5 to 6 oktas. Although there was considerable variation in the day to day values, the standard errors of the means in Table 5.5 are small and mean radiance values in the East are equal to those in the West within the confidence limits of the measurements. The mean values are thus considered reliable and are used in Section 5.4 to estimate the relative diffuse irradiance of sloping surfaces.

Table 5.5 Mean values of relative radiance for partly cloudy skies (5 to 6 oktas).

Zenith Angle θ	Aspect	$N/\hat{N}$	Standard deviation	Standard error
0		1.07	0.10	0.01
30	S	1.13	0.08	0.01
60	S	1.04	0.22	0.02
30	E	1.07	0.10	0.01
60	E	0.92	0.11	0.01
30	W	1.06	0.07	0.01
60	W	0.90	0.11	0.01
30	N	0.96	0.09	0.01
60	N	0.80	0.07	0.01

5.4 The Diffuse Irradiation of Slopes by Cloudy Skies

An analytic approximation symmetrical about the N-S axis was fitted to the radiance distribution of Table 5.5 using the method described in Chapter II, Section 2.5. The approximation had the form

$$N/\hat{N} = a_1 + a_2 \cos\theta + a_3 \cos\phi + a_4 \cos\theta \cos\phi \qquad 5.5$$

where ϕ is the azimuth from S and the coefficients a_i at the best fit are given in Table 5.6. The accuracy of the fit was good,

Table 5.6 Fitted values of coefficients in Eq. 5.5.

Coefficient	Value	Standard error
a_1	0.77	0.04
a_2	0.32	0.05
a_3	0.18	0.05
a_4	- 0.14	0.07

the residual standard deviation being only 0.02 and the largest difference between the fitted function and the radiance values was less than 0.04. The spatial distribution of the differences was not systematic.

The fitted approximation to the radiance distribution of partly cloudy skies was integrated numerically using the method of Chapter III, Section 3.1. The integrated irradiance on a horizontal surface using $N/\hat{N}$ from Eq. 5.5 was 0.98. The $N/\hat{N}$ values in Table 5.5 can thus be converted to N/D, within the limits of accuracy of the function fitting and integrating procedures, by dividing by 0.98. The integrated irradiation values of a number of planes of different tilt α and

Table 5.7 Relative diffuse irradiance of slopes by partly cloudy skies.

	$D(\alpha,\psi)/D$				
	Azimuth ψ relative to S				
Tilt α	0°	45°	90°	135°	180°
15°	1.00	1.00	0.98	0.96	0.96
30°	0.96	0.95	0.92	0.89	0.88
45°	0.88	0.87	0.83	0.80	0.78
60°	0.77	0.76	0.72	0.68	0.67
75°	0.65	0.63	0.59	0.56	0.54
90°	0.51	0.49	0.46	0.43	0.41

azimuth ψ relative to South are given in Table 5.7 in which the tabulated values are the daily irradiation of slopes relative to D for partly cloudy skies (5 to 6 oktas).

The diffuse irradiance of slopes derived from radiance measurements may be compared with irradiance measured with a tilted solarimeter. A Kipp solarimeter was mounted at the meteorological site as shown in Fig. 4.8, tilted at an angle of 45° at azimuth 133° (approximately NW). The output of the solarimeter was recorded as in Section 5.1. From the 'sunless' data records, days were selected when n_o/n_t was 0.65 to 0.70 or D/G was 0.85 to 0.91 corresponding roughly to the mean values for which Table 5.5 is valid. This procedure provided 24 daily averages for comparison. For these days the values D(45) of daily diffuse irradiation of the tilted solarimeter were expressed as fractions of D . The mean was 0.86 with standard deviation 0.03. However this value included a fraction of reflected radiation from the ground for which

allowance must be made. The mean value of the albedo of grass measured at the Meteorological Site was about 0.2. Assuming that reflection was isotropic the reflected component of the irradiance of the tilted solarimeter was 0.03 D. The corrected mean value of $D(45)/D$ is thus 0.83. The corresponding integrated value from Table 5.7 was 0.80. For comparison, the ratio $D(45)/D$ for an isotropic sky would be 0.85.

The difference between the measured diffuse irradiance on a sloping surface and the estimate based on measurements of radiance is small and may be due to several factors. Some of the sources of uncertainty have been discussed in Chapter III in the context of clear sky radiation, but the most obvious source of uncertainty in the integrated values is the sparcity of radiance measurements over the hemisphere. The analytic approximation Eq. 5.5 used for integration is based on only 9 points and the function is entirely extrapolated for $\theta > 60^{\circ}$. There may however be errors in the measurements of a tilted radiometer. The convective term in the energy balance of a thermopile varies with tilt and Anderson (1967) showed that convective transfer is a major factor in the Kipp solarimeter. Experiments with an Eppley pyrheliometer by Fuquay and Buettner (1957) indicated that the instrument sensitivity decreased with tilt, by as much as 3% for a vertically mounted instrument. There appear to be no comparable studies for the Kipp radiometer but the effect of tilt is likely to be small. The most likely reason for the difference of 0.03 between the measured values and integrated estimates of $D(45)/D$ is that the region of sky near the horizon is brighter than suggested by extrapolation from the measured radiance values.

5.5 Overcast Skies

A separate investigation was performed on the radiance distribution of overcast skies. The computer files of 'sunless data' were used to obtain hourly averages for those occasions when all six ten-minute scans within an hour were present. A file of 'sunless hours' was created, containing hourly mean values of each radiance measurement for 355 hours through the year. Not all the sunless hours can be regarded as overcast however. Each hour average is based on only six measurements and some of the sunless hours are from partly cloudy skies. For example with 6 oktas of cloud the probability that no direct sunshine will be recorded is $\{6/8\}^6$ or about 18%. The proportion of non-overcast hours in the total cannot be determined however without knowledge of the frequency distribution of different levels of cloudiness.

To eliminate 'pseudo-overcast' hours, a total of 99 overcast hours were selected from the sunless hours by choosing occasions where the variation of radiance with azimuth was minimal. In all the hours selected the coefficient of variation (the ratio of the standard deviation to the mean) of radiance with azimuth was less than 0.1 both at $\theta = 30^\circ$ and $\theta = 60^\circ$. Partly cloudy hours are expected to have greater azimuthal variation in radiance due to the influence of the sun's position.

Radiance distributions from overcast skies were measured by Grace (1971) who noted wide variations within a short period of time. In the present work the coefficient of variation of D within the hour was typically about 20% and the coefficient of variation of N was typically about 25%. Hourly average values however were more stable.

The 'Standard Overcast Sky' is described by the formula of Moon and Spencer (1942), given in Eq. 1.7. This formula may be modified to give a relationship which is linear in $\cos\theta$ but with a coefficient β which can be varied, Eq. 5.6.

$$N(\theta) = N(0) \{1 + \beta \cos\theta\} / \{1 + \beta\} \qquad 5.6$$

Goudriaan (1977) gave a theoretical basis for this form of distribution but the coefficient β in his analysis was subject to uncertainties in the assumptions made. The radiance values from the 99 overcast hours were used to test Eq. 5.6 and values of β for each case were found by linear regression. Fig. 5.3(a) shows the frequency distribution of the values of β, expressed as frequency per unit range of β to allow for unequal ranges. The residual variances of the regressions were in most cases well within the uncertainty from the calibration of the instruments. The distribution of β appears slightly skewed towards larger values but may be regarded as a normal distribution for many purposes. The mean value of β was 1.4 with 95% confidence limits of $\pm$ 0.15. No significant variation in the distribution of β could be found with season or with the magnitude of D as shown in Fig. 5.4. These data show that the Standard Overcast Sky formula Eq. 1.7 where $\beta = 2$, overestimates the value of β but the formula proposed by Walsh (1961) in Eq. 1.8 (for luminance distributions) is within the confidence limits of the present work.

The cumulative frequency diagram, Fig. 5.3(b) also shows the frequency distribution of β when Eq. 5.6 was tested on all sunless hours. The mean value of β was somewhat lower and the spread of the distribution

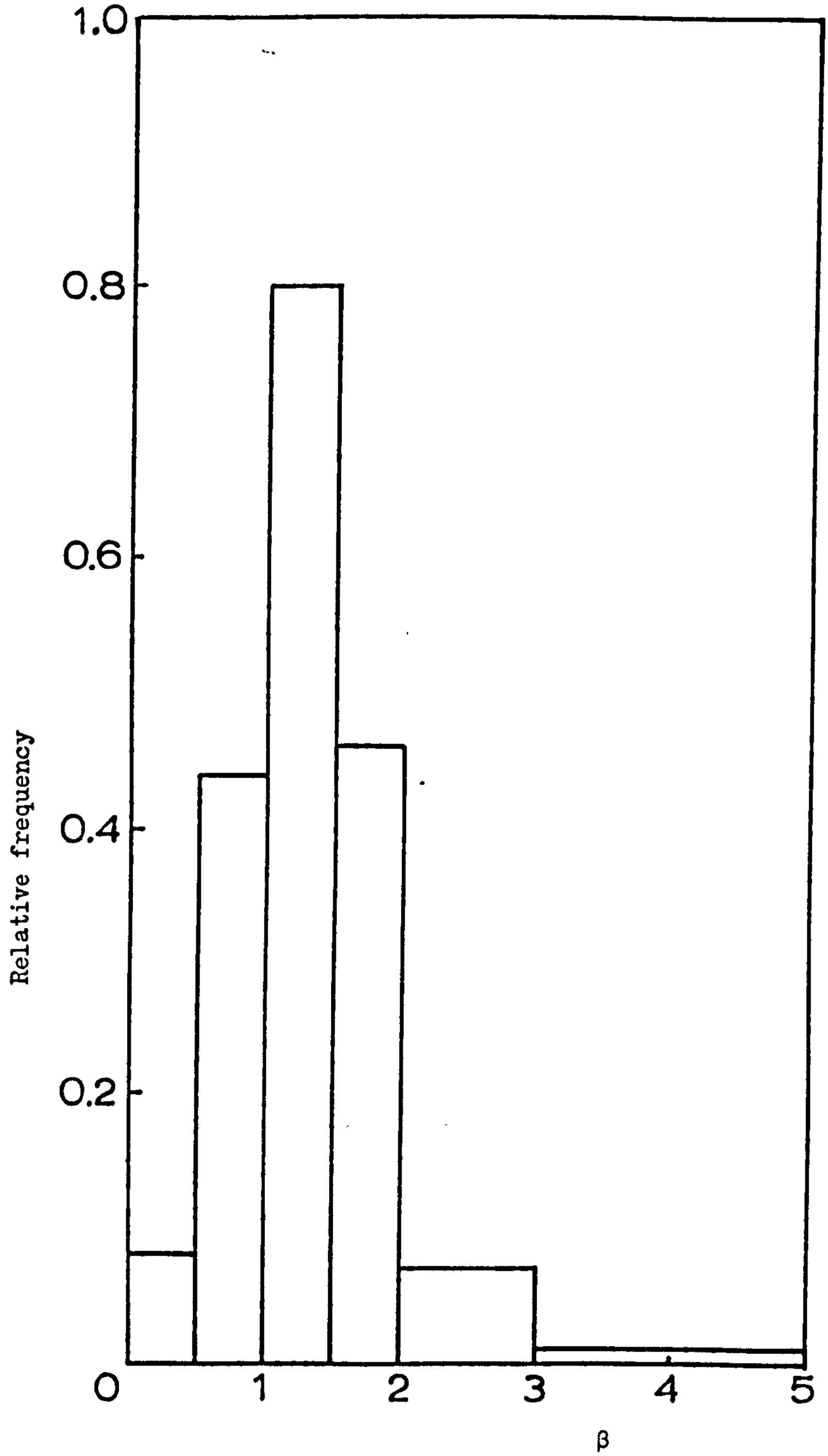

Fig. 5.3(a) Frequency distribution of β for overcast hours.

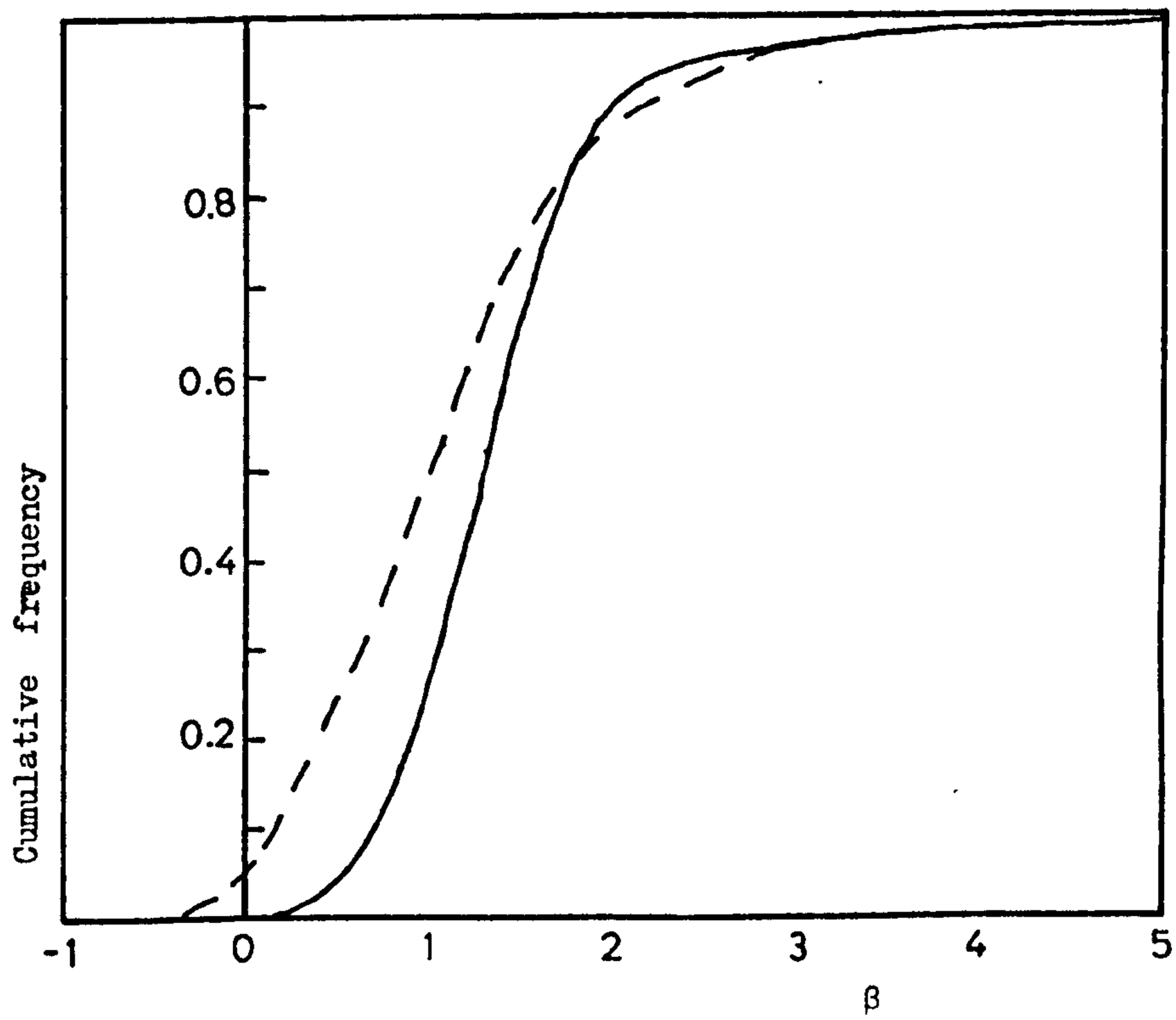

Fig. 5.3(b) Cumulative frequency distribution of β for overcast hours (solid line) and all 'sunless hours' (dashed line).

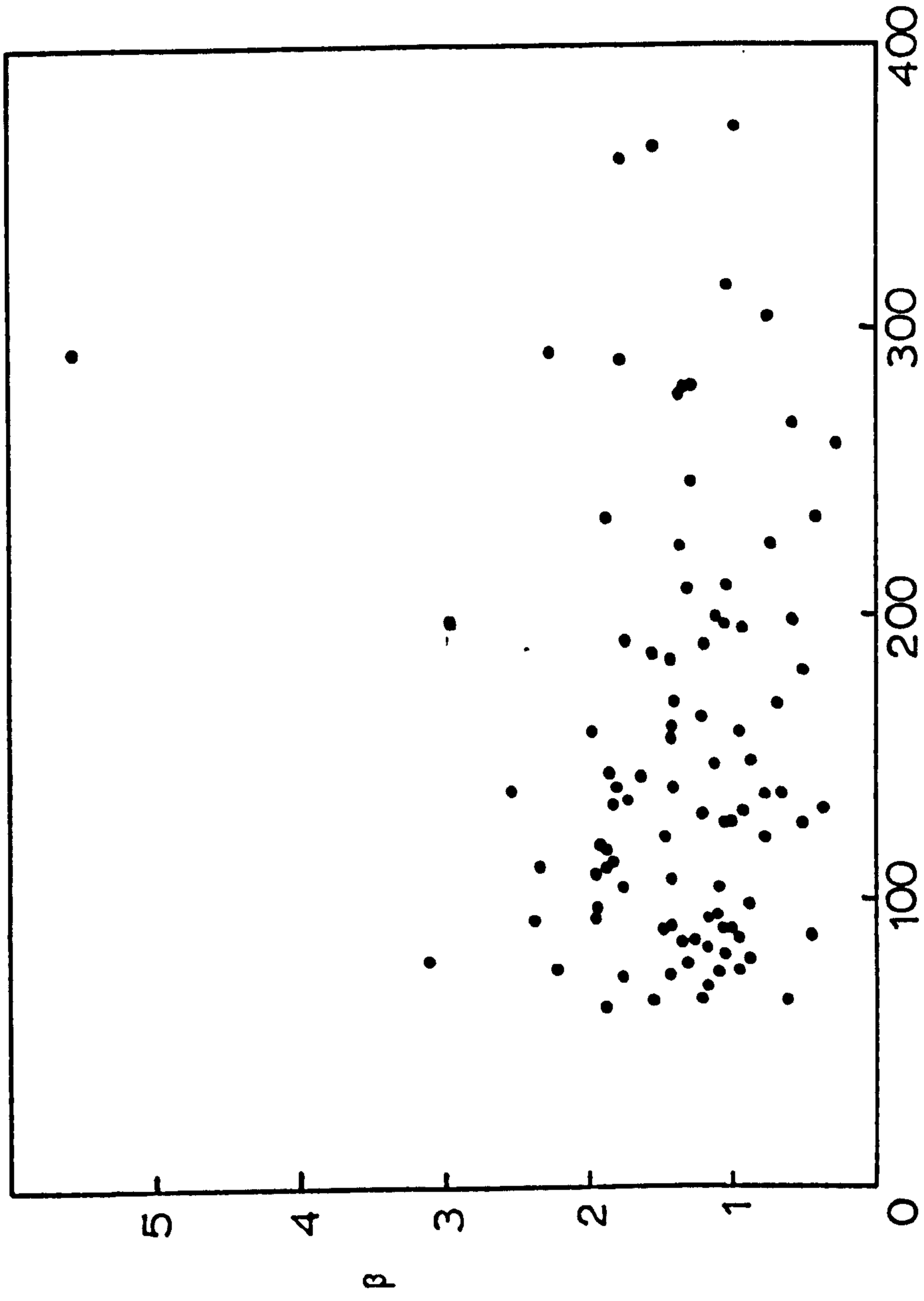

Fig. 5.4 The distribution of β as a function of D.

was larger. The residual variance however was in many cases much larger than with overcast hours alone and Eq. 5.1 should not be regarded as a good representation for all sunless hours.

The radiance distribution of Eq. 5.6 can be integrated analytically to give the diffuse irradiance $D(\alpha)$ of any plane surface of inclination α. The relative irradiance is given by

$$\frac{D(\alpha)}{D} = \left\{\frac{1 + \cos \alpha}{2}\right\} + \frac{2\beta}{\pi[3 + 2\beta]} \left\{\sin \alpha - \alpha \cos \alpha - \frac{\pi}{2}[1 - \cos \alpha]\right\} \qquad 5.7$$

as shown in Chapter III. The effect of the value of β on the relative irradiance of inclined surfaces under an overcast sky is shown in Fig. 5.5 for values of α of 45° and 90°. Fig. 5.5 indicates that the maximum error in using a value of β of 2 instead of 1.4 is about 2% and for irradiance estimates this error is negligible when compared with other sources of uncertainty. The value of β however may be significant if knowledge of the radiance distribution itself is important rather than relative values of irradiance.

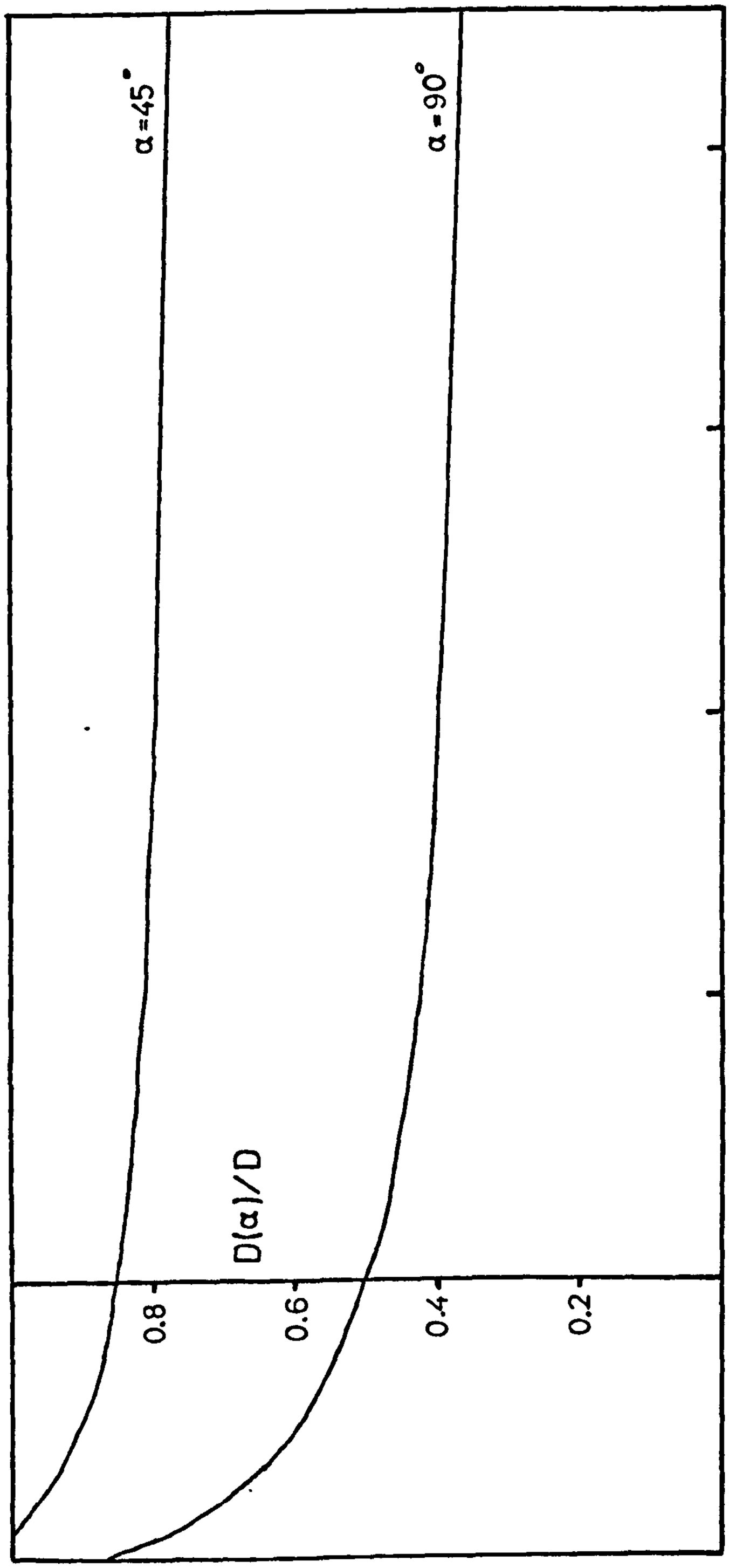

Fig. 5.5 The relative irradiance of 45° and 90° tilted planes as a function of the parameter β.

VI. A COMPUTER MODEL OF THE IRRADIANCE OF SLOPING SURFACES

6.1 Introduction

Several methods of estimating the global irradiance of sloping surfaces were reviewed in Chapter I and their relative merits were discussed. Different approaches require different data, but the more reliable approach which is applicable to surfaces of all aspect is to use measurements on a horizontal surface of global radiation G and diffuse radiation D and to consider the components of radiation separately. The bulk of this thesis has been concerned with establishing the geometric characteristics of diffuse radiation. The irradiance of planes however involves diffuse, direct and reflected radiation components. In this Chapter a computer model for the calculation of slope irradiance from hourly values of G and D is described, some results calculated from mean radiation data from sites in Britain are presented and a sensitivity analysis is conducted to investigate the effect of uncertainties in the modelling of diffuse radiation. In addition, particular problems studied using the model were : the optimisation of the tilt of a solar collector; the energy gain of a collector which tracks the sun through the sky; and the effect on slope irradiance of anisotropic reflection by an adjacent water surface.

6.2 Formulation of the Model

The model calculates hourly values of the irradiance of up to nine sloping planes given their angles of inclination and azimuth, and sums the irradiance values to give daily (or monthly) and yearly irradiation totals. The components of radiation are summed separately

and the output of the program gives daily and yearly totals of each of the components as well as hourly values of global irradiance. Data required are the latitude and longitude of the site, the reflection coefficient ρ of the surroundings, the mean turbidity τ of the atmosphere and hourly values of G and D. The computer program, written in FORTRAN, is given in Appendix F.

The radiation data used were monthly means of hourly averages derived from Meteorological Office records over a ten year period at Kew, Aberporth, Eskdalemuir and Lerwick. To calculate the sun's position for calculations of slope irradiance, it was assumed that these data could be treated approximately as instantaneous values for the middle of each hour on the 15th day of the month. The declination and the equation of time were calculated for each date after the method of Dogniaux (1975) using Fourier series approximations (Subroutine DECTIM). The sun's position was then calculated from the time using standard astronomical formulae (Subroutine SOLOC).

When the zenith angle z of the sun was greater than 85°, the radiation was all treated as isotropic diffuse radiation to avoid large errors in the calculation of the direct beam irradiance I at normal incidence. The elimination of the direct beam at low solar elevations will affect the daily irradiation estimates for E and W facing planes by at most 5% due to the small values of irradiance concerned. When z was less than 85°, G and D were separated into four radiation components as follows, and geometrical conversion factors for each receiving plane were calculated for each component. The direct beam $B = G - D$ was used to calculate I. The reflected radiation on an inverted 180°

surface was calculated as ρG . The diffuse radiation D was separated into a part D_b due to blue cloudless sky and a part D_g due to cloud, each having different geometrical characteristics.

To separate the two components of diffuse radiation it was assumed that the ratio D_b/B was on average the same below partly cloudy skies as below cloudless skies. This ratio was determined from mean relationships between D/G and atmospheric turbidity τ in cloudless skies. For values of z less than 60°, Unsworth and Monteith (1972) showed that $(D/G)_b$ for cloudless skies was well represented by a linear function of τ

$$(D/G)_b = 0.097 + 0.68\,\tau \qquad 6.1$$

For z greater than 60°, Page (1975) tabulated values of D/G for cloudless skies as a function of z and τ based on data from Kew. These values are shown in Fig. 6.1. For the purposes of this model a crude approximation was adopted in which the values of Unsworth and Monteith were used for $z > 60^\circ$ and a linear approximation to the values of Page for $60^\circ < z < 85^\circ$ as shown in Fig. 6.1. The approximation tends to under estimate the D/G values of Page when $z > 75^\circ$ but because irradiance values are low at large zenith angles this will not introduce serious errors in daily irradiation estimates. The slopes of the linear approximations for $z > 60^\circ$ were found to be linear functions of τ , Fig. 6.2. This enabled the ratio $(D/G)_b$ for $z > 60^\circ$ to be estimated by a linear function of z and τ .

$$(D/G)_b = 0.097 + 0.68\,\tau + \{z - 60\}\{3.5 + 44\,\tau\} \times 10^{-3} \qquad 6.2$$

These calculations in the program were performed by subroutine RAT , (Appendix F). The blue sky radiation for the hour D_b , was then

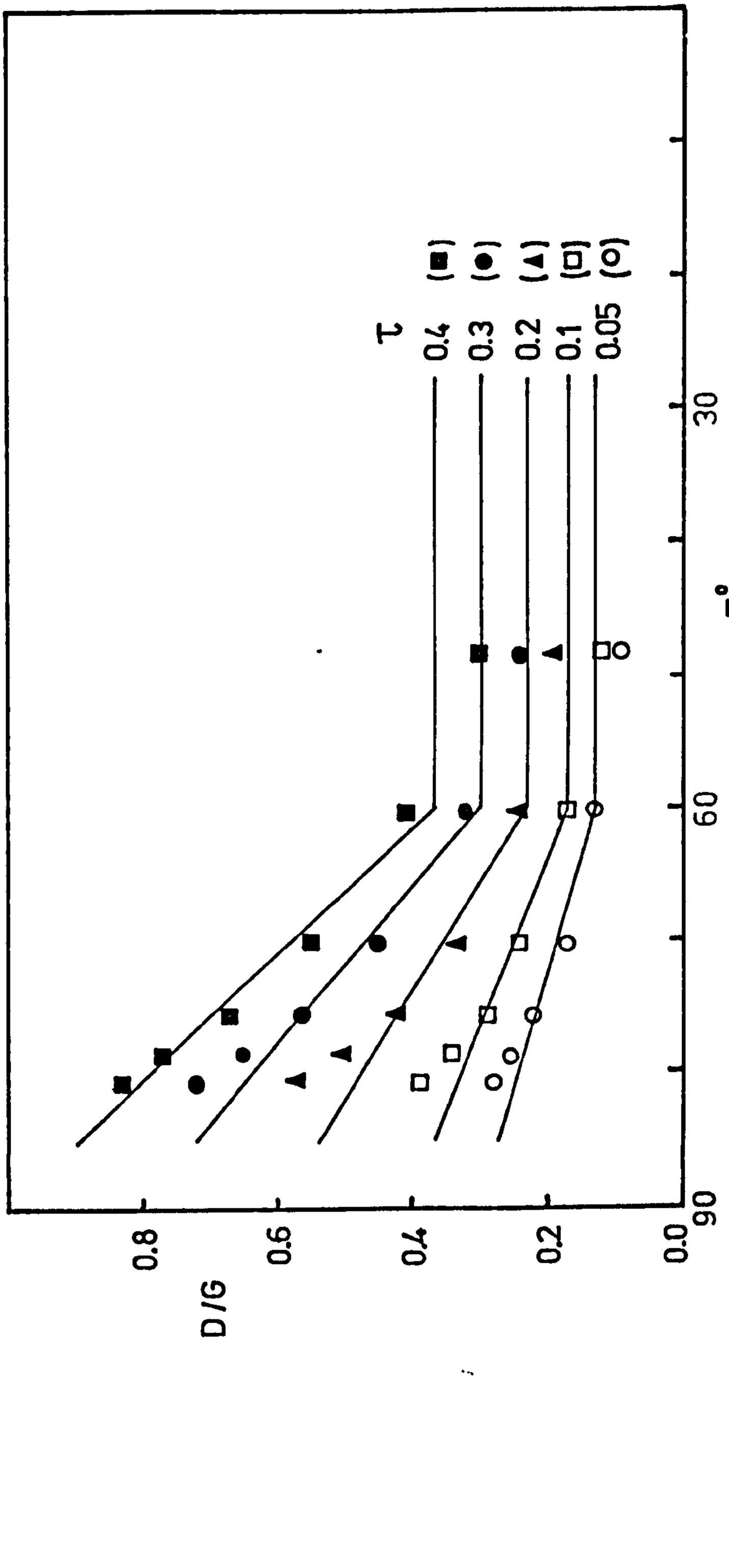

Fig. 6.1 The ratio D/G for cloudless skies as a function of z and τ. The plotted points are from Page (1975); the curves give the ratios used in the model.

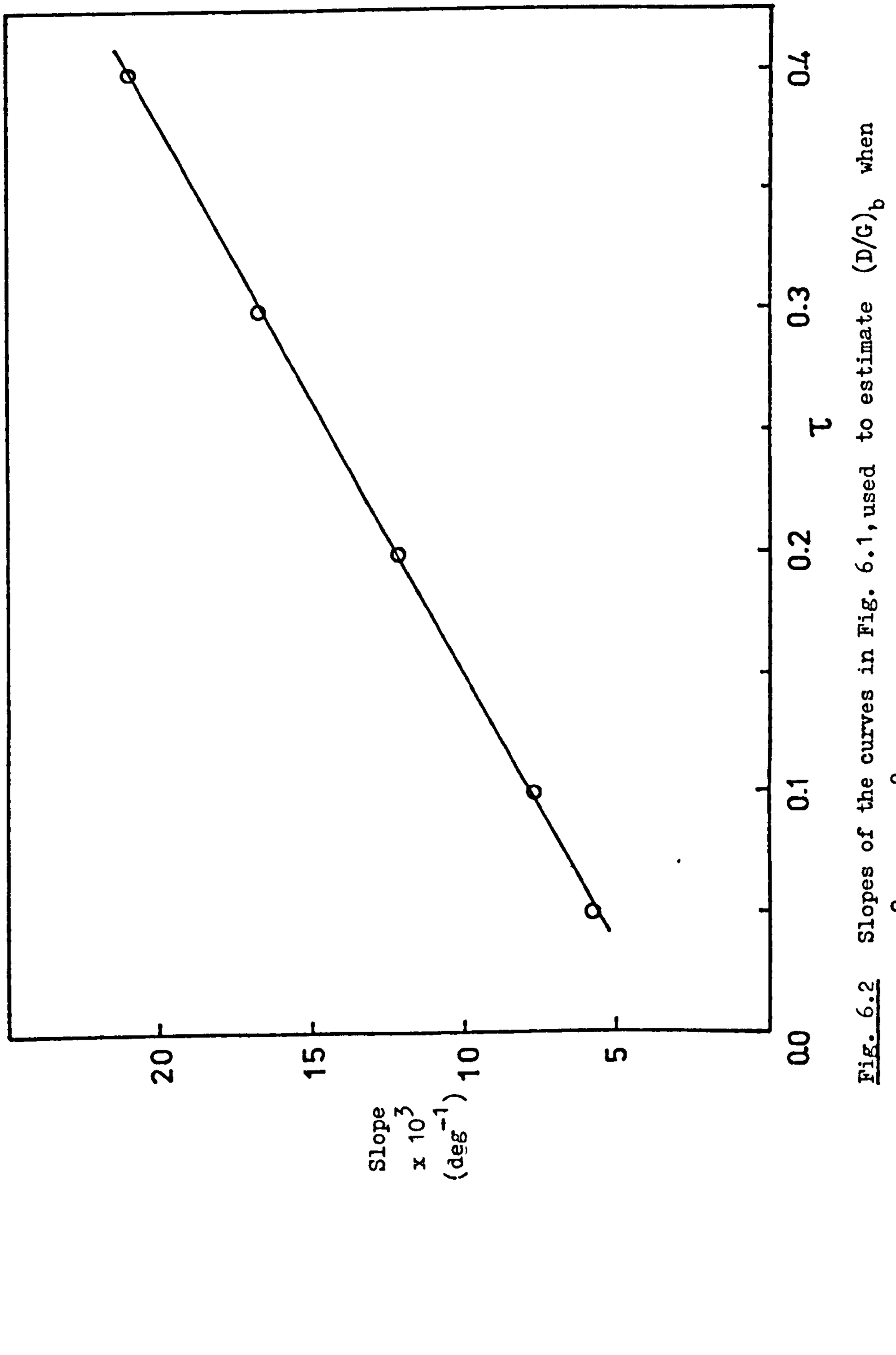

Fig. 6.2 Slopes of the curves in Fig. 6.1, used to estimate $(D/G)_b$ when $60^o < z < 85^o$.

estimated from B using

$$D_b/B = (D/G)_b/\{ 1 - (D/G)_b \} \qquad 6.3$$

The calculated value of D_b could not exceed D and since the monthly mean radiation data included both cloudy and blue sky radiation, the ratio D_b/D should in fact be considerably less than 1 . The ratio was arbitrarily prevented from exceeding 0.65 and the results of the model indicate that this condition only operated at low solar elevations when the uncertainties in the estimations were large. The value of D_g was taken as $D - D_b$.

Geometric conversion factors for each plane were calculated for the radiation components. The direct beam irradiance was calculated from I using standard trigonometrical relationships. The reflected radiation component was calculated assuming that the reflection was isotropic. The cloudy diffuse component was calculated in subroutine DIFF by assuming that the mean radiance distribution was similar to that of an overcast sky, linear in cos θ as found in Chapter V, Eq. 5.6, where θ is the zenith angle. The value of the coefficient β in Eq. 4.5 was 1.2, slightly lower than the mean for overcast skies but more appropriate for cloudy skies in general (Fig. 5.3(b)). The blue sky diffuse component on a sloping surface was calculated according to the model of Chapter III, section 3.4. A circumsolar component of radiation was calculated as a fraction s of D_b and was treated as a supplement to the direct beam. The remaining 'background diffuse' radiation was treated as if the radiance distribution were linear in cos θ with slope $\beta = -0.87$ used in Eq. 3.7 (Subroutine DIFF). The basic value of s , 0.51 was corrected for disparities in the shade

ring corrections according to the method of Chapter III, section 3.3. The diffuse radiation data supplied by the Meteorological Office contained a geometric correction calculated by Drummond's formula (Eq. 3.5), but no correction had been made for anisotropy. The value of s was therefore reduced using Eq. 3.9, for example to 0.43 in January when the anisotropy correction was largest and 0.48 in June when the overestimation of the geometric correction by Drummond's formula (Fig. 3.6) partly compensated for the missing correction for anisotropy.

6.3 Results of the Model

The model was applied to mean radiation data from four sites in Britain using representative values of the parameters ρ and τ. In all cases the value of ρ was 0.25, typical of grass and many other types of vegetation (Monteith, 1973). Unsworth and Monteith (1972) suggested ranges of turbidity τ in urban and rural Britain but their observations were biased towards cloudless conditions. McWilliams (1973) reported that at Valentia rainfall caused a reduction of about 30% in atmospheric aerosol and that the annual variation of turbidity closely paralleled the variation of rainfall. It was assumed for this study that partly cloudy conditions have lower turbidities than clear sky conditions and the mean values of Unsworth and Monteith were reduced towards the lower end of the ranges which they suggest. The values employed were 0.25 for Kew, 0.20 for Eskdalemuir, 0.15 for Aberporth and 0.15 for Lerwick and were constant throughout the year. Although there is evidence of seasonal variation in τ (Unsworth and Monteith, 1972; McWilliams, 1973), the mean values were not regarded as sufficiently well established for seasonal variation in the model to be justified.

The effect of using different values of turbidity is considered in Section 6.6.

A comparison was made between E and W facing surfaces at Kew. The differences in daily irradiation varied from month to month, both in magnitude and direction, but over the year E facing surfaces received more radiation, the differences being as much as 8% on vertical surfaces. About 2% of this difference may be due to errors in the estimation of irradiation at large values of z . The effect was predominantly due however to asymmetry in the mean diurnal variation of radiation at Kew. In all months values of B observed in the morning were larger than those in the afternoon. At the other sites this phenomenon was not so marked. For the purposes of this study the differences between E and W facing slopes were disregarded and the sloping surfaces selected for evaluation faced N , W and S .

Tables 6.1 to 6.4 give annual irradiation totals calculated by the model for inclined planes at each of the four sites facing S , W and N with tilt α of 30°, 60° and 90°. The contributions to the global irradiation by the four components in the model are also given. Tables 6.5 and 6.6 give the daily mean irradiation values of inclined planes at Kew for June and December respectively. The tabulated values indicate that the blue sky radiation is on average between about 1/5 and 1/3 of D depending on the site. The circumsolar component of D_b is a significant element in the global irradiation of slopes, in effect increasing the direct beam component by about 15 to 20%.

Table 6.1 Slope irradiation values for the year, GJ m^{-2}.
Kew - 51.5° N , 0.3° W , $\rho = 0.25$, $\tau = 0.25$.

Tilt α	Aspect	Beam	Blue sky	Cloud	Ground	Global
0°		1.40	0.64	1.24	0.00	3.27
30°	S	1.79	0.75	1.13	0.05	3.72
60°	S	1.73	0.73	0.85	0.20	3.52
90°	S	1.23	0.57	0.52	0.41	2.73
30°	W	1.24	0.63	1.13	0.05	3.06
60°	W	1.02	0.60	0.85	0.20	2.67
90°	W	0.71	0.47	0.52	0.41	2.11
30°	N	0.70	0.50	1.13	0.05	2.39
60°	N	0.18	0.39	0.85	0.20	1.63
90°	N	0.07	0.30	0.52	0.41	1.30

Table 6.2 Slope irradiation values for the year, GJ m^{-2}.
Aberporth - 51.5° N , 0.3° W , $\rho = 0.25$, $\tau = 0.15$.

Tilt α	Aspect	Beam	Blue sky	Cloud	Ground	Global
0°		1.72	0.51	1.63	0.00	3.86
30°	S	2.21	0.59	1.49	0.06	4.35
60°	S	2.14	0.57	1.13	0.24	4.08
90°	S	1.52	0.44	0.69	0.48	3.14
30°	W	1.61	0.51	1.49	0.06	3.67
60°	W	1.35	0.47	1.13	0.24	3.19
90°	W	0.94	0.37	0.69	0.48	2.48
30°	N	0.85	0.39	1.49	0.06	2.80
60°	N	0.20	0.30	1.13	0.24	1.87
90°	N	0.08	0.23	0.69	0.48	1.48

Table 6.3 Slope irradiation values for the year, GJ m^{-2}
Eskdalemuir - 55.3° N , 3.2° W , ρ = 0.25 , τ = 0.20.

Tilt α	Aspect	Beam	Blue sky	Cloud	Ground	Global
0°		1.09	0.43	1.40	0.00	2.92
30°	S	1.50	0.53	1.28	0.05	3.35
60°	S	1.53	0.54	0.97	0.18	3.22
90°	S	1.17	0.44	0.59	0.37	2.57
30°	W	0.99	0.43	1.28	0.05	2.75
60°	W	0.85	0.41	0.97	0.18	2.41
90°	W	0.61	0.33	0.59	0.37	1.90
30°	N	0.50	0.33	1.28	0.05	2.15
60°	N	0.13	0.26	0.97	0.18	1.54
90°	N	0.06	0.20	0.59	0.37	1.22

Table 6.4 Slope irradiation values for the year, GJ m^{-2}.
Lerwick - 60.1°N , 1.2° W , ρ = 0.25 , τ = 0.15 .

Tilt α	Aspect	Beam	Blue sky	Cloud	Ground	Global
0°		1.02	0.31	1.42	0.00	2.74
30°	S	1.40	0.38	1.29	0.05	3.12
60°	S	1.42	0.38	0.98	0.17	2.96
90°	S	1.09	0.31	0.60	0.34	2.34
30°	W	0.95	0.31	1.29	0.05	2.60
60°	W	0.82	0.30	0.98	0.17	2.27
90°	W	0.59	0.24	0.60	0.34	1.77
30°	N	0.45	0.23	1.29	0.05	2.02
60°	N	0.11	0.18	0.98	0.17	1.44
90°	N	0.06	0.14	0.60	0.34	1.14

Table 6.5 Daily mean slope irradiation values, MJ m^{-2} for Kew in June. $\rho = 0.25$, $\tau = 0.25$.

Tilt α	Aspect	Beam	Blue sky	Cloud	Ground	Global
0°		8.3	3.4	5.8	0.0	17.5
30°	S	8.2	3.3	5.3	0.3	17.1
60°	S	6.3	2.8	4.0	1.1	14.2
90°	S	2.9	1.8	2.5	2.2	9.4
30°	W	7.2	3.3	5.3	0.3	16.1
60°	W	5.6	3.0	4.0	1.1	13.7
90°	W	3.7	2.3	2.5	2.2	10.6
30°	N	6.1	3.1	5.3	0.3	14.8
60°	N	2.3	2.4	4.0	1.1	9.8
90°	N	0.9	1.7	2.5	2.2	7.3

Table 6.6 Daily mean slope irradiation values, MJ m^{-2} for Kew in December. $\rho = 0.25$, $\tau = 0.25$.

Tilt α	Aspect	Beam	Blue sky	Cloud	Ground	Global
0°		0.6	0.6	0.5	0.0	1.7
30°	S	1.7	1.1	0.5	0.0	3.3
60°	S	2.3	1.5	0.4	0.1	4.3
90°	S	2.4	1.4	0.2	0.2	4.3
30°	W	0.6	0.6	0.5	0.0	1.8
60°	W	0.6	0.6	0.4	0.1	1.7
90°	W	0.5	0.6	0.2	0.2	1.5
30°	N	0.0	0.3	0.5	0.0	0.9
60°	N	0.0	0.3	0.4	0.1	0.8
90°	N	0.0	0.3	0.2	0.2	0.7

6.4 Solar Energy Collectors

Investigations have been made by several authors of the optimum tilt and orientation of a solar energy collector, using a variety of different models for the diffuse radiation. Kern and Harris (1975) however pointed out that the optimum tilt depends on the use to which the energy is put. Their results, and the results of Szokolay (1975), indicate that the collector tilt can differ by 10° from the optimum value without seriously affecting the efficiency. Szokolay also showed that change in azimuth by as much as 50° from the optimum value reduced the collection of radiation by only 10%. To determine the slope receiving the most radiation over the year and on a month to month basis, the present model was applied to nine S facing planes tilted at 10° intervals from 10° to 90°. The irradiation of an equatorially mounted plane was also studied to determine the energy gained by tracking the sun through the day. The results shown in Table 6.7 give the ratios $G(\alpha)/G$ of collector irradiation values to

Table 6.7 Mean annual energy gain of solar collectors intercepting maximum radiation

Site	D/G	τ	tilt α	$G(\alpha)/G$	$G(z)/G$ (tracking)
Kew	0.57	0.25	35°	1.14	1.49
Aberporth	0.55	0.15	35°	1.13	1.41
Eskdalemuir	0.63	0.20	40°	1.16	1.45
Lerwick	0.63	0.15	35°	1.14	1.40

the global irradiation of a horizontal surface. The ratio for a tracking collector is also given. The results indicate that τ has a

particularly important effect on the ratio found for the tracking collector and is a major source of uncertainty. The energy gain of a tracking collector compared to the best fixed surface is about 25 to 30%, depending on the site.

Table 6.7 may be compared with the results of Szokolay (1975) who used a crude model based on hourly values of G at London. His model used the results of Loudon (1965) for clear skies to estimate the background diffuse radiation D' as a function of solar height. D' was assumed to be isotropic and the difference between measured values of D and D' was regarded as circumsolar radiation and left as part of the direct beam. Szokolay did not use the D' values of Loudon for partially cloudy skies because he found that these values nearly always exceeded the measured values of D and would have resulted in a negative component of circumsolar radiation. Szokolay's results indicated an optimum tilt of 34° which is in agreement with the present work, but the ratio $G(\alpha)/G$ was about 1.2 which is considerably larger.

An alternative method of increasing the radiation interception of a solar collector is to adjust the tilt to obtain the maximum energy on a month to month basis. The optimum tilt for each month at Kew, together with the irradiation of the tilted and the horizontal surfaces are shown in Table 6.8. Over the year the ratio $G(\alpha)/G$ of a surface with tilt adjusted to the monthly optimum was 1.19 and the relative gain of a tracking collector to this method was only about 25%.

Table 6.8 Monthly mean daily irradiation of solar collectors with optimum tilt at Kew, MJ m^{-2}.

Month	G	Optimum tilt α	G(α)	G(z) tracking
Jan	2.1	70°	4.5	4.9
Feb	3.7	60°	6.1	7.1
Mar	7.8	50°	10.6	13.5
Apr	11.1	30°	12.2	15.6
May	15.5	20°	15.9	21.5
June	17.5	10°	17.7	23.2
July	15.7	10°	15.9	20.1
Aug	13.5	25°	14.3	18.1
Sept	10.1	40°	12.4	15.3
Oct	5.8	55°	8.8	10.2
Nov	2.8	65°	5.3	5.8
Dec	1.7	75°	4.4	4.8

6.5 The Anisotropy of Reflected Radiation

The reflected component of radiation when $\rho = 0.25$ accounts for up to 1/3 of the global irradiance of vertical planes in Tables 6.1 to 6.4 and the simplistic model of isotropic reflection with a constant reflection coefficient (albedo) may be a serious source of error in irradiance estimates. Several authors have noted an increase in the albedo of certain surfaces with solar zenith angle z under clear sky conditions. Kondratyev (1969) reviewed results of measurements over snow and water surfaces and Geiger (1965) reported similar studies for sand. Few measurements have been made however of the anisotropy of the radiation reflected from natural surfaces. Actinometric measurements by Monteith and Szeicz (1962) over long grass indicated a complex pattern of radiation which varied both with zenith and azimuth. The maximum

reflection measured was in the direction away from the sun and towards the horizon, but this pattern is not typical of smooth surfaces and may not be typical of all vegetation.

Water surfaces are one case when the reflective properties are comparatively well known. Nunez et al (1972) measured the surface albedo of Lake Ontario and reviewed the reflection processes involved. The direct solar beam is reflected specularly by a smooth water surface according to the Fresnel formula for unpolarised light. The Fresnel reflection coefficient ρ_f is given by

$$\rho_f = \frac{1}{2} \left\{ \frac{\sin^2 (z - \zeta)}{\sin^2 (z + \zeta)} + \frac{\tan^2 (z - \zeta)}{\tan^2 (z + \zeta)} \right\} \qquad 6.4$$

where the angle of reflection ζ is related to z by Snell's Law : $\sin z / \sin \zeta = \mu$. The value of μ , the coefficient of refraction for fresh water is 1.33 . The reflection coefficient ρ_d for diffuse radiation may be calculated by integrating the Fresnel formula for all directions over the sky. Kondratyev (1969) reported that calculations of ρ_d for isotropic diffuse radiation gave a value of 0.066 and the corresponding calculated values for clear and lightly clouded skies using measured radiance distributions varied from 0.08 to 0.11. In addition, part of the radiation transmitted by the water surface is scattered back to the atmosphere by particles in the water. The coefficient of back scattering ρ_b depends on the turbidity of the water (Kondratyev, 1969), but the measurements of Nunez et al (1972) suggest that a mean value of 0.02 was appropriate for Lake Ontario. The effect of roughness of the water surface is not so well determined. The results of theoretical calculations given by Kondratyev (1969) suggest

that the albedo increases with roughness for small values of z and decreases for larger values ($z > 60^{o}$). Measurements by Nunez _et al_ however indicated that water roughness increases the albedo for all values of z and that otherwise the general pattern of behaviour with z remains the same.

The present model of reflection from water was based on a smooth surface with $\rho_b = 0.02$ and $\rho_d = 0.07$. The Fresnel coefficient ρ_f was calculated using Eq. 6.4. Appendix F gives the subroutine (FRESNEL) in which this was done but the rest of the program is for the version of the model with isotropic reflection. The reflected radiation was calculated as the sum of the specularly reflected direct solar beam and a diffuse component treated as isotropic which incorporated the reflected sky radiation and the backscattered radiation. Specular reflection is directional and has its maximum effect on planes facing the sun's reflected image in the water. The reflected irradiance of an inverted horizontal surface R(180) is given by Eq. 6.5 :

$$R(180) = \rho_f B + \rho_d D + \rho_b \{G - \rho_f B - \rho_d D\} \qquad 6.5$$

and the albedo ρ is $R(180)/G$. The circumsolar portion of D was reflected isotropically in this model. Also, since the model allows no direct solar beam radiation for $z > 85^{o}$, there was no specular reflection in the early morning or evening. Although irradiance values then are small the Fresnel reflection coefficient is large and this may be a serious source of error in the model. Both these practices will cause the specular component of reflection to be underestimated.

Measured values of the albedo of water are affected critically by the ratio D/G. For overcast skies, $D/G = 1$ and the value of ρ

is approximately 0.09. For clear skies the albedo depends strongly on atmospheric turbidity τ and Fig. 6.3 shows the variation of ρ with z as a function of τ using the relationships between D/G and τ described in Section 6.2. The albedo for Fresnel reflection alone is also shown. For values of z less than 40°, ρ is roughly constant. The predicted albedos in this model agree well with measured values given by Nunez et al (1972) and Kondratyev (1969) both for clear and overcast skies.

Daily and annual means of reflected radiation interception calculated for tilted planes adjacent to a water surface are given in Table 6.9 for the Kew data. The global irradiation is also given

Table 6.9 Global and reflected irradiation of planes adjacent to a water surface at Kew.

Tilt α	Aspect	June (MJ m^{-2} dy^{-1})		December (MJ m^{-2} dy^{-1})		Year (GJ m^{-2})	
		$G(\alpha)$	$R(\alpha)$	$G(\alpha)$	$R(\alpha)$	$G(\alpha)$	$R(\alpha)$
0°		17.49	0.00	1.68	0.00	3.27	0.00
30°	S	16.92	0.06	3.55	0.24	3.70	0.03
60°	S	13.32	0.23	4.77	0.58	3.43	0.12
90°	S	7.77	0.54	4.83	0.78	2.54	0.22
30°	W	15.96	0.14	1.79	0.06	3.04	0.04
60°	W	13.08	0.47	1.80	0.17	2.58	0.11
90°	W	9.28	0.83	1.53	0.25	1.89	0.19
30°	N	14.65	0.09	0.84	0.01	2.35	0.01
60°	N	9.10	0.35	0.72	0.03	1.48	0.06
90°	N	5.75	0.69	0.54	0.05	1.00	0.12
tracking collector		23.33	0.77	5.45	0.82	4.99	0.28

and the other components of radiation are the same as Tables 6.1, 6.5 and 6.6. Over the year the reflected radiation for a given tilt appears

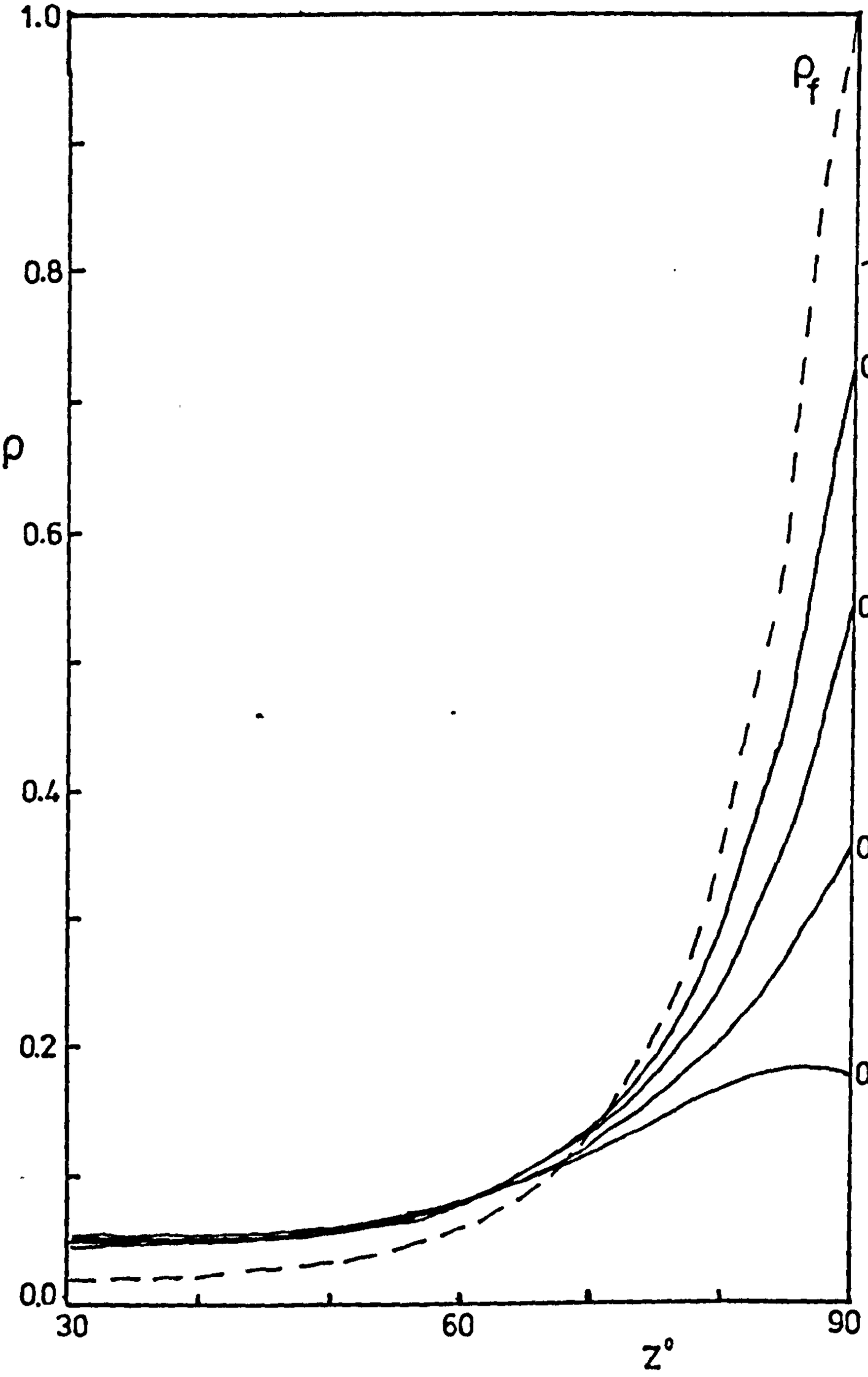

Fig. 6.3 The Fresnel coefficient of reflection ρ_f and the calculated albedo of a water surface as a function of z and τ.

to be roughly proportional to the global, the ratio $R(\alpha)/G$ being about 1%, 4% and 10% on 30°, 60° and 90° slopes respectively, independent of azimuth. Specular reflection is thus an important factor in the global irradiation of vertical planes but its effect on planes of less than 30° tilt is negligible. The Fresnel reflection coefficient increases sharply at larger values of z and absolute values of reflected radiation are greater on S facing planes in winter than in summer, in spite of lower values of B in winter. North facing planes receive more reflected radiation in summer than S facing planes. The results thus indicate that in the case of a water surface the anisotropy of reflection has an important bearing on the irradiance of steeper slopes and this may also be true for reflection by other types of surface.

6.6 Sensitivity Analysis

To measure the effect of uncertainties in the modelling of slope irradiance, parameters in the model were varied about their basic values. The tests were performed on Kew data with N , S and W facing surfaces and for the sun tracking collector. The parameters varied were turbidity τ ; the coefficient β_1 (β in Eq. 5.6) used to describe the distribution of cloud radiance; the coefficient β_2 (β in Eq. 3.7) used to model the radiance distribution of D' , the background part of D_b ; and s , the proportion of circumsolar radiation in D_b . When any one parameter was changed the others were held at their basic values. An additional test was done using the irradiation values for partly cloudy skies (Chapter V, Section 5.4) for the diffuse radiation. Finally, a comparison was made with the results of a simple irradiation

model where the diffuse radiation was treated as isotropic. The effect of different values of ρ in the present model can be found using Tables 6.1 to 6.6 and the problem of anisotropic reflection was considered separately in Section 6.5.

The value of τ is used to partition the mean values of D into blue sky and cloud radiation according to Eqs 6.1 to 6.3. This has an important effect on the irradiance of slopes, particularly those facing the sun, due to the modelling of blue sky radiation as the sum of a circumsolar and a background component. However when τ was increased from 0.25 to 0.30, the estimated annual irradiation changed by a maximum of +2% on S facing slopes and on the tracking collector. There was little effect on other surfaces. The change in τ had a negligible effect on irradiation estimates for June, but for December the values changed by +5% on S facing and tracking planes and -5% on the N facing plane with tilt $\alpha = 30^{\circ}$.

The value of s determines the circumsolar fraction of D_b that is treated as part of the direct beam. It is sensitive to errors in shade ring corrections and the value of s in the model was adjusted monthly for these (Section 6.2). When s was reduced by 0.06 the effect over the year was small. The greatest changes in irradiation estimates were +2% on N facing slopes. The effect in June was similar to the yearly pattern but deviations were about twice as large in December, amounting to -3% on S facing slopes and the tracking collector, and +4% on N facing slopes.

The value of β_2 determines the slope of the radiance distribution with zenith angle for the background component of blue sky radiation, Eq. 3.7. When this was changed from - 0.87 to - 0.6 the net effect

over the year in estimates of irradiation was a decrease, -1% to -2% on steeper slopes. The disparity was slightly greater in December amounting to -5% on N facing slopes.

The diffuse radiation D_g from clouds was evaluated using the isotropic ($\beta_1 = 0$) and the standard overcast assumptions ($\beta_1 = 2$). The changes in irradiation estimates were a maximum on vertical surfaces. When D_g was treated isotropically these changes ranged from +4% to +8% over the year, the differences being somewhat larger in June than in December. With the standard overcast assumption the differences were -2% or less for all slopes.

The present model implicitly assumes that partly cloudy skies can be represented by a combination of clear sky and overcast conditions. To investigate the validity of this assumption the diffuse irradiance of planes was estimated from D using the values of $D(\alpha, \psi)/D$ for 5 to 6 oktas of cloud (Table 5.7). No separation of blue sky from cloud was done. The diffuse irradiance values are only valid for daily averages so the effect on the tracking collector which moves during the day, cannot be assessed. Over the year the irradiation of planes of all orientations decreased, the difference being -5% on vertical surfaces. The differences in December however were -20% to -25% on S facing planes and +20% on the N facing plane with $\alpha = 30^{\circ}$. In June the differences were smaller, about -2% for most planes facing N and W and +2% to + 4% for those facing S .

The results of the model were compared with results obtained assuming that all the measured diffuse radiation was isotropically distributed, with no separation into blue sky and cloud. Over the year

the simple model predicted 10% more radiation on the steeper N facing slopes, 5% less on S facing slopes and 8% less for the tracking collector. In December differences from the present model were as large as +27% on N facing slopes and -25% on S facing slopes and on the tracking collector. In June the differences were not so marked, but still as high as +6% on the N facing slope with $\alpha = 90^{o}$.

6.7 Concluding Remarks

The model of the irradiation of slopes brings together the findings of this study and may be used to assess the importance of different factors in the irradiation of inclined surfaces. The results of Section 6.6 indicate that the present model is a considerable improvement on the simple method, commonly used to estimate slope irradiance, of assuming that the diffuse radiation is isotropic,

The results of the model are relatively insensitive to small changes in the parameters. There is however considerable uncertainty in the mean value of τ and this may affect the estimates of irradiance of planes facing the sun. Also, the comparison using diffuse irradiation estimates based on partly cloudy skies indicate that these conditions are only approximately represented by combining clear sky and overcast conditions. However the mean radiation data used included both clear sky, overcast and partly cloudy conditions so the estimation of mean irradiation will not be greatly affected. The sensitivity analysis allows a rough estimate of the overall accuracy of the calculated irradiation values. Since the model uses radiation data on a horizontal surface the uncertainty on slopes with $\alpha < 30^{o}$ is minimal. Over the year the model probably evaluates the irradiation of steeper slopes to

±5%, within the limits of accuracy of the basic data. Monthly values, particularly in winter are somewhat more uncertain.

There are several areas, in the context of slope irradiance, in which future research would be useful. A closer description of the radiance distribution of partly cloudy skies would help to reduce uncertainties in the modelling of diffuse radiation. Shade ring corrections for measurements of D under cloudy skies should be studied in more detail. Accurate estimations of the mean irradiation of sloping surfaces may also require analysis of the frequency distribution of different types of sky conditions and different turbidities. Finally, reflected radiation is an important part of the radiation intercepted by inclined surfaces, and a study of the anisotropy of reflection by various natural surfaces would make a useful contribution to the estimation of the irradiance of steeper slopes.

REFERENCES

ANDERSON, M.C. 1967 The role of heat transfer in the design and performance of solarimeters. J. appl. Met., 6, 941-947.

ANDERSON, M.C. 1970 Interpreting the fraction of solar radiation available in forest. Agric. Met., 7, 19-28.

ARNOLD, G.P. 1975 The measurement of irradiance with particular reference to marine biology. In Evans, G.C., Bainbridge, R. and Rackham, O. Light as an ecological factor : II., 1-26, Blackwell Scientific Publications, Oxford.

BENER, P. 1950 Untersuchung über die Wirkungsweise des Solarigraphen Moll-Gorczynski. Arch. Met. Geoph. Biokl., B2, 188-249.

BENER, P. 1963 Der Einfluss der Bewölkung auf die Himmelsstrahlung. Arch. Met. Geoph. Biokl., B12, 442-457.

BLACKWELL, M.J. 1954 Five years continuous recording of total and diffuse solar radiation at Kew observatory. Air Ministry Res. Comm., London, M.R.P. No. 895.

BRINKWORTH, B.J. 1972 Solar energy for man. Compton Press, Salisbury.

BULLRICH, K. 1964 Scattered radiation in the atmosphere and the natural aerosol. Adv. Geoph., 10, 99-260.

COLLINGBOURNE, R.H. 1975 The United Kingdom solar radiation network and the availability of solar radiation data from the meteorological office for solar energy applications. International Solar Energy Society, UK Section. Proc. Conf. UK meteorological data and solar energy applications, 2-17, London, February 1975.

DINES, W.H. and DINES, L.H. 1927 Monthly mean values of radiation from various parts of the sky at Benson, Oxfordshire. Mem. Roy. Met. Soc., 11, 1-8.

DOGNIAUX, R. 1954 Etude du climat de la radiation en Belgique. Inst. Roy. Met. Belg., Contr. No. 18.

DOGNIAUX, R. 1975 Variations geographiques et climatiques des expositions energetiques solaires sur des surfaces receptrices horizontales et verticales. Inst. Roy. Met. Belg., Misc. ser. B, no. 38.

DRUMMOND, A.J. 1956 On the measurement of sky radiation. Arch. Met. Geoph. Biokl., B7, 413-436.

EBERT, H. 1967 Physics pocketbook. Oliver and Boyd, Edinburgh.

FUQUAY, D. and BUETTNER, K. 1957 Laboratory investigation of some characteristics of the Eppley pyrheliometer. Trans. Am. Geoph. Union, 38, 38-43.

GARNIER, B.J. and OHMURA, A. 1968 A method of calculating the direct short-wave income of slopes. J. appl. Met., 7, 796-800.

GARNIER, B.J. and OHMURA, A. 1970 The evaluation of surface variations in solar radiation income. Solar Energy, 13, 21-34.

GEIGER, R. 1965 The climate near the ground. Harvard Univ. Press, Cambridge Mass., U.S.A.

GOUDRIAAN, J. 1977 Crop micrometeorology : a simulation study. Centre for Agricultural Publishing and Documentation, Wageningen, the Netherlands.

GRACE, J. 1971 The directional distribution of light in natural and controlled environment conditions. J. appl. Ecology. 8, 155-164.

HEYWOOD, H. 1966 The computation of solar radiation intensities : Part 2 Solar radiation on inclined surfaces. Solar Energy, 10, 46-52.

HEYWOOD, H. 1970 A general equation for calculating total radiation on inclined surfaces. International Solar Energy Society Conference, Paper no. 3/21, Melbourne - Australia, 2-6 March 1970.

HOPKINSON, R.G. 1954 Measurements of sky luminance distribution at Stockholm. J. Opt. Soc. Am., 44, 455-459.

KALMA, J.D. and FLEMING, P.M. 1972 A note on estimating the direct and diffuse components of global radiation. Arch. Met. Geoph. Biokl., B20, 191-205.

KERN, J. and HARRIS, I. 1975 On the optimum tilt of a solar collector. Solar Energy, 17, 97-102.

KIMBALL, H.H. and HAND, I.F. 1921 Sky-brightness and daylight-illumination measurements. Mon. Weath. Rev., 49, 481-488.

KIMBALL, H.H. and HAND, I.F. 1922 Daylight illumination on horizontal, vertical and sloping surfaces. Mon. Weath. Rev., 50, 615-628.

KONDRATYEV, K.Y. 1969 Radiation in the atmosphere. Academic Press, London.

KONDRATYEV, K.Y. and FEDORORA, M.P. 1976 Radiation regime of inclined surfaces. UNESCO/WMO Solar Energy Symposium, Eng. S/Doc. 2, Geneva, 30 August- 3 September 1976.

KONDRATYEV, K.Y. and MANALOVA, M.P. 1960 The radiation balance of slopes. Solar Energy, 1 14-19.

LECARPENTIER, M. 1974 Developpement d'un procede numerique pour le calcul automatique des pentes et de leur insolation. McGill Univ. Climat. Bull., 15, 1-10.

LIU, B.Y.H. and JORDAN, R.C. 1960 The interrelationship and characteristic distribution of direct, diffuse and total solar radiation. Solar Energy, 4, 1-19.

LIU, B.Y.H. and JORDAN, R.C. 1961 Daily insolation on surfaces tilted towards the equator. ASHRAE J., 3, 53-59.

LOUDON, A.G. 1965 The interpretation of solar energy measurements for building problems. CIE, Proc. Conf. Sunlight in Buildings, 111-118, Newcastle.

MANTELL, C.L. 1960 Electrochemical engineering. McGraw Hill, New York.

McCARTNEY, H.A. 1975 Spectral distribution of solar radiation within and above crops. Ph.D. thesis, Nottingham Univ.

McCREE, K.J. 1972 Tests of current definitions of PAR against leaf photosynthesis data. Agric. Met., 10, 443-453.

McWILLIAMS, S. 1973 Atmospheric turbidity at Valentia observatory. Irish Met. service, Tech. note 36.

METEOROLOGICAL OFFICE 1956 Observers Handbook. HMSO, London.

MOLL, W.J. 1923 A thermopile for measuring radiation. Proc. Phys. Soc., 35, 257-260.

MONTEITH, J.L. 1959 Solarimeter for field use. J. Sci. Instrum., 36, 341-346.

MONTEITH, J.L. 1973 Principles of environmental physics. Edward Arnold, London.

MONTEITH, J.L. and SZEICZ, G. 1962 Radiative temperature in the heat balance of natural surfaces. Quart. J. Roy. Met. Soc., 88, 496-507.

MOON, P. and SPENCER, D.E. 1942 Illumination from a non-uniform sky. Trans. Illum. Engng. Soc. N.Y., 37, 707-726.

NAG 1975 NAG library manual : Mark 5. Numerical Algorithms Group, Oxford.

NORRIS, D.J. 1966 Solar radiation on inclined surfaces. Solar Energy, 10, 72-76.

NUNEZ, M., DAVIES, J.A. and ROBINSON, P.J. 1972 Surface albedo at a tower site in Lake Ontario. Boundary Layer Met., 3, 77-86.

OHMURA, A. 1970 The influence of the skyline on the incidence of direct short wave radiation. McGill Univ. Climat. Bull., 7, 17-24.

PAGE, J.K. 1975 Supplementary note on values of D/K↓ on cloudless days for solar altitudes below 30°. Int. Solar Energy Soc., U.K. Sect. Proc. Conf. UK meteorological data and solar energy applications, 37-39, London, February 1975.

PAGE, J.K. 1976 The estimation of monthly mean values of daily short wave radiation on vertical and inclined surfaces from sunshine records for latitudes 60°N to 40°S. Univ. of Sheffield, Dept. of Bldg. Sci., Rep. no. BS32.

PARMALEE, G.V. 1954 Irradiation of vertical and horizontal surfaces by diffuse solar radiation from cloudless skies. Trans. Am. Soc. Heat. Vent. Engrs, 60, 341-358.

PETHERBRIDGE, P. 1965 Sunpath diagrams and overlays for solar heat gain calculations. Bldg. Res. Curr. Papers, Res. Ser. 39 with supplement.

PEYRE, J. 1927 Mesure de la brillance du ciel diurne - répartition de la lumière sur la voute céleste. Revue d'Optique, 6, 73-80.

POKROWSKI, G.I. 1929 Über einer scheinbaren Mie-Effect und seine mögliche Rolle in der Atmosphärenoptik. Z. Phys., 53, 67-71.

RAYLEIGH, Lord (J.W. Strutt) 1871 On the light from sky, its polarisation and colour. Phil. Mag., 41, 107-120.

RAYLEIGH, Lord 1899 On the transmission of light through an atmosphere containing small particles in suspension and on the origin of the blue of the sky. Phil. Mag., 47, 375-384.

ROBINSON, N. 1966 Solar radiation. Elsevier, Amsterdan - The Netherlands.

RUTH, D.W. and CHANT, R.E. 1976 The relationship of diffuse radiation to total radiation in Canada. Solar Energy, 18, 153-154.

SCHMID, W. 1976 Aufbereitung und Qualitätskontrolle langjähriger Messunterlagen der Globalstrahlung und Himmelsstrahlung. Swiss Met. Inst., Working Rep. no. 59.

STAGG, J.M. 1947 Solar radiation at Kew observatory. Air Ministry Res. Comm., London, M.R.P. no. 372.

STEVEN, M.D. 1977 Standard distributions of clear sky radiance. Quart. J. Roy. Met. Soc., 103, 457-465.

SZOKOLAY, S.V. 1975 Solar energy and building. The Architectural Press, London.

TEMPS, R.C. and COULSON, K.L. 1977 Solar radiation incident upon slopes of different orientations. Solar Energy, 19, 179-184.

THEKAEKARA, M.P. 1976 Solar radiation measurement : techniques and instrumentation. Solar Energy, 18, 309-326.

THRELKELD, J.L. 1963 Solar irradiation of surfaces on clear days. ASHRAE Trans., 69, 24-36.

TONNE, F. and NORMANN, W. 1960 Die Berechnung der Sonnenwärmestrahlung auf senkrechte und beliebig geneigte Flächen unter Berücksichtigung meteorologischer Messungen. Z. Met., 14, 166-179.

UKISES 1976 Solar energy, a UK assessment. International Solar Energy Society, UK Section, London.

UNSWORTH, M.H. and MONTEITH, J.L. 1972 Aerosol and solar radiation in Britain. Quart. J. Roy. Met. Soc., 98, 778-797.

UNSWORTH, M.H. and MONTEITH, J.L. 1975 Long wave radiation at the ground, I. Quart. J. Roy. Met. Soc., 101, 13-24.

VALKO, P. 1969 Short wave irradiation of cylindrical and rectangular bodies. Swiss Met. Inst., Working Rep. no. 14.

VALKO, P. 1970 Radiation load on buildings of different shape and orientation under various climatic conditions. In Building Climatology. WMO Tech. Note 109, 87-109.

VALKO, P. 1975 Solar radiation impact on buildings of different shape and orientation. Meteoplan 1, Hallwag, Berlin.

VALKO, P. 1976 Meteorologische Daten zur Sonnenenergienutzung. German Solar Energy Soc., Symp. Solar Engng., 22 October 1976, Stuttgart-Fellbach.

WALSH, J.W. 1961 The science of daylight. MacDonald, London.

WILSON, W.M. and EPPS, T.D. 1920 The construction of thermopiles by electrodeposition. Proc. Phys. Soc., 29, 326-340.

APPENDIX A

Fitted Functions for Clear Sky Distributions of Relative Radiance

The mean distributions of normalised radiance of clear skies, Table 2.1, were fitted by Eqs 2.5 and 2.6 as described in Chapter II. The equations were given by

$$N(\theta,\xi) = \{c_1 + c_2 \exp(c_3 \xi) + c_4 \cos^2 \xi\} \{1 - \exp(c_5 \sec \theta)\} \qquad 2.5$$

$$N(\theta,\phi) = \sum_{i=1}^{10} d_i f_i(\theta,\phi) + d_{11} \exp(-d_{12} \sin \xi) \qquad 2.6$$

The coefficients c_i are given in Table A1, the functions f_i in Table A2 and the coefficients d_i in Table A3.

The uncertainties given with the coefficient values in Tables A1 and A3 are standard errors. Some of the coefficient values are not significantly different from 0, but they are included because of correlations with the other coefficients. If the insignificant values were omitted, the optimum values of the other parameters would change.

Table A1. Coefficients for use with Eq. 2.5

z	35°	45°	55°	65°
c_1	0.61 ± 0.02	0.65 ± 0.02	0.73 ± 0.02	0.76 ± 0.03
c_2	11.91 ± 0.62	10.77 ± 0.53	11.12 ± 0.40	12.95 ± 0.49
c_3	- 2.97 ± 0.09	- 2.82 ± 0.06	- 2.97 ± 0.06	- 3.09 ± 0.07
c_4	- 0.12 ± 0.16	- 0.02 ± 0.11	0.07 ± 0.06	0.17 ± 0.05
c_5	- 0.45 ± 0.03	- 0.48 ± 0.03	- 0.48 ± 0.02	- 0.42 ± 0.02

Table A2. Functions for use with Eq. 2.6.

f_1	1.0
f_2	$\sin\theta \cos\phi$
f_3	$\cos\theta$
f_4	$\sin^2\theta \cos 2\phi$
f_5	$\sin\theta \cos\theta \cos\phi$
f_6	$\{3\cos^2\theta - 1\}/2$
f_7	$\sin^3\theta \cos 3\phi$
f_8	$\sin^2\theta \cos\theta \cos 2\phi$
f_9	$\sin\theta \cos\theta \{5\cos^2\theta - 1\}$
f_{10}	$\{5\cos^3\theta - 3\cos\theta\}/2$

Table A3. Coefficients for use with Eq. 2.6

z	35°	45°	55°	65°
d_1	1.1 ± 0.5	1.0 ± 0.5	0.4 ± 0.05	1.6 ± 0.5
d_2	0.12 ± 0.09	0.7 ± 0.1	0.9 ± 0.2	1.5 ± 0.2
d_3	-2.6 ± 0.7	-0.7 ± 0.9	0.7 ± 0.9	-1.6 ± 0.9
d_4	0.04 ± 0.04	0.26 ± 0.04	0.38 ± 0.05	0.42 ± 0.06
d_5	-0.04 ± 0.3	-0.5 ± 0.4	-0.7 ± 0.5	-2.0 ± 0.4
d_6	1.4 ± 0.5	-0.04 ± 0.7	-1.3 ± 0.7	0.2 ± 0.6
d_7	0.01 ± 0.01	0.04 ± 0.02	0.09 ± 0.02	0.12 ± 0.02
d_8	-0.1 ± 0.1	-0.3 ± 0.1	-0.3 ± 0.1	-0.32 ± 0.08
d_9	-0.16 ± 0.05	0.01 ± 0.06	0.006 ± 0.07	0.19 ± 0.07
d_{10}	-0.6 ± 0.2	0.06 ± 0.2	0.6 ± 0.2	0.1 ± 0.2
d_{11}	5.6 ± 0.6	5.8 ± 0.3	7.0 ± 0.5	9.8 ± 0.8
d_{12}	2.3 ± 0.5	3.9 ± 0.6	4.4 ± 0.6	5.2 ± 0.5

APPENDIX B

Cloudless Sky Corrections for Narrow Shade Rings

For narrow shade rings $(b/r < 0.2)$, the shade ring correction factor K can be calculated using the relation

$$K = 1/\{1 - q\, f\} \qquad B1$$

The factor f is given approximately by Drummond's formula, Eq. 3.5

$$f = \frac{2b}{\pi r} \cos^3 \delta \left\{\sin L \sin \delta\, t_o + \cos L \cos \delta \sin t_o\right\} \qquad 3.5$$

and q is the ratio of the irradiance from the obscured section of sky to the corresponding irradiance from an isotropic sky. For narrow shade rings q is relatively independent of b and r and the values may be found by a line integral approximation (Eq. 3.4). This was done numerically as described in Chapter III.

The values of q were found to be almost independent of z for $z = 65^\circ$, 55° and 45° but were significantly larger for $z = 35^\circ$. Tables B1 and B2 give values of q for the 15th of every month at latitudes 0° to 60° for large and for small zenith angles. Shade ring corrections can be calculated by substituting q values from the tables together with f from Eq. 3.5 into Eq. B1. Southern hemisphere corrections may be made by adding 6 months to the date. The tabulated values of q are accurate to $\pm$ 0.1 and calculated K values will be accurate to $\pm$ 0.01 so long as $b/r < 0.2$. The values do not account for circumsolar radiation within a 5° radius of the sun, which is in effect considered to be part of the direct solar beam.

Table B1. Values of q for $z > 40^{\circ}$

Latitude ($^{\circ}$N)	0	10	20	30	40	50	60
Date							
15/1	1.4	1.6	1.9	2.3	3.2		
15/2	1.3	1.4	1.5	1.8	2.3	3.2	
15/3	1.2	1.3	1.3	1.5	1.7	2.1	2.8
15/4	1.2	1.2	1.2	1.3	1.4	1.5	1.8
15/5	1.3	1.3	1.2	1.2	1.3	1.3	1.5
15/6	1.4	1.3	1.2	1.2	1.2	1.3	1.4
15/7	1.4	1.3	1.2	1.2	1.2	1.3	1.4
15/8	1.3	1.2	1.2	1.2	1.3	1.4	1.6
15/9	1.2	1.2	1.3	1.4	1.5	1.7	2.1
15/10	1.2	1.3	1.4	1.6	1.9	2.5	
15/11	1.3	1.5	1.7	2.1	2.7		
15/12	1.4	1.6	1.9	2.5	3.5		

Table B2. Values of q for $z \leq 40^{\circ}$

Latitude ($^{\circ}$N)	0	10	20	30	40	50
Date						
15/1	1.6	1.9				
15/2	1.4	1.6	1.9			
15/3	1.2	1.3	1.5	1.8		
15/4	1.3	1.2	1.3	1.4	1.6	
15/5	1.5	1.3	1.2	1.3	1.4	1.6
15/6	1.6	1.4	1.3	1.2	1.3	1.4
15/7	1.6	1.4	1.3	1.2	1.3	1.5
15/8	1.4	1.3	1.2	1.3	1.5	
15/9	1.2	1.2	1.4	1.6		
15/10	1.3	1.4	1.7			
15/11	1.5	1.8				
15/12	1.6	2.0				

APPENDIX C

Thermopile construction

The thermopile shown schematically in Fig. 4.1 was made by winding 50 s.w.g. constantan wire around a Tufnol former, 36 mm square and 3 mm thick. The two ends of the wire were soldered to short pins and the wire was turned around a similar pin in the centre of the former to reverse the position of the hot and cold junctions. This procedure left a gap of 4 mm in the centre of the thermopile which is the reason for the stepped nature of the angular response functions in Fig. 4.4. In most of the thermopiles there were 60 windings on each half.

The junctions were formed by selective copper plating. Nail varnish was painted across the windings in a central strip 10 mm wide and the remaining exposed wire was copper plated after the method of Wilson and Epps (1920) and Monteith (1959). Standard data for copper plating from Mantell, (1960) are given in Table C1. Mantell also suggested that the solution should be agitated. For a hard deposit on the cathode the formation of small crystals from many nucleating centres is preferred to the growth of crystals from a few nuclei. Too low a current density favours the growth of single crystals producing a brittle deposit, whereas too high a current density favours the growth of dendritic crystals due to ion depletion at the cathode (Mantell, 1960).

The plating solution had 100 g/l of copper sulphate and 25 g/l of sulphuric acid. To prevent different rates of plating on different sections of the wire, the cathode resistance was lowered by placing a contact wire across the windings. Most of the thermopiles were plated at 36 ma (20 ma cm^{-2}) for 27 minutes to provide a copper coating with cross sectional area 0.6 of that of the wire.

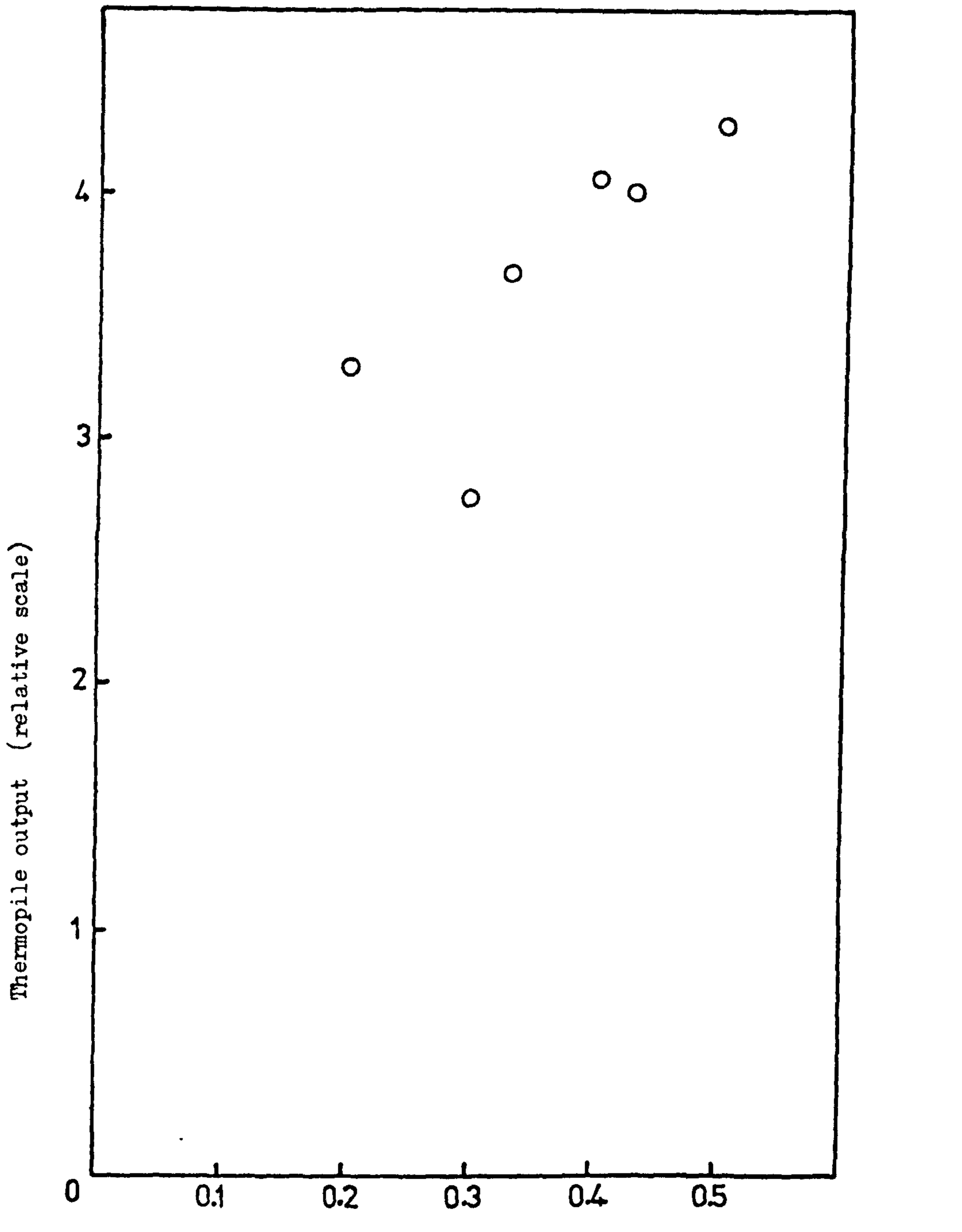

Fig. C.1 Thermopile sensitivity as a function of plating thickness.

Table C1. Recommended data for copper plating from Mantell (1960).

Bath composition	180 - 230 g/l $Cu\ SO_4.5\ H_2O$
	28 - 70 g/l $H_2\ SO_4$
Temperature	20 - 50 °C
Voltage	< 6 V
Current Density	23 - 110 ma cm^{-2}
Cathode efficiency	95 - 100 %

It was very difficult to control the plating quality and many of the wires showed patchy plating (Fig. 4.3), although they were thoroughly cleaned before plating. It was assumed that any additional junctions formed in this way would have no serious effect since the temperature difference developed between junctions depends on the painted surface. When the thermopiles were complete with their surfaces painted, tests were made of their relative sensitivity. Sensitivity generally increased with plating thickness as shown in Fig. C.1. The scatter can be attributed to differences in plating quality.

After plating, the nail varnish masking was removed and the thermopile was coated in vinyl for protection. The top surface was then painted in the form shown in Fig. 4.1(b) using 'Nextel velvet coatings' manufactured by 3M; type 101 A10 for the white and 101 C10 for the black. These paints were chosen for their optical and thermal properties, in particular for their matched emittances in the infra red and their similar thermal conductivities. The important physical properties of the materials used in thermopile construction are given in Table C2.

Table C2. Physical properties of thermopile materials

(a) Optical properties of Nextel paints 101 C10 (Black) and 101 A10 (White) from manufacturer's data.

	Black	White
Total reflectance	< 2½%	> 85%
Solar absorption	0.98	0.21
Infrared emittance at 25°C	0.89	0.88
Infrared reflectance		
· 700 - 1400 nm	½%	
1400 - 2500 nm	2%	
400 nm		60%
500 nm		85%
600 nm		90%
800 nm		88%
1000 nm		82%
1500 nm		70%
2000 nm		65%
2600 nm		50%

(b) Thermal conductivities of thermopile materials, W m^{-1} K^{-1}

Tufnol	0.19
Paint (black)	0.29
Constantan	22
Copper	403
Air	0.025

Note : 3M would not commit themselves in writing on the thermal conductivity of the white paint, but it should be similar to the black as the paints have, except for pigment, the same composition.

APPENDIX D

Construction of the Instrument Body

The body of the instrument was machined out of aluminium. The design is shown in longitudunal section in Fig. D.1. The outer filter collar and the instrument base screwed into the tube. The inner filter collar made a sliding fit into the base and was held by a thin layer of silicone rubber compound SR300. The same compound was used to hold the glass filters in place and to seal all the holes and cracks at the joints. Schott glass WG395 with a transmission factor of 0.93 for wavelengths between 350 and 2800 nm was used for the filters. Two holes were drilled in the base for wiring to the thermopile. A third hole was made in some of the instruments to attach a bottle of silica gel via a short tube. Diodes were inserted into three of the instruments to act as temperature sensors. They had a temperature coefficient of -2.1 mV $^{o}C^{-1}$ and in field operation they were attached to a 25V regulated power supply.

All parts of the instrument were thoroughly dried by heating in an oven. The instrument was then filled with dry air in a cold room at -20 ^{o}C and sealed. The whole surface except for the outer glass filter was insulated with 4 mm of polystyrene foam and covered with aluminised Melanex film for weatherproofing and radiation shielding.

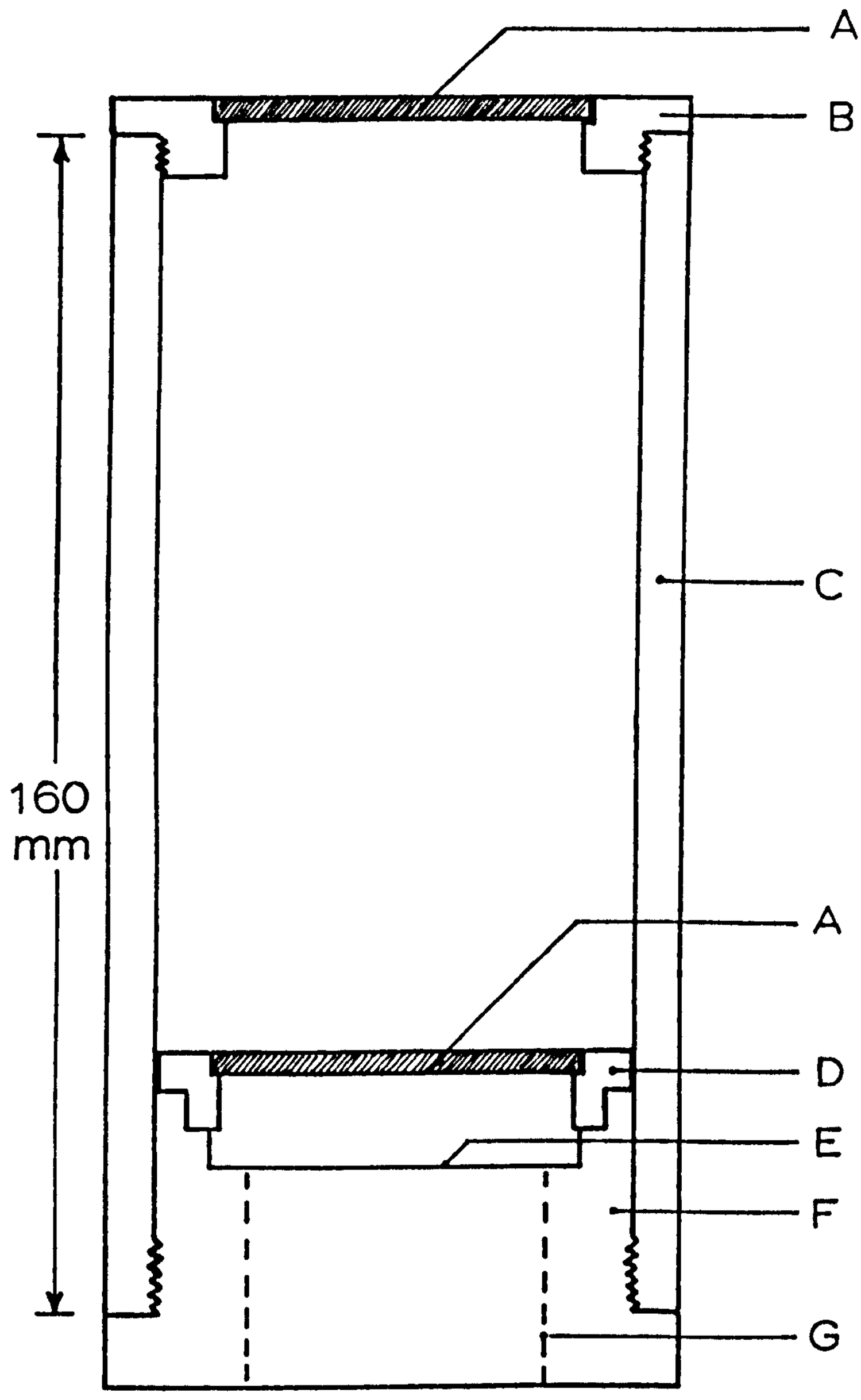

Fig. D.1 Longitudinal section through the actinometer body.

A - Glass filters
B - Outer filter collar
C - Tube
D - Inner filter collar
E - Thermopile
F - Instrument base
G - 1 mm diameter hole for wiring

APPENDIX E

Instrument Calibrations and Field Operation

The calibration procedures were discussed in Chapter IV, Section 4.6(a) and the organisation of the field site was described in Section 4.7. Table E1 gives the calibration values of the actinometers and Table E2 gives their orientations in the field. Actinometer no. II was only used in April 1977 for a limited series of measurements and consequently the calibration value adopted for this was the 1977 value. In most other cases a mean value was adopted. The thermopile in instrument no. III was changed in February 1977 and the adopted value is for measurements before this date. Later measurements used the 1977 calibration.

Table E3 gives the calibration values used for the Kipp solarimeters on the Meteorological site. The sensitivity of solarimeter no. CM5-690254 was measured in October 1977 and is about 5% higher than the original calibration of 1969. There are no records of any calibration done on this instrument since 1970. The new calibration however gives closer agreement with irradiance estimates based on measured radiance distributions (Chapter V).

Table E1 Actinometer sensitivities $\mu V/W\ m^{-2}\ (\pi\ st)^{-1}$

Calibration date	Feb. 1976	July 1977	Adopted value
Instrument no.			
I	0.65	0.60	0.63
II	0.77	0.61	0.61
III	0.67	0.48	0.65
IV	0.66	0.65	0.66
V	0.74	0.64	0.69
VI	0.64		0.62
VII	0.72	0.63	0.67
VIII	0.75	0.73	0.74
IX	0.52	0.51	0.51
X	0.70	0.67	0.68

Table E2 Actinometer orientations

Instrument	Azimuth Before Feb. 1977	Zenith	Azimuth After Feb. 1977	Zenith
I	E	30°	E	30°
II			S	60°
III	S	60°	N	60°
IV	S	30°	S	30°
V	E	60°	E	60°
VI	W	60°	W	60°
VII		0°		0°
VIII	W	30°	W	30°
IX	N	30°	N	30°
X	N	60°	S	60°

Table E3 Calibrations of Kipp solarimeters

Serial no.	Use	Sensitivity $\mu V/W\ m^{-2}$
CM2 - 683135	Global radiation	12.62
CM2 - 683062	Diffuse radiation	11.69
CM5 - 690254	Global radiation on tilted plane	11.80

APPENDIX F

A computer program for the estimation of the irradiation of sloping surfaces.

```
      MASTER IRRADIATION
      REAL LAT,LONG
      LOGICAL HIGH
      DIMENSION X(10),Y(10) , Z(10),TILT(10),AZI(10),R(10)
      DIMENSION TITLE(10),TEXT(5),C(4,5,10),G(5,10),S(5),SDY(5),SYR(5)
      DIMENSION COR(12)
      COMMON PI,DTR
      DATA IMIN/0/
      PI = 3.1415926536
      DTR = PI/180.
      READ(55,1200) TITLE
      READ(55,1000) LAT,LONG
C***  LONG IS USED TO CORRECT LOCAL TIME TO GMT. ONLY VALID IN GMT TIME ZONE.
C***  TAKE LONGITUDE WEST AS POSITIVE.
      READ(5,1000) TAU,RHO,BETA1,GAMMA,BETA2
      READ(15,1000) COR
      DO 22 I = 1,5
   22 READ(15,1200) TEXT(I)
C
      READ(25,1100) NP
C*** NP IS THE NUMBER OF FIXED PLANES CONSIDERED.
C***  SET UP COORDINATES OF PLANES. X,Y AND Z ARE DIRECTIONAL COSINES OF THE
C***  NORMAL TO THE SURFACE.
 1000 FORMAT(99F0.0)
 1100 FORMAT(99I0)
 1200 FORMAT(10A8)
      DO 30 I = 1,NP
      READ(25,1000) TILT(I),AZI(I)
      TT = TILT(I) *DTR
      AA = AZI(I)*DTR
      X(I) = SIN(TT)*COS(AA)
      Y(I) = SIN(TT)*SIN(AA)
      Z(I) = COS(TT)
   30 CONTINUE
C
      CALL ZERO(SYR,C,1,5,10)
      WRITE(6,6000) TITLE
      WRITE(6,6100) LAT,LONG
      WRITE(6,6200) RHO,TAU
      WRITE(6,6300) BETA1,GAMMA,BETA2
 6000 FORMAT(1H1,10A8)
 6100 FORMAT(1H0,'LATITUDE ',F6.2,10X,'LONGITUDE  ',F6.2,'     DEGREES')
 6200 FORMAT(////1H0,'REFLECTED RADIATION ISOTROPIC  WITH ALBEDO ',F5.2
     */1H0,'MEAN TURBIDITY TAKEN AS ',F5.2)
 6300 FORMAT(1H0,'DIFFUSE RADIATION SEPARATED INTO BLUE SKY AND CLOUDY F
     *RACTIONS'/1H0,'CLOUD RADIANCE IS ASSUMED LINEAR IN COS(THETA) WITH
     *  SLOPE',F5.2,'  (SOC HAS SLOPE 2)'/1H0,'A FRACTION',F5.2,
     *' OF THE BLUE SKY DIFFUSE IS ADDED TO THE DIRECT BEAM'/1H0,
     *'THE REMAINDER IS TREATED IN THE SAME WAY AS CLOUD BUT WITH SLOPE'
     *,F6.2)
C*** C(I,J,K) IS THE IRRADIATION OF SURFACE K.
```

```
C***  I REFERS TO THE TIME PERIOD. 1 = YEAR, 2 = MONTH ,3 = DAY, 4 = HOUR.
C***  J REFERS TO THE COMPONENTS OF RADIATION. 1 = GLOBAL, 2 = DIRECT BEAM
C***  3 = BLUE SKY DIFFUSE, 4 = CLOUDY DIFFUSE, 5 = GROUND REFLECTION.
C
C
      DO 10 MONTH = 1,12
      READ(55,1100) NDAYS, IHOUR, LHOUR
      CALL ZERO(SDY,C,3,5,10)
      CALL DECTIM(15,MONTH,DECL,ETIME)
C***  CORGM IS THE PROPORTION OF CIRCUMSOLAR IN THE BLUE SKY RADIATION
C*** CORRECTED FOR SHADE RING DISPARITIES.
      CORGM = 1. - COR(MONTH)*(1. - GAMMA)
      WRITE(6,7000) MONTH
      WRITE(6,7050) DECL,ETIME
      WRITE(6,7055) CORGM
      WRITE(6,7100) (TILT(I),I=1,NP),(AZI(I),I=1,NP)
 7000 FORMAT(1H1,'COLLECTOR IRRADIATION VALUES FOR MONTH ',I2//
     *1H ,'HOURLY SURFACE IRRADIANCE (W.M-2)'//)
 7050 FORMAT(1H0,'ON 15TH DAY OF MONTH, DECLINATION = ',F8.3,' DEGREES',
     *'  EQUATION OF TIME = ',F8.3,' MINUTES')
 7055 FORMAT(1H0,'GAMMA CORRECTED FOR SHADE RING = ',F6.2)
 7100 FORMAT(1H0,70X,'TILT,AZIMUTH DEGREES'//1H0,48X,9F7.0,6X,'Z'/
     *1H ,'HR',4X,'Z',3X,'AZ',9X,'ST',5X,'SD',4X,'SDB',5X,'SB',4X,9F7.0,
     *5X,'AZ'//)
      DO 20 NHOUR = IHOUR,LHOUR
C***  IMIN IS AN INCREMENT IN MINUTES TO BE ADDED IF TIME INTERVAL IS NOT
C***  CENTRED ON THE HOUR
      CALL SOLOC(NHOUR,IMIN,DECL,ETIME,LAT,LONG,XS,YS,ZS)
C
C***  MEASURED RADIATION VALUES : ST -- GLOBAL; SD-- DIFFUSE.
      READ(55,1000) ST,SD
      ZEN = ACOS(ZS)/DTR
      AZ = ATAN(YS/XS)/DTR
      IF(XS.LT.0.0) AZ = AZ + SIGN(180.0,YS)
      HIGH = ZS.GT.0.087
      IF(HIGH) GO TO 413
      S(2) = 0.0
      S(3) = 0.0
      S(4) = ST
      GO TO 423
  413 SB = ST-SD
      S(2) = SB/ZS
C***  RAT GIVES THE RATIO OF BLUE SKY RADIATION TO TOTAL IN A CLEAR SKY.
C***  USED TO SEPARATE BLUE SKY FROM CLOUDY DIFFUSE
      Q = RAT(ZEN,TAU)
      S(3) = SB*Q/(1.-Q)
C*** THE NEXT CARD LIMITS THE BLUE SKY PORTION OF THE DIFFUSE FOR MEAN DAY
C***  OR PARTLY CLOUDY DAYS.SHOULD BE REMOVED IF USING CLEAR DAY DATA.
      IF(S(3).GT.0.65*SD) S(3) = 0.65*SD
      S(4) = SD - S(3)
  423 S(5) = RHO*ST
      S(1) = ST
C
C***  G(J,K) ARE GEOMETRICAL MULTIPLIERS TO CONVERT THE RADIATION COMPONENTS
C***  S(J) INTO THEIR INTERCEPTED VALUES ON THE SURFACES C(I,J,K).
      DO 60 JP = 1,NP
      DOT = XS*X(JP) + YS*Y(JP) + ZS*Z(JP)
      IF(DOT.LT.0.0) DOT = 0.0
      G(2,JP) = DOT
      G(3,JP) = CORGM*DOT/ZS + (1. - CORGM)*DIFF(BETA2,TILT(JP),Z(JP))
      G(4,JP) = DIFF(BETA1,TILT(JP),Z(JP))
      IF(.NOT.HIGH) G(4,JP) = DIFF(0.0,TILT(JP),Z(JP))
      G(5,JP) = (1. - Z(JP))/2.
      C41J = 0.0
      DO 50 KR = 2,5
      C4KJ = G(KR,JP)*S(KR)
```

```
      C41J = C41J + C4KJ
      C(4,KR,JP) = C4KJ
   50 CONTINUE
      C(4,1,JP) = C41J
   60 CONTINUE
      C4110 = 0.0
      G(2,10) = 1.0
      G(3,10) = CORGM/ZS + (1. - CORGM)*DIFF(BETA2,ZEN,ZS)
      G(4,10) = DIFF(BETA1,ZEN,ZS)
      IF(.NOT.HIGH) G(4,10) = DIFF(0.0,ZEN,ZS)
      G(5,10) = (1. - ZS)/2.
C
      DO 70 KR = 2,5
      C4K10 = G(KR,10)*S(KR)
      C4110 = C4110 + C4K10
      C(4,KR,10) = C4K10
   70 CONTINUE
      C(4,1,10) = C4110
      S(2) = ST - SD
      DO 75 LR = 1,5
      SDY(LR) = SDY(LR) + S(LR)*3.6E-3
      DO 75 IP = 1,10
      C(3,LR,IP) = C(3,LR,IP) + C(4,LR,IP)*3.6E-3
   75 CONTINUE
      WRITE(6,7500) NHOUR,ZEN,AZ,ST,SD,S(3),S(2),(C(4,1,I),I = 1,10)
 7500 FORMAT(1H ,I2,2F5.0,4X,4F7.1,4X,10F7.1)
   20 CONTINUE
C***  R VALUES ARE THE RATIOS OF COLLECTOR TOTALS TO ST.
      DO 80 IP = 1,10
      R(IP) = C(3,1,IP)/SDY(1)
      DO 80 JR = 1,5
      C(2,JR,IP) = C(3,JR,IP)*NDAYS
      C(1,JR,IP) = C(1,JR,IP) + C(2,JR,IP)
   80 CONTINUE
      DO 95 I = 1,5
      SM = SDY(I)*NDAYS
      SYR(I) = SYR(I) + SM
   95 CONTINUE
      WRITE(6,8000)
 8000 FORMAT(//1HO,'MEAN DAILY RADIATION TOTALS     MJ.M-2'//
     *1H ,15X,'HORIZONTAL'/)
      DO 85 J = 1,5
      WRITE(6,8100) TEXT(J),SDY(J),(C(3,J,I),I = 1,10)
 8100 FORMAT(1H ,A8,8X,F7.2,25X,10F7.2)
   85 CONTINUE
      WRITE(6,8200) R
 8200 FORMAT(//1HO,'RATIOS OF SURFACE TO HORIZONTAL IRRADIATION'//
     *1H ,48X,10F7.2)
   10 CONTINUE
      DO 100 I = 1,10
      R(I) = C(1,1,I)/SYR(1)
  100 CONTINUE
      WRITE(6,9000)
 9000 FORMAT(1H1,'COLLECTOR IRRADIATION VALUES FOR THE YEAR'/1HO,10X,
     *'MJ.M-2'///1H ,15X,'HORIZONTAL')
      DO 98 J = 1,5
      WRITE(6,9100) TEXT(J),SYR(J),(C(1,J,I),I = 1,10)
   98 CONTINUE
 9100 FORMAT(1H ,A8,8X,F7.0,25X,10F7.0)
      WRITE(6,8200) R
      STOP
      END
```

```
      SUBROUTINE ZERO(B,A,I,J,K)
      DIMENSION A(4,J,K),B(J)
      DO 10 JJ = 1,J
      B(JJ) = 0.0
      DO 10 KK = 1,K
      A(I,JJ,KK) = 0.0
10    CONTINUE
      RETURN
      END
```

```
      FUNCTION RAT(Z,T)
C***  RAT GIVES THE RATIO OF BLUE SKY RADIATION TO TOTAL IN A CLEAR SKY.
C***  USES RELATIONSHIPS WITH TURBIDITY (T) FROM UNSWORTH(1976) AND PAGE(1976).
      RAT = 0.097 + 0.68*T
      IF(Z.LT.60.0) RETURN
      RAT = RAT + (Z-60.0)*(3.5 + 44.0*T)/1000.
      RETURN
      END
```

```
      FUNCTION DIFF(B,AL,CSA)
      COMMON PI,DTR
C***  DIFFUSE IRRADIANCE OF TILTED SURFACES FOR RADIANCE
C***  DISTRIBUTIONS LINEAR IN COS(THETA)
C***  WHEN B = 2 ,THE FORMULA IS THE SAME AS THAT OF MOON AND SPENCER (1942).
      F = (2.0*B)/(PI*(3.0 + 2.0*B))
      A = AL*DTR
C***  B IS THE SLOPE OF THE RADIANCE DISTRIBUTION WITH COS(Z).
C***  AL IS THE SURFACE TILT IN DEGREES AND CSA IS COS(AL)
      DIFF = (1.0 + CSA)/2.0 + F*(SIN(A) + CSA*(PI/2.0 - A) - PI/2.0)
      RETURN
      END
```

```
      FUNCTION FRESNEL(ZS)
      DATA RI/1.33/
C***  COMPUTES FRESNEL REFLECTION COEFFICIENT OF WATER SURFACE FOR
C***  UNPOLARISED LIGHT.
      ZT = ACOS(ZS)
      SIZ = SQRT(1.-ZS*ZS)
      SIR = SIZ/RI
      R = ASIN(SIR)
C***  R IS THE ANGLE OF REFRACTION, ZT THE ZENITH ANGLE AND RI THE REFRACTIVE
C***  INDEX.
      A = SIN(ZT-R)
      B = SIN(ZT+R)
      C = TAN(ZT-R)
      D = TAN(ZT+R)
      FRESNEL = 0.5*((A*A)/(B*B) + (C*C)/(D*D))
      RETURN
      END
```

```
      SUBROUTINE DECTIM(ND,MONTH,TD,TE)
      COMMON PI,DTR
      DIMENSION IMONTH(12),D1(3),D2(3),E1(3),E2(3)
C***  DECTIM CALCULATES THE DECLINATION AND EQUATION OF TIME FOR
C***  ANY DAY OF THE YEAR.
      DATA IMONTH/0,31,59,90,120,151,181,212,243,273,304,334/
      DATA D1/-22.9943,-0.3761,-0.1457/
      DATA D2/3.5677,0.0373,0.0740/
      DATA E1/0.5638,-3.1358,-0.08165/
      DATA E2/-7.3434,-9.41858,-0.30829/
      DATA D0/0.3747/
      DATA E0/0.00408/
C*** USES COEFFICIENTS FROM FITTING OF 1976 LEAP YEAR DATA. ERROR IS SMALL.
C***  < 0.6 DEG IN DECL AND < 0.8 MIN IN TIME.
```

```
      W = 2.0*PI/365.25
      JRDAY = IMONTH(MONTH) + ND
      TD = D0
      TE = E0
      DO 555 I = 1,3
      QT = FLOAT(I*JRDAY)*W
      CS = COS(QT)
      SN = SIN(QT)
      TD = TD + D1(I)*CS + D2(I)*SN
      TE = TE + E1(I) *CS + E2(I)*SN
  555 CONTINUE
C*** TD IS THE DECLINATION IN DEGREES, TE IS THE EQUATION OF TIME IN MINUTES.
      RETURN
      END


      SUBROUTINE SOLOC(NH,IM,DECL,FTIME,LAT,LONG,XS,YS,ZS)
      COMMON PI,DTR
      REAL LAT,LONG
C*** SOLOC CALCULATES DIRECTIONAL COSINES (XS,YS,ZS) OF THE SUN
C***  FOR TIME OF DAY ,DATE, LATITUDE AND LONGITUDE.
      DCL = DECL*DTR
      ET = ETIME/60.
      RLAT = LAT*DTR
      RLONG = LONG/15.
      HRANGL = (FLOAT(NH) + FLOAT(IM)/60. + ET - 12. - RLONG)*PI/12.
C**   HRANGL USES THE CONVENTION THAT LONGITUDE MEASURED WEST IS POSITIVE.
      COZ = SIN(RLAT)*SIN(DCL) + COS(RLAT)*COS(DCL)*COS(HRANGL)
      SIZ = SQRT(1. - COZ*COZ)
      SNAZ = COS(DCL)*SIN(HRANGL)/SIZ
      CSAZ = (SIN(RLAT)*COZ - SIN(DCL))/(COS(RLAT)*SIZ)
      XS = SIZ*CSAZ
      YS = SIZ*SNAZ
      ZS = COZ
      RETURN
      END
```

```
C**********************************************************************
```

APPENDIX G

Dates of measurement

Measurements of the radiance distribution of cloudless skies with the Linke-Feussner actinometer were made on the following dates :

1975	June	11 , 12 , 13 , 22 , 23 , 25 , 26
	July	2 , 3 , 4 , 6 , 7 , 28
	August	2 , 4 , 7 , 8 , 11 , 13 , 14 , 28 , 29
	September	4
	October	22
1976	March	2 , 5
	May	7

The following table shows the number of days selected in each month for the analysis of cloudy skies, using the 'sunless data' and the 'corrected data'

Month	'sunless data'	'corrected data'
May 1976	9	12
June	13	10
July	8	8
August	5	6
September	8	8
October	9	8
November	10	12
December	4	7
January 1977	4	8
February	0	0
March	15	20
April	8	10
May	2	0